Lawrence Berkeley National Laboratory
Recent Work

Title
UTILIZATION OF METALS IN OIL SHALE RETORT COMPONENTS

Permalink
https://escholarship.org/uc/item/7zj85830

Author
Levy, A.V.

Publication Date
1982-11-01

eScholarship.org Powered by the California Digital Library
University of California

LBL-16018
UC-25 c.1

Lawrence Berkeley Laboratory
UNIVERSITY OF CALIFORNIA

Materials & Molecular Research Division

RECEIVED
LAWRENCE
BERKELEY LABORATORY
JUN 8 1983
LIBRARY AND
DOCUMENTS SECTION

UTILIZATION OF METALS IN OIL SHALE RETORT COMPONENTS

Alan V. Levy

November 1982

For Reference
Not to be taken from this room

Prepared for the U.S. Department of Energy under Contract DE-AC03-76SF00098

LBL-16018

DISCLAIMER

This document was prepared as an account of work sponsored by the United States Government. While this document is believed to contain correct information, neither the United States Government nor any agency thereof, nor the Regents of the University of California, nor any of their employees, makes any warranty, express or implied, or assumes any legal responsibility for the accuracy, completeness, or usefulness of any information, apparatus, product, or process disclosed, or represents that its use would not infringe privately owned rights. Reference herein to any specific commercial product, process, or service by its trade name, trademark, manufacturer, or otherwise, does not necessarily constitute or imply its endorsement, recommendation, or favoring by the United States Government or any agency thereof, or the Regents of the University of California. The views and opinions of authors expressed herein do not necessarily state or reflect those of the United States Government or any agency thereof or the Regents of the University of California.

LBL-16018

UTILIZATION OF METALS IN OIL SHALE RETORT COMPONENTS

Alan V. Levy
Materials and Molecular Research Division
Lawrence Berkeley Laboratory
University of California
Berkeley, California 94720

Research sponsored by the Department of Energy under DOE/FEAA 15 10 10 0, Advanced research and Technical Development, Fossil Energy Materials Program, Work Breakdown Structure Element LBL-3.5 and under Contract No. DE-AC03-76SF00098.

INTRODUCTION

A program to determine the corrosion behavior of candidate commercially available alloys in in-situ and above-ground oil shale retorting environments has been conducted. Both laboratory tests in simulated operating conditions and actual field exposures in both types of retorts have been carried out. In addition performance analyses have been performed on metal sections from several components that were used in actual and simulated in-situ retorts.

The program was initiated to provide metallic corrosion information to the operators of experimental retorts that were experiencing significant loss of components by corrosion in retorting operations. These losses occurred in critical components such as thermowells and product oil sumps that severely compromised the experiments that were being conducted. A brief review of the oil shale retorting processes will provide a basis for understanding the corrosion environments that are present and the degree of attack that can occur in relatively short time exposures in in-situ retorts.

The Green River oil shale deposits, located in the Utah-Wyoming-Colorado Three Corners region, and the Antrim shale formation centered in Michigan and also occurring down the center of the country constitute a major source of national fossil energy reserves in a form

that can be refined into liquid/gas hydrocarbon fuels. Since this national resource could make a major contribution to future energy needs, considerable effort has been undertaken to develop the processes to extract the organic material, called kerogen, from its marlstone rock depository. The process to separate the kerogen from the marlstone uses a pyrolysis type reaction that involves heating the oil shale to a temperature near 550°C to convert the organic material into a vapor which is collected, condensed and further refined to produce various usable product fractions.

OIL SHALE COMPOSITIONS

The composition of oil shale differs within oil shale formations as well as between formations. The chemical composition of the various shales directly relate to their corrosion potential. Sulfur is a particularly reactive element that participates in the major corrosion reactions that can occur in retorting operations. Table I lists some of the constituents in Green River-western and Antrim-eastern shales. It can be seen that there are major differences in composition between the relatively low sulfur content Green River shale and the high sulfur Antrim shale that directly relates to their corrosivity.

Table II shows how the sulfur content in shales distribute themselves in Green River shales of varying oil content. There is a general trend for the higher oil content shales to have a higher sulfur content. Typical shales contain 25 - 40 gal/ton and have a sulfur content around 0.5 - 0.75 wt/%. Table III lists the distribution of compounds in the inorganic portion of various grades of Green River

shale and of the retorted or spent shale. Some of these constituents can enhance and others retard the corrosion reactions that can occur during retorting. For example CaO can act as a corrosion inhibitor by gettering the sulfur and forming calcium sulfide if conditions are favorable.[3] A review of the sulfur reactions that occur in a shale retorting operation is contained in reference 4.

ABOVE GROUND RETORTS

The heat required to raise the rock to the kerogen's pyrolysis temperature is generated, basically, in two manners. In above ground retorting, the crushed rock containing the kerogen is placed in a vessel and the heat required to raise it to the pyrolysis temperature is developed from a source outside the vessel. This process, which has been demonstrated over a period of years but never commercialized, utilizes different heating schemes that generally separates the higher temperature areas from the shale. Because the corrosive constituents in the shale never exceed the pyrolysis temperature, $\sim 500^{\circ}C$, the corrosion potential is quite low in above ground retorting and material selection can be based on general experience in the chemical process industry. For some components, abrasive selection criteria used by the mining industry may be appropriate. At any rate, current materials selection practices can be utilized in above-ground oil shale retorting reasonably well.

IN-SITU RETORTS

In-situ oil shale retorting, the other pyrolysis method, has been under development for a relatively short period of time, has much more severe operating environments for metallic components and has caused considerable elevated temperature corrosion degradation of components in retorts that have been operated to date. The principal elements that result in a severe corrosion environment are a localized reducing atmosphere, the presence of significant amounts of sulfur and operating temperatures for some metallic components that can exceed 1000° C.

Renewed interest in oil shale deposits has led to extensive investigations during the past several years of the technical, economical and environmental aspects of in-situ retorting of oil shale. Such firms as Occidental Oil Shale, Inc.[5-6], Rio Blanco Oil Shale project[7-8], and Geokinetics, Inc. among others have carried out pilot scale operations to obtain oil from the Green River formation. The Dow Chemical Co. has experimented to recover product from the Antrim shales of Michigan.

Three types of in-situ processes have been investigated by industry: modified, true and additional modified. Only the true and the modified in-situ processes are described here as they have been developed nearest to commercial status. Fig. 1 shows a representative commercial retort field consisting of a series of chimneys of rubblized oil shale. These rubblized chimneys, called retorts, are created in-situ by first removing from 15% to 30% of the raw oil shale and then blasting to distribute small pieces of rock through the void volume. Fig.2 shows the extensive mining necessary to develop such a field.

Many horizontal drifts are drilled; vertical shafts are drilled from the drifts into the shale bed for the placement of explosives for rubblization. The 15% to 30% raw oil shale removed is retorted in above-ground retorts using such processes as Tosco II, Paraho or Lurgi. A rubblized chimney is shown schematically in figure 3. The dimensions shown are for an experimental chimney that was retorted by Occidental Oil Shale, Inc. Typical commercial prototype chimneys designed by the Rio Blanco Oil Shale Project have dimensions of from 100' x 150' x 400' to 150' x 300' x 700'. The overburden above the chimneys can range from 40' to greater than 200'.

A description of the process, taken from reference 5, follows:

> "In the Modified In-Situ Process, retorts are created by mining out only enough shale to provide a void fraction for rubblizing the remaining shale by blasting and to provide permeability for gas flow during operation. These in-situ retorts consist of groups or clusters of eight 200'x200'x300'-high rubble columns or chimneys. Undisturbed pillars function as control partitions between operating retorts.
>
> The processing of a cluster of retorts consists of several steps. First, a retort within a cluster is kindled from the top by externally fueled burners. When the temperature at the top of the retort is sufficient to sustain reaction, the burners are shut off and a regulated mixture of air and steam is drawn into and through the retort by exhaust blowers on the surface. Residual organic material is combusted with the air in the feed gas. The hot combustion gases flow down through the retort and supply heat to the raw unretorted shale below. As the shale is heated, the organic material or kerogen decomposes into oil vapor and other gases that are carried along with the combustion gases while some residual organic material remains in the rubble. Steam in the feed gas acts as a dilutent to the oxygen in the air to control the reaction temperature and reacts with some of the residual organic material forming carbon monoxide and hydrogen to improve the heating value of the product gas. Some of the mineral carbonates in the shale are also decomposed to carbon dioxide gas and mineral oxides. As the gas mixture flows down through the retort, it preheats the raw shale. At the same time, the oil and gas leave the bottom of the retort and move to the surface for further processing as product oil, product fuel gas, and water.

As retorting progresses, the combustion and retorting zones move slowly down through the in situ retort. Between 7 and 8 months are required to process a cluster. When retorting is complete, the air and steam feed are stopped and the in-situ retort is closed off. The spent shale remains underground with no need for surface disposal.

Surface process facilities consist only of oil/water separation equipment, exhaust blowers, a sulfur removal unit for treatment of product gas, and boilers to produce process steam from fuel values in the product gas."

A schematic of a horizontal type true in-situ retort such as is operated by Geokinetics, Inc. is shown in Fig. 4. The various thermal regions are shown in this drawing along with a temperature curve. The same thermal areas occur in a vertical retort such as that described above. The time that any region of the retort behind the pyrolysis front or distillation zone is in the temperature range where sulfidation corrosion can occur ranges from days to a few weeks. Any metal component that must remain functional in this region is susceptable to damaging elevated temperature corrosion.

The reports of oil shale retorting companies stress the importance of the measurement and control of the temperatures in the retorting chimneys to control the actual retorting operation. The temperatures at various locations are measured by thermowells that can extend in from the sides or the top of the chimney for distances of over 100 feet. To assure the integrity of the thermocouples in the rubblized shale bed, they must be protected by tough metallic sheaths so that the shifting shale during retorting does not break them. The integrity of these metal sheaths, which are critical to the control of the retorting operation, can be severely compromised by elevated temperature corrosion in the sulfidizing-oxidizing environments present in the

retorts. Temperatures are expected to reach 1000° C and higher in commercial in-situ retorts. Other metallic components are also planned to be used in the retorts that will be exposed to high temperatures. Low temperature, aqueous type corrosion may also be a problem in retorting operations.

CORROSION OVERVIEW

The Materials and Molecular Research Division (MMRD) of the Lawrence Berkeley Laboratory (LBL) has been working closely with the Laramie Energy Technology Center (LETC) and the Lawrence Livermore National Laboratory (LLNL) as a part of the program reported herein to determine the behavior of metals operating in experimental, simulated, in-situ oil shale retorts. In addition, specimens have also been exposed in underground retorts developed by Geokinetics, Inc. Specimens of 14 commercially available alloys ranging from 1018 mild steel to Incoloy 800, uncoated and coated with a commercial aluminized coating, have been exposed in simulated in-situ retorting experiments at LETC and LLNL and subsequently analyzed at LBL.

The performance analyses of stainless steel thermocouple sheaths, flexible piping components, and down-hole mild steel piping and pump components have also been conducted. In these investigations, it has been determined that corrosion, principally by sulfidation reactions, can completely corrode a cross section to scale products in a relatively few hours or days. The extent of the corrosion attack varies as a function of the type of retort, the alloy composition, the

type of shale and the temperature-time profile that the material is exposed to.

PROGRAM PLAN

The program was conducted in three major tasks:

task 1. performance analyses of materials from actual components

task 2. specimen exposures in large scale, simulated in-situ and experimental above-ground retorts.

task 3. specimen exposures in small scale, laboratory retorts and crucibles.

Commercial alloys were used for all exposures. The exposure conditions were not controlled in the large scale retorts, but were monitored to as great a degree as was possible by measuring and recording temperature, time, position in the retort, and the type of shale that was used. In the laboratory scale exposures, temperature and time were controlled and representative shale compositions were used. All specimens were carefully fabricated to the same dimensions and surface finish. The scheduling of all large scale retort tests were at the convenience of the retort operators in the case of retorts operated by LETC and LLNL. Laboratory tests were carried out and the specimens analyzed during periods between availability of specimens from the large scale tests.

PERFORMANCE ANALYSES

Sections of components from large scale tests were obtained from retort operators at their convenience. The conditions under which the

materials were exposed were obtained from the retort operators. In all cases, these conditions were loosely defined. It was never known what the exact location, retort operating conditions (especially temperature), and exposure times were. In some instances, the number of exposures cycles was not known.

The pieces were sent to LBL for analysis generally wrapped in newspaper or in a plastic bag. Protection of the scales formed was not very good and pieces of scale were knocked off the surface in transit. Because the scale formation was so extensive, there was always sufficient scale to make a good analysis. However, the thicknesses of scales, particularily outside scales on pipes and tubes could not be absolutely determined unless the scale was relatively thin and coherent. In several instances, the types and relative positions of scales formed on a component made it possible to speculate quite well on what the operating conditions of the component were in the retort. Performance analyses representing each of the several types of behavior observed on parts analyzed during the program were selected for presentation in this report.

310SS THERMOCOUPLE SHEATH

Operating Conditions:

A Chromel-Alumel thermocouple in a mullite insulator and sheathed in 310 stainless steel was exposed to a Green River oil shale retorting environment in the LETC 10-ton simulated in-situ retort. A maximum temperature of 980°C (1800°F) was reached at the flamefront for each run and the isothermal advance of the flamefront was 1.4 inches/hours.

Each retorting run lasted approximately 72 hours. The thermocouple was exposed to two or more runs; the exact number is not known.

The thermocouple wires in mullite insulators were originally sheathed in 310 stainless steel to protect the brittle mullite thermocouple housing from shale rock during loading that could cause premature thermocouple failure. This design prevented premature failure, but during the course of the retorting runs heavy attack on the 310 stainless steel occurred. Enough of the sheathing was eventually removed by corrosion that the mullite cracked due to the rock loading and enabled some sulfur to penetrate through to the thermocouple wires (Fig. 5). Thermocouple failure resulted.

Analysis Description:

A one-inch length of 310 stainless steel sheathed thermocouple wires was received for analysis. The length was cross-sectioned and a section was mounted, polished, and examined using the scanning electron microscope (SEM) and optical microscope. A qualitative analysis of the elements present in the scales was obtained using the SEM for x-ray mapping and EDAX peak analyses. The EDAX also was used to investigate segregation of the alloying elements in the 310 stainless steel. A more detailed identification of the actual compounds present as oxides and sulfides was obtained using powder x-ray diffraction.

Results:

Three areas of the 310 stainless steel sheath were examined. These areas are shown in a multiple scale cross section in Fig. 5. The original thickness of the stainless steel sheath was 0.6mm. This was

reduced to 0.2mm, or 30% of the original thickness. The areas examined were: (1) the inside face of the sheath next to the mullite tube (Fig. 6); (2) the metal-outer scale interface (Fig. 7); and (3) the outer surface of the scale where it was exposed to the atmosphere (Fig. 8).

At the mullite-310SS interface shown in Fig. 6 there was strong evidence of Cr_2O_3 formation on the alloy. Some traces of sulfur and silicon were in the sheath-mullite interface and also on the thermocouple wires themselves. There was also evidence of Cr_2O_3 on the thermocouple wire.

Examination of the 310 sheath-outer scale interface in Fig. 7 also showed strong evidence of Cr_2O_3 in areas of Fe-Ni alloy devoid of chromium. Note the sulfur concentration map. This indicates that small areas of chromium sulfide occurred in conjunction with the Cr_2O_3.

The outer scale area on the 310 stainless steel exhibited a large amount of porosity and consisted of multiphase regions of various corrosion products, see Fig. 8. The Ni has segregated into alloy pockets in a predominately Fe-Cr-S matrix. Some areas of Fe-Cr-S showed evidence of some nickel being present. A small number of areas showed the presence of $Fe_{1-x}S$, and $FeCr_2O_4$, with traces of S. To more clearly show the mixed distribution of corrosion products in the outer scale, a tracing of the 1000X closeup of Fig. 8 is shown in Fig. 9. The tracing is coded for easy identification of the corrosion products that were indicated by SEM x-ray maps.

A higher magnification (5000X) of this particular area is shown in Fig. 10. Qualtitative examination using EDAX peak analysis was done at three points. Different concentrations of Fe, Cr, Ni and S occurred at

each point, verifying the presence of the constituents identified above. Location #1 shows existence of a Cr-depleted Fe-Ni alloy with a trace of S. Location #2 shows an iron sulfide, $Fe_{1-x}S$, with some Ni in it, while #3 shows 310 stainless steel with a small amount of S in it.

Four x-ray maps were made at 5000X of the area pictured in Fig. 10. These are shown in Fig. 11. They verify the EDAX peak identifications and also reveal the distribution of Fe, Cr, Ni, and S over the entire area photographed.

To further identify the several compounds in the outer scale, the scale on the sheath was scraped off, powdered, and examined using powder x-ray diffraction methods. The resulting experimental peak readings and the corresponding peaks of standard compounds are shown in Table 4. The closest agreements of the thermocouple sheath scale data with specific standard peaks were those readings for CrS, $Fe_{1-x}S$, and $FeCr_2O_4$. These x-ray analyses were done using corrosion scale scraped off a small section of sheathed thermocouple approximately 1/2 inch long. Consequently, the amount of powder obtained for analysis was only enough for a Deby-Scherer camera, thus limiting the accuracy of the experimental peaks.

Discussion:

The results of this investigation of in-situ sulfidation were compared with results obtained from controlled laboratory sulfidation experiments in an argon-sulfur gas mixture. These experiments were carried out on 310 stainless steel at temperatures from 730°C to 953°C and $P_{S_2} = 10^{-7}$ atm. No oxygen was present in the laboratory furnace

atmosphere. They yielded a scale formation similar to that obtained on the shale retort-exposed 310 specimens (see Fig. 12). For example, the interior scale of the laboratory specimens was found to be Cr_xS_y in a Ni-rich base metal. This agrees with the scale found adjacent to the 310SS sheath consisting of Cr_xS_y and Cr_2O_3 mixed with pockets of Cr-depleted alloy. In addition, the outer portion of the scale on the laboratory specimens was found to be a $FeCr_xS_y$ spinel. Extensive evidence of this spinel occurred in the outer scale on the 310SS sheath. Such close agreement suggests that an estimation can be made of the partial pressure of sulfur seen by the 310SS sheath in the retorting atmosphere.

Referring to the thermodynamic equilibrium stability diagram[9] in Fig. 13 shows that the CrS is stable at $P_{S_2} > 10^{-9}$ atm., and Cr_2S_3 is stable at $P_{S_2} > 10^{-7}$ atm. This suggests that the 310 sheath saw a $P_{S_2} > 10^{-9}$ atm during shale retorting, since a form of Cr_xS_y was indicated by the x-ray diffraction analysis. Also, the presence of $FeCr_2O_4$ in the scale suggests a $P_{O_2} > 10^{-19}$ atm at the alloy-atmosphere interface. It can be surmised from these observations that the Cr_xS_y probably formed by internal sulfidation and outgrew the protective Cr_2O_3 on the metal surface. The Fe-Cr-S spinel subsequently grew on this Cr_xS_y layer by a diffusion process.

As mentioned earlier, the exact determination of chemical composition of the sulfide and oxide scales formed on the 310SS sheath was difficult due to both the complex nature of scale growth and also the small amount of material available.

Conclusions:

Based on the results of this analysis and supporting laboratory sulfidation tests, the following conclusions can be made:

1. The retorting temperature of 980°C and the sulfur content of the Green River shale worked in combination to create a high P_{S_2}-low P_{O_2} atmosphere that caused destructive sulfidation of the 310 stainless steel.
2. A complex mixture of scale products formed on the 310 stainless steel sheath indicating that complex gas mixtures had occurred in very local areas.
3. The partial pressure of sulfur (P_{S_2}) at the thermocouple sheath surface is estimated to be $>10^{-9}$ atm.
4. Based on the presence of $FeCr_2O_4$ found in the sheath scale, the partial pressure (P_{O_2}) of oxygen would be $>10^{-19}$atm.
5. The laboratory sulfidation experiments closely compared to the sulfidation behavior of 310 stainless steel in the Green River shale retorting environment indicating that a strongly reducing atmosphere was present in the retort.

MILD STEEL THERMOWELL CASING

Operating Conditions:

Two badly corroded thermocouple well casings from an in-situ oil shale retort operation by Geokinetics, Inc. were analyzed.

The well casings were originally 3/4 inch dia. mild steel pipe. One of the casings had a thermocouple of stainless steel still attached to its inside wall. Each casing had been exposed to an in-situ

retorting environment at temperatures from 540°C (1000°F) to 1100°C (2000°F). The length of the exposure time was not known nor was the composition of the retorting gases, but conditions were severe enough to completely corrode the casing.

Analysis Description:

The specimens were photographed in their initial state, Fig. 14. The white appearing tube on the right side of each specimen is a rolled up piece of paper used to identify the specimen. Using standard metallographic procedures, the specimens were cross-sectioned, mounted in bakelite molds, and polished to a 1 micron finish. Three sections were cut along the long axis of casing A and B and the Casing A attached thermocouple. Specimens were observed using the optical metallograph and the scanning electron microscope (SEM) equipped with EDAX. Encrusted scale material from the exterior of each pipe was scraped and powdered for examination by x-ray diffraction.

Results:

Mild Steel - Specimen B shows heavy scale development on either side of the metal matrix (Fig. 15-A). Note the extent of the corrosion and the layered nature of the scale. The rough handling of the specimen in withdrawing it from the retort and shipping it to the laboratory knocked off most of the scale on the outer surface of the tube, leaving only a few layers of scale (Fig.15-B). At its thickest portion, there is only 0.7 mm of casing left. There appears to be some metal islands in the inner scale (Fig. 15-C) while none was observed in the outer scale.

Specimen A had been too heavily attacked to permit a useful optical examination to be performed. The metal had been completely transformed to scale; no metal remained. Speciman A did have a fairly intact thermocouple assembly that was removed and photographed (see Fig. 16). A heavy scale is present and there is also considerable selective attack along the grain boundaries that extends throughout the sheathing. The sensing wires appear undamaged, probably due to the protective ceramic casing.

A low magnification SEM micrograph of Specimen B was taken to show the thick, layered interior surface scale and the remaining exterior surface scale, see Fig. 17. Also visible is a thin layer of internal sulfidation on either side of the metal matrix that only appears in the peak analysis of Fig. 18. No grain boundary attack is observed. The primary scale layers on either side of the remaining metal shows only iron present in the form of Fe_2O_3, as determined by x-ray diffraction.

The thin scale layers immediately adjacent to the specimen were examined at a higher magnification and show significant quantities of sulfur as well as iron in Fig. 18. This indicates the presence of iron sulfide ($Fe_{1-x}S$), (FeS_2), or iron sulfate ($FeSO_4$), depending on retorting conditions such as temperature and the gas partial pressures of sulfur and oxygen.

To more clearly identify this sulfide layer, a high magnification micrograph of the area was made. EDAX analyses of various sections show the presence of iron and sulfur (see Fig. 19). EDAX analysis of the round inclusion in the base metal indicates manganese sulfide. The presence of MnS is probably not due to the corrosion conditions. In

the production of the alloy, manganese is commonly added to the melt to form the sulfur present into stable round sulfide inclusions that are less deleterious to the material's overall characteristics. A summary of the composition of the scale products on Specimen B is detailed in the Fig. 20 schematic. The limited outer scale depicted reflects its being knocked off in handling. Ref. 10 is an analysis of the same component by D. Douglass of UCLA.

Stainless Steel - An examination of the stainless steel thermocouple sheath removed from Specimen A (see Fig. 21A) shows the heavy scale and the internally attacked sheathing. The material was a 300 series stainless steel, probably 304SS. At approximately half-way through the sheathing the internal grain boundary attack changes markedly in nature. In the outer portion the attack is heavy, the grain boundaries are very thick, and the grains are large. Toward the inner portion, the attack is still heavy, but it is concentrated in thinner boundaries around smaller grains.

In Fig. 21-B the external scale, the scale metal interface and the internal attack along the grain boundaries are shown at higher magnification. The locations of sulfur, chromium, nickel and iron are shown in the x-ray maps for these elements which were obtained over a more highly magnified area at the scale-metal interface (Fig. 22). From these maps it is seen that the scale layer nearest the remaining metal is primarily Cr_2O_3 with some chromium sulfide (Cr_xS_y) present. The internal attack is chromium sulfide in a heavily chromium-depleted iron-nickel matrix.

Fig. 23 shows the region of the remaining metal noted earlier

where the nature of the grain boundary attack changes abruptly. In the upper left hand corner a section of the ceramic tubing is visible. In the lower right hand corner can be seen the internal grain boundary attack that extends inward from the exterior surface of the sheathing which was identified in Fig. 22 to be chromium sulfide. The EDAX peak confirms that it is chromium sulfide.

The inclusions in Fig. 23 change at this boundary, gradually becoming lighter in color and less continuous along the grain boundaries further in, toward the ceramic tube of the thermocouple. In a higher magnification micrograph of these inclusions, their nature is examined using EDAX, Fig. 24. No sulfur is detected within them so they are not chromium sulfides. An EDAX of the surrounding matrix shows nickel, chromium and iron but no sulfur. It is probable that this area of inner grain boundary attack consists of chromium carbides in the stainless steel base metal. The base metal does not show the high chromium depletion that it did in the outer areas of the thermocouple. EDAX of the internal portions of the wire show mostly nickel and chromium while EDAX of the scale show much higher chromium concentrations but there is no sulfur detected. The thin scale layer is protective chromium oxide. A summary of the scale products that formed on and in the thermocouple sheathing is given in the Fig. 25 schematic.

The electron micrograph results from Specimen A are shown in Fig. 26. The heavy multi layered external scale and the porous internal scale can be seen;no metal remains. There appears to be a significant

amount of iron sulfide present, particularily in the outer scale, along with iron oxide.

X-ray diffraction: While there are slight differences, each powder scraped from the exterior of the two speciment is remarkably similar and a close match was obtained for iron oxide, Fe_2O_3, both gamma and alpha phases (see Table V). This is a final confirmation of the results of the electrom microscope analysis.

No significant quantities of the sulfur compounds were detected as most of the sulfide scale was formed on the inner surfaces of the scales layers and the total percentage of sulfur scale as compared with oxide scale was small and could have escaped determination.

Conclusions

1. The major corrosion reaction that occurred on the mild steel casing was the formation of the heavy oxide scale. A thin band of sulfide formed at the scale metal interface that probably enhanced the iron oxide reaction which accounted for the greater part of the deterioration of the well casings.
2. The 304SS thermocouple sheath underwent a classic sequential corrosion with chromium carbide forming furthest in from corroding gases, then chromium sulfide and, finally, an outer scale of a porous Fe-Cr-O spinel.
3. Mild steel has no corrosion resistance for service in reactive gases of the type that occurs in in-situ oil shale retorts at service temperatures above 650°C and should not have been used in this application.

DOWN-HOLE BURNER COMPONENTS

Operating Conditions:

Specimens from two failed components used in two separate in-situ Antrim oil shale retorting tests were received for analysis from the Dow Chemical Company in Midland, Michigan. One specimen was a 321 stainless steel tube, part of a molybdenum resistance heating element sheathed in silica. This heating element was used in an in-situ retort where only pyrolysis occurred, no combustion. The 321 sheath achieved temperatures as high as 700°C. The heating element shorted out in the first 21 hours of the test. After retorting was completed, the element was taken out and examined. It had a bend in the 321 pipe with extensive cracking in the bend area.

The other specimen was a portion of a corroded, burned fin from a burner stop in an in-situ Antrim shale combustion test. The burner fin was originally 0.6cm wide and was used in a channel to direct air to the combustion zone. It was exposed to gas temperatures up to 1375°C (2500°F).

Analysis Decription:

Microscopic and x-ray analyses were used, along with thermodynamic predictions from the literature to analyze observed behavior. Color photos of each of the component parts were taken before the parts were sectioned for metallographic examination.

Two specimens were mounted from the cracked area of the 321 stainless steel tube. The specimens were mounted in a special edge-retaining bakelite, fine polished, and etched in a solution of 5ml HF,

15ml HNO3, and 200 ml H20 for three minutes. Optical photomigrographs and SEM photos and EDAX analyses were made.

Three specimens were sectioned from the burned fin part. A chemical analysis showed the fin to be made from 304 stainless steel. The fin specimens were prepared for metallographic examination using the technique previously described. Optical photomicrographs and SEM photos and EDAX analyses were also made.

Results:

Fig. 27 shows the 321SS sheath. Multiple cracks occurred at the bend in the tube. Fig. 28 is a closeup photo of the bent area showing the multiple cracks that occurred. Fig. 29 shows what was left of the burner stop fin.

321SS Sheath on heating element - Two specimens were taken from the cracked surface of the 321SS tube. Cracking patterns in these specimens were analyzed to determine whether the mode of failure was stress-corrosion cracking or high-temperature rupture, or a combination of the two. The etched specimens were first observed on the optical metallograph to see if the crack pattern was intergranular or transgranular. A typical crack tip area is shown in Fig. 30. In the lower photo the cracking is seen to be primarily transgranular and is of a feathery nature. Both of these conditions indicate the probability of stress-corrosion cracking.

An analysis of the root of a major system of cracks was made using the SEM. Photographs of this area are shown in Fig. 31. The inside surface of the crack root area was analyzed at 1000X using EDAX analysis. It can be seen that the crack fracture surface is dimpled,

suggesting ductile fracture at elevated temperature. The EDAX analysis has significant indication of chlorine in the crack root, further suggesting stress-corrosion cracking had occurred.

The metallographic evidence indicates that the sheath cracked due to stress-corrosion cracking, thereby causing the eventual shorting of the heater element by exposing the silica and the molybdenum element to the atmosphere in the retort. This proposed mechanism is supported by the following findings: 1. A network of large cracks occurred perpendicular to the axis of the 321 tube, that branched out into many smaller, feather-like cracks that are transgranular. 2. A sizable amount of chlorine in the crack fracture surface was detected, as shown in the EDAX probe picture in Fig. 31. The 700°C temperature which occurred for approximately 12 hours, the presence of chlorine in the retort atmosphere and an appreciable bending load applied to the tube, probably from a shifting in the shale bed, could combine to initiate stress-corrosion cracking.

304SS Burner Stop Fin - Three specimens were taken from the 304SS burned fin: two cross-sections and one side section at the tip. No cracking was observed in the specimen, although evidence of high-temperature rupture was anticipated. An optical photomicrograph of the cross section of one specimen is shown in Fig.32. Heavy carbide precipitates were observed both between grains and inside them. The same cross-section was analyzed on the SEM.

The area analyzed is shown in Fig. 33. In scanning the surface of the specimen, it was observed that no one type of uniform corrosion surface scale existed over the entire surface. Instead, isolated

pockets of oxide and sulfide spinels were found.

The scale pocket on the left side of Fig. 33 was found by EDAX analysis to contain a large amount of chromium and iron, but no nickel or sulfur. The scale to the right was found by EDAX to contain a large amount of sulfur and some nickel in addition to chromium and iron. These findings are further established by examining the x-ray maps and EDAX probe analyses in Figs. 34 and 35. Fig. 34 shows an enlargement of the left side Fe-Cr scale pocket with a Cr x-ray map and an EDAX analysis of the scale. The most noticeable characteristic of this figure is the lack of sulfur in the EDAX analysis and the large concentration of Cr in the x-ray map. Fig. 35 shows an enlargement of the right side sulfide scale pocket with a sulfur x-ray map and an EDAX analysis of the scale. The x-ray map shows the sulfur concentration to be higher in the scale area of the photograph. This high concentration is also shown in the EDAX analysis in Fig. 35. A large concentration of Cr in this scale is also shown in the EDAX analysis, in addition to the iron and nickel detected. Also noticeable in both Fig. 34 and 35 is the dendritic structure of carbide precipitates throughout the base metal.

The temperature of operation of the fin, 1375°C, is far beyond an acceptable operating limit for an 18-8 type stainless steel, which is about 1000°C with low loads on it. In fact, 1375°C is within 95°C of the alloy's melting temperature. If any sizable load were applied to this part while it was at or near 1375°C, high temperature rupture would occur. The high temperature also explains the absence of any uniform corrosion scale, since very large partial pressures of oxygen

and sulfur would be required for the oxides and/or sulfides that form scales to be stable at 1375°C.

Conclusions:

321 stainless Tube - The feathery appearance of the crack patterns on the surface coupled with the presence of chlorine in the crack fracture surface strongly suggest that stress-corrosion cracking took place. The dimpled fracture surface in the crack root indicates a ductile failure at elevated temperature, indicating that a reasonable large load was applied, possibly due to a shift in the shale bed.

Burner Stop Fin: The extremely high temperature of operation was beyond the normal operational limit of the steel making high-temperature rupture a probability.

IN-SITU RETORT EXPOSURES

Specimens of 14 different commercial alloys used in the chemical process industry were tested in large scale,(>10 ton of shale/run), above ground, simulated, in-situ oil shale retorts. Table 6 lists the alloys tested and their compositions. Several of the alloys, those marked with asterisks, were also tested with an aluminized coating applied by the commercial Alonizing process. Table 7 lists the retorts in which specimens were placed, which materials were exposed, and, to the degree known, the operating conditions of the retort.

Since the inclusion of alloy specimens into the large scale retorts to determine their corrosion behavior was not a priminary objective of any of the retort operations, no control of the test

conditions was possible. By placing the specimens near thermocouples it was possible in all but one case to get time-temperature histories. Some of the retorts were operated at temperatures and times that turned out to not be very corrosive to most or all of the specimens exposed. In most of the retorts, corrosive time-temperature histories only occurred at certain levels in the retort. After the corrosivity of the various levels was established in early 10 ton retort tests at LETC, specimens were only placed at the corrosive levels in subsequent retort exposures.

The specimens were notched in patterns shown in Fig. 36 so that they could be identified after the test, regardless of how severe the corrosion had been. An 18" length of 304SS wire was attached to each specimen so it could be retrieved after the test. The specimens were dumped out of the retort when it had cooled in the midst of a 10 ton pile of spent shale. The shale was combed through to find the specimens. Some specimens were not retrieved after exposure.

Thus, the large scale retort exposures were a bit of a hit and miss operation. Diligence on the part of LETC and LLNL personnel resulted in the major part of the exposed specimens being recovered. Combining the factors of lost specimens, low temperature-time operating cycles for some retorts, and only certain levels in the retorts providing the corrosivity to result in observable corrosion, made it impossible to perform complete analyses on all specimens exposed. However, there was sufficient corrosion on sufficient numbers of specimens to obtain an extensive documentation and understanding of the corrosion of steels in in-situ retorts.

Specimens from certain retorts were analyzed in detail and the behavior of various alloy compositions were related to each other and to the operating conditions in the retort. Each retort exposure will be discussed below. Some of the exposures will be analyzed in detail; others will be described more briefly. Of the several hundred specimens exposed in large, simulated in-situ retorts during the course of the program less than 100 will be described in any detail. It can be assumed that those that are not described either behaved like those that are described, or underwent very little corrosion because of mild conditions, or were lost in the tons of spent shale.

RETORT RUN S49

Test Conditions:

Carbon steel (1018) and stainless steel (304) were exposed to Antrim oil shale at simulated production temperatures in the 10-ton retort, a 10 foot high, 6 foot diameter above-ground, in-situ simulation retort at the North Site of LETC. The shale was ignited by hot methane gas, and the resulting flamefront was moved through the length of the retort with air forced in from the top. The maximum temperature reached at the flamefront was 980°C (1800°F), and the isothermal temperature advance was 1.4 inches/hour. The entire retorting experiment lasted 72 hours, with each inch of the retort seeing an average of 9 hours at 980°C.

The 1018 carbon steel and 304SS alloys were chosen to get a comparison of scaling behavior between low-cost, low carbon and high-

cost, stainless steel. The specimens were located in the 10-ton retort on two different levels approximately 5 and 8 feet from the bottom grate. The specimens were exposed in the as-received conditions. The 304SS specimens measured approximately .252 in. thick by 3 in. long by 1 in. wide, and the 1018 specimens were approximately .222 in. thick by 3 in. by 1 in.

After exposure, the specimens were photographed in the as-exposed condition, sectioned, mounted, and polished for metalllographic examination. Photomicrographs were taken with optical metallographs and the scanning electron microscope (SEM) for scale thickness determination. A qualitative analysis of the elements present in the scales was obtained by x-ray mapping and EDAX unit peak analyses. The EDAX was also used to investigate segregation of the alloying elements in the stainless steel. A more detailed investigation of the compounds present as oxides and sulfides required powdering the surface scales for x-ray diffraction analyses.

Experimental Results:

Examination of the corrosion scales found on the exposed 1018 and 304SS specimens indicated occurrence of heavy sulfidation and oxidation on the 1018 and less attack on the 304SS. Exposure to Antrim shale, a high-sulfur content shale, resulted in thick crystalline pyrites and pieces of shale bonded onto the surface of the 1018. This indicated the probability of formation of molten product (Fig. 37).

SEM and EDAX analyses of the 1018 indicated the scale structure to consist of iron oxide 0.075 mm thick, containing minute flakes of iron

sulfide next to the 1018 (Fig. 38). Above this was a porous sulfide 0.175mm thick followed by the more porous crystalline sulfide, 0.38mm thick. Above the sulfide were iron pyrite crystals up to 1.5mm diameter at the oxide-atmosphere interface. The shale particles were buried in these crystals. No internal corrosion was observed below the scale-metal interface. X-ray diffraction of the sulfide scale showed it to be FeS_2. This scale structure suggests an initial formation of iron oxide with Fe cations diffusing through it to combine with the sulfur at the oxide-scale interface to form the sulfides. The large iron pyrite crystals on the outer scale suggest occurrence of surface melting. Specimen thickness was reduced from an average of 5.6mm to an average of 5mm thick, or a 10% reduction in thickness in 72 hours.

SEM and EDAX examination of the 304SS after exposure to the Antrim shale enviornment revealed some internal sulfidation and less exterior scale formation than occurred on the 1018 (Fig. 39). As can be seen in Fig. 40, the 304SS exhibited widespread chromium diffusion internally to the austenite grain boundaries where chromium carbides formed (light-colored boundaries in Fig. 40). Closer to the scale-metal interface, the chromium carbide had transformed to chromium sulfide (dark boundaries in Fig. 40) 2.5mm from the surface. Areas of Fe-Cr sulfide also formed (area 2 in Fig. 40), and Cr-depleted alloy pockets were observed in the scale itself (area 1 in Fig. 40), along with Fe-Cr and Fe-Ni sulfide spinels. The outer surface of the scale contained amounts of Al, Si, and Ca, in addition to Cr and Fe (Fig. 41). This would be expected considering the relative percentages of Al,Si and Ca in the raw Antrin shale listed in Table 8.

A closer look at the EDAX analysis in Fig. 41 shows larger concentrations of Fe/Cr compounds near the scale-metal interface than in areas farther out (EDAX Nos. 1-4 in Fig. 41.) Note also in EDAX Nos. 1 and 2 the presence of Fe-Cr sulfides in surface intrusions into the base metal. Note also the large concentration of Si in much of the exterior scale (EDAX No. 5). X-ray diffraction of the scale showed it to consist of the compounds CrS, $Fe_{1-x}S$, and Fe_xNi_yS. This suggests the diffusion of Cr and Ni cations outward to the surface along with diffusion of C and S anions inward to form internal carbides and sulfides. There was negligible reduction in thickness after 72 hours exposure.

Discussion:

The thermodynamic equilibrium stability diagram (Fig. 42) for Cr in oxygen and sulfur vapor at the 10-ton retort temperature of 980°C indicates that the chances of internal Cr_xS_y formation would depend on the presure and amounts of H_2S, SO_3, and liquid sulfur produced during the retorting process. From Fig. 42 it can be seen that a P_{S_2} $>10^{-9}$ atm. is required just inside the metal surface if internal Cr_xS_y is to be a stable compound. The presence of internal Cr_xS_y formation in the Antrim shale-exposed 304SS indicates a concentration of S in the Antrim retorting product that was sufficient to increase the P_{S_2} inside the 304SS to $>10^{-9}$ atm., encouraging internal sulfidation.

Using the thermodynamic equilibrium stability diagrams for Fe and Ni at 980°C (Fig. 42), it can be seen that a P_{S_2} $>10^{-7}$ atm. is needed for Ni_xS_y and Fe_xS_y to exist as stable compounds. Since the P_{S_2} for CrS at 980°C is 10^{-9} atm., it would possibly form in 304SS before the other

two sulfides became thermodynamically stable. This agrees with the observation made in Fig. 40 of the internal sulfidation of Antrim shale exposed 304SS at 980°C. The CrS was obviously stable and formed internally, while Fe-Cr and Fe-Ni sulfide spinels began to form in the outer scale.

It should be metioned that the use of thermodynamic equilibrium stability diagrams to predict scale formation in oil-shale retorting materials is limited to determining what can happen, not what will happen. The diagrams are for equilibrium gas-metal reactions under controlled laboratory conditions, whereas the oil shale retorting process involves complex gas-metal and liquid-metal reactions involving several interacting constituents such as sulfur, oxygen, carbon and calcium with iron, chromium, and nickel. The kinetics of the reactions are not considered in these diagrams. Sulfur concentration and temperature are not the only determining factors in scale formation. Scale morphologies, the presence of minor constituents, and the formation of certain compounds can also affect the formation of the principal scale constituents.

RETORT RUN S-54

Test Conditions:

The six stainless steel (SS) alloys exposed in the simulated in-situ retorting test in the LETC 10 ton retort represented three types: (1) Fe-Cr martensitic steel (410); (2) weldable 18-8 austenitic steel (321 - 347); and (3) more corrosion-resistant alloys (316, 309, 310). Table 6 lists the compositions of the alloys exposed. Fig. 43 shows the 10-ton retort at LETC. Fig. 44 shows the specimens after exposure.

Two specimens of each of the six alloys were placed in the retort at each of the four thermocouple levels shown by the sketch in Fig. 45. After exposure specimens were selected for detailed analysis from level 1, where the flame front was initiated and retorting began, and from level 2, where the combustion front generated temperatures above 980°C for more than 24 hours. The specimens from level 3 and 4 were not attacked as much as those at levels 1 and 2 (see Fig. 44). Fig. 46 shows a time-temperature profile for each level.

The specimens were photographed. Those selected for detailed analysis were cross-sectioned and mounted in bakelite, polished, and examined using the scanning electron microscope (SEM) and optical metallography. Qualitative and quantitative analyses of the scales were obtained by using the energy dispersive x-ray analysis unit (EDAX) on the SEM. Powder x-ray diffraction was also used to verify the accuracy of these analyses. Thickness measurements of the base metal after exposure were made of cross sections using a micrometer stage on an optical microscope.

Experimental Results:

All three types of stainless steels examined exhibited similar corrosion attack, consisting of some internal sulfidation, a Fe-Cr-S spinel layer next to the base metal, and an exterior solidified from a melted FeS layer. Because of the longer exposure time at higher temperature (Fig. 46) the level 2 specimens showed heavier scale formation and more pronounced internal attack than did the level 1 specimens. The level 3 and 4 specimens underwent <20 mil/yr corrosion.

Fig 47 - 50 show the surface of specimens of 410, 321, 347, 310SS from level 2. The large deposits of melted iron sulfide and other corrosion products are readily seen. Some shale particles that were embedded in the melted layer are also seen. The black shale particles have carbon deposits from the shale pyrolsis process on them. The other specimen surfaces can be seen in Fig. 44.

The 410SS specimens exposed at the first level exhibited light to moderate attack with only a 1.2% reduction in metal thickness. The outer sulfide scale was .075mm thick. The 410SS specimens on the second level had an 8.3% reduction in metal thickness and a total scale thickness of .56mm, as shown by the sulfur x-ray map in Fig. 51. The $(Fe,Cr)_{1-x}S$ (Inner Scale EDAX peak analysis in Fig. 51) and FeS or FeS_2 layer (Outer Scale EDAX peak analysis) seemed to be approximately the same thickness on the level 2 specimens examined, 0.28mm each.

More severe scaling behavior was observed on the 347SS exposed at levels 1 and 2. The specimen from the first level showed no evidence of an inner sulfide scale but had a 5.8% reduction in metal thickness. The specimen from the second level shown in Fig. 52, showed much more severe scaling, having a 17.8% reduction in cross section and a total scale thickness of 3.3mm. Evidence indicates that the $(Fe, Cr)_{1-x}S$ formed as an inner scale after an initial formation of Cr_2O_3. Fig. 52 shows the scale formation pattern on the 347SS surface. Successive EDAX peak analyses from the base metal through the scale to the outside scale are shown. A SEM closeup of the middle layer area of Fig. 52 is shown in Fig. 53. Concentrations of Cr, Fe, and S are shown by x-ray maps. These maps reveal a high-chromium, sulfur-free

concentration in the middle horizontal layer, and relatively little chromium in the outer layer at the top of the photograph. This suggests that the composition of this middle layer is Cr_2O_3. This layer was approximately 0.02mm thick, compared to the $(Fe,Cr)_{1-x}S$ layer below it at 0.3mm and the $(Fe, Cr)_{1-x}S$ scale above it at 3mm thick.

More pronounced grain-boundary sulfidation was observed in the 310 samples. As in the case of the 410SS and 347SS, the second level specimens showed more material loss and thicker scales than the first level specimens did. The second level specimen is shown in Fig. 54. The 310SS differed from the 410SS and 347SS in scale morphology in that a layer of Cr_2O_3 was found near the surface of the 310SS, with the $(Fe, Cr)_{1-x}S$ and FeS layer above it. The total scale thickness was 0.15mm. Compare this morphology to that of the 347SS in Fig.53. Differences in thermodynamic conditions in the two alloys inslde the gas-scale interface caused differences in scale morphologies. Iron, chromium, and sulfur x-ray maps of a level 2 310SS specimen are shown in Fig. 54. Note the more pronounced Cr next to the metal surface and the light concentration of S in the same region. The Cr concentration decreased in the direction away from the alloy, while the sulfur concentration increased to a maximum at the outermost scale. This suggests the presence of an $(Fe, Cr)_{1-x}$ outerlayer.

Discussion:

Based upon the analyses of these oil shale retort specimens, an attempt was made to estimate the partial pressures of sulfur and oxygen

in the retorting system during operation. This job was difficult for a number of reasons: First, and most important, is the fact that the thermodynamic equilibrium stability diagrams used for this estimation describes partial pressures of S_2 and O_2 at the metal interface in contact with the atmosphere and not at the shale-metal, shale-scale, scale-metal, or scale-atmosphere interface. The P_{O_2} and P_{S_2} values in the following calculations are, at best, estimates of activities at these latter interfaces and not the interface described by the diagram.

Second, the diagrams only describe what reactions can happen at a specific partial pressure and temperature, and do not take into account the scale growth kinetics of various sulfides and oxides formed. For example, a scale that may appear as originally Fe-Cr sulfide may actually have started as Cr_2O_3. FeS forming on the Cr_2O_3 surface could impede any further oxide growth while Cr^{+++} ions diffused from the base metal through the oxide to combine with$S^{=}$ ions and Fe^{++} ions could form the Fe-Cr sulfide spinel.

Third, it is evident from visual observation and x-ray analysis of the surfaces of the specimens exposed in the 10-ton retort that the outermost scale is an FeS crystallized from molten product. The molten iron sulfide could contain more dissolved iron than is predicted by the formula, FeS. This dissolved iron probably came from the shale and not from the alloy. So non-stoichimetry could lead to a composition of the form $Fe_{(1-x)}S$.

Since the following calculations are based on the formulas FeS and FeS_2, it is possible that the P_{S_2} calculated would be different than

the "real" non-stoichiometric P_{S_2} This possibility would present difficulty in obtaining an accurate estimation of P_{S_2} in the system. Finally, the diagram used is for a single temperature, while a variety of temperatures occur at the reaction surfaces.

Keeping these considerations in mind, analyses of the data obtained are discussed below.

Every specimen analyzed showed evidence of solidified FeS on its outer surface. Assuming a reaction of the form

$$Fe(S) + 1/2\ S_2(g) \rightarrow FeS(s) \qquad [1]$$

at 1255°K (1800°F), and $\Delta G_f^\circ = -20$ kcal/mole[9] ,a value $P_{S_2} = 1.07 \times 10^{-7}$ atm was obtained.

However it is probable that the FeS could have originally been molten FeS_2. Assuming a reaction of the form

$$FeS_2(1) \rightarrow FeS(s) + 1/2\ S_2(g) \qquad [2]$$

at 1255°K and $\Delta G_f^\circ = -12.08$ kcal/mole[11], a value of $P_{S_2} = 6.18 \times 10^{-5}$ atm was obtained.

These two reactions suggest a range of P_{S_2} in the retort atmosphere from 10^{-5} to 10^{-7} atm. In addition, the presence of Cr_xS_y in the grain boundaries of these specimens suggests an internal P_{S_2} of approximately 10^{-9} atm (See Fig. 13). Thus it is thermodynamically feasible for the P_{S_2} at the metal-atmosphere interface during retorting at 980°C to range anwhere from 10^{-5} to 10^{-7} atm. and the P_{S_2}

internally to be $>10^{-9}$ atm. This --- gradient from the outer surface to the base metal is indicative of sulfur distribution in scale-metal morphologies of this type.

Every specimen analyzed had an inner layer next to the substrate that consisted of $(Fe, Cr)_{1-x}S$. Assuming a stoichiometric composition in the reaction

$$FeS(s) + 2CrS(s) + 1/2\ S_2(g) \rightarrow FeCr_2S_4 \qquad [3]$$

at 1255°K and $G_f = -21$ kcal/mole[11], a value of --- $= 4 \times 10^{-8}$ atm was obtained. This value is within the range described above.

Evidence of differences in scale growth rates were observed on the 10-ton retort specimens. For example, on the 410SS there was no evidence of expected Cr_2O_3 formation (Fig. 51), while on the 347SS, the specimen exposed in the second retort level showed definite evidence of a Cr_2O_3 layer suspended between the inner $(Fe, Cr)_{1-x}S$ and the outer FeS scales (Fig. 52).

Two possible explanations can be considered as to the absence of Cr_2O_3 on the 410 and the presence of Cr_2O_3 on the 347: (1) Cr_2O_3 formed initially on the 410 surface, but after exposure for >20 hours at 1255°K in molten iron sulfide, the chromia was dissolved in the molten product. Upon cooling, an FeCrS spinel was formed. Simultaneously, the remaining molten sulfide in the shale retorting atmosphere solidified into FeS with some Cr in it, forming the outer sulfide layer; (2) The Cr_2O_3 formed initially on the 347 but because of the relatively low --- ($<10^{-22}$ atm) and the high --- (10^{-5} to 10^{-7} atm), growth of the oxide was retarded while FeS solidified on the chromia surface. Diffusion of Fe^{++} and $S^{=}$ ions inward from the sulfide

encouraged formation of the inner FeCrS spinel on the 347SS.

The 310SS specimens also had $(Fe, Cr)_{1-x}S$ inner layers and FeS outer layers, but the innermost scale next to the substrate was found to be Cr_2O_3 (see Fig. 54) This scale morphology was different from that observed on the 347SS sample analyzed. Differences in the formation of the Cr_2O_3, FeS, and FeCrS scales between 347 and 310SS could be due to differences in local specimen temperature, or chromium content, or both. For example, it is possible that the 310SS level 2 specimen was in a section of level 2 that had a different temperature profile than the section where the 347SS was placed (see Fig. 55). Note from the x-ray maps that the Cr concentration decreases with distance away from the alloy while the S concentration increases. This is in agreement with results found in laboratory experiments.

RETORT RUN S-57

None of the specimens exposed in simulated in-situ retort run S-57 in the 10-ton LETC retort were recovered after the run and, thus, were not available for analysis.

RETORT RUN S-59

Test Conditions:

Specimens of bare and aluminized steels of 10 compositions were exposed in this 10-ton retort run using low sulfur, Green River shale. The highest temperature achieved at the level where the specimens were placed,level 2, was only 825°C (1500°F). With a total operating duration of only 68 hours, the time that the specimens saw even the

825°C was of the order of 30 hours. Therefore the amount of corrosion observed on the specimens was light and the retort turned out to not be a sufficiently severe test of the aluminized coatings to determine their enhancement of the stainless steels. On the other hand, the diffusion rate of aluminum in the 1018 steel was low and the enhancement of the service temperature limit of the 1018 steel could be studied.

Experimental Results:

The corrosion resistance of some of the samples was enhanced by the addition of an aluminide coating applied from a pack by the Alon process. Depending on the substrate composition, the coatings tested consisted of iron, nickel or chromium aluminides. Particles of aluminum oxide from the aluminizing pack material were entrapped in the coating by the outward growing aluminide and distributed randomly in the surface layer.

The 1018 aluminized specimen is shown in cross section in Fig. 56. The alumina particles embedded in the surface are effective markers of the surface of the as-coated specimen. It can be seen that no corrosion products formed on the surface other than a very thin Al_2O_3 barrier scale. The embedded particles are Al_2O_3 as can be seen in peak analysis 1. Peak analyses 2 and 3 show a small indication of sulfur penetration. However, the protection provided by the aluminide layer can be seen by comparing Fig. 56 with Fig. 38 of the attack on unprotected 1018 steel from retort S-49. The difference in type of shale and exposure temperatures between the 1018 steel exposure in

retort S-49 and S-59 must be kept in mind when making the comparison, see Table 7.

The 310SS aluminized specimens, Fig. 57, had a chrome-nickel-iron aluminide with some Al_2O_3 particles from the aluminizing pack distributed within and at the surface of the coating, see Al x-ray map. There is no clear coating, metal interface as is seen in Fig. 56 indicating that the aluminum diffused deeply into the metal. No sulfidation of the sample was observed.

Optical polarized micrographs of 316 and 347 stainless steel specimens (Figs. 58 and 59 respectively) both show a distinct metal-coating interface indicating that the nature of the aluminide coatings on these stainless steels are somewhat different from those formed on the 310SS. No evidence of sulfidation was seen on either of these steels. The 347SS sample, Fig. 60, shows a layered aluminide with a top layer of chromium and iron aluminides and a lower layer of nickel aluminide as determined by SEM x-ray analysis.

Discussion:

Particles of Al_2O_3 have been embedded in the surface layers of all of the aluminized steels. The appearance of surface scalloping and voids in Fig. 59 are the locations of Al_2O_3 pack particles that were removed in the specimen polishing operations. Higher quality aluminide coatings with little or no entrapped alumina particles should be utilized in actual applications. The presence of the Al_2O_3 particles could compromise the performance of the coatings in more severe operating environments.

This retort exposure shows the value of aluminizing mild steel to protect it against combined oxidation-sulfidation in in-situ oil shale retort environments. While the exposure in retort S-59 was for a short duration, the potential of using aluminized 1018 steel was shown. The low diffusion rates of aluminum in carbon steel should permit 1018 to be used in the protected condition for the single, limited life cycle in oil shale retorts into the 850°C service temperature range.

While the service temperature was too low in retort S-59 to evaluate the use of aluminizing to protect 300 series stainless steels, it appeared that the aluminizing process did result in a compatible coating on stainless steels having different levels of chromium content. Whether aluminizing could extend the service temperature of stainless steels for the required single cycle life is problematical. However the extensive diffusion of the aluminum into the steel during the coating operation makes its retention at the surface of the steel in service for the required life cycle somewhat questionable if the service temperature was above the approximate 1000°C that the bare metal could serve at.

RETORT RUN S-60

Test Conditions:

A broad range of bare alloys was tested in the 10-ton retort which operated for 64 hours on Green River shale, reaching a maximum temperature of 925°C (1700°F) at the level that the specimens were placed, see Table 7.

Experimental Results:

The 1018 steel specimens exhibited the heaviest corrosion attack in this retort, forming a two layer scale with the morphology of both scales being quite crystalline in nature. Figs. 61 and 62 show SEM micrographs of the scales. X-ray maps and EDAX spectra in Fig. 62 show that the outer scale consists of mixed iron sulfides and iron oxides (see EDAX 2) while the inner scale has heavy concentrations of iron sulfide in it. EDAX 4 shows that below the inner scale-metal interface essentially no sulfur has penetrated. The absence of internal sulfidation is representative of how the mild steel behaved in oil shale retorts. The stainless steels, while undergoing considerably less corrosion did have some internal attack in several instances.

The 316SS shown in Fig. 63 was representative of the austenitic stainless steel tested. It had a thin scale consisting of mixed oxides and sulfides similar to those observed in Fig. 9. The composition variation of the scale was determined by EDAX peak analyses shown in Fig. 64. Peak analyses 1 and 2 indicate areas that contained an iron-chromium sulfide spinel. Peak analysis 3 representas an area of iron sulfide containing some nickel. Peak analysis 4 shows that this area contained an iron oxide with Cr in it and no nickel present. There was some evidence of internal sulfur penetration, see peak analysis 5. The x-ray maps in Fig. 63 show areas in the scale where chromium was present and sulfur was absent indicating Cr_2O_3 formation. Note that the sulfur x-ray map is upside down.

The 410SS specimen underwent very little corrosion as can be seen in Fig. 65. Peak analysis 1 shows that no internal sulfidation

occurred. The localized scale area shown consisted of chromium and iron oxides, peak analysis 2, with some isolated occurence of iron-chromium sulfide spinel, peak analysis 3.

Discussion:

Retort S-60 caused scales to occur on the 1018 and stainless steels tested that were representative of the type of scales formed at the higher exposure temperatures. Since this retort only achieved a temperature of 875°C (1600°F) in the area where the specimens were located, the scales were quite thin, especially for the stainless steels. The mix of oxides, sulfides and sulfide spinels in the scales have been seen on specimens from several retorts that reached temperatures near 900°C or above . The fact that the 1018 steel did not develop a thicker scale was somewhat unusual. The partial pressures of oxygen and sulfur that were discussed in retort S-49 appeared to be present in retort S-60 as the scale products were similar even though the temperature was lower.

RETORT L2

Test Conditions:

A series of nine alloys, bare and aluminized, were exposed in a different retort at the Lawrence Livermore National Laboratory. The test conditions were different from those in the LETC 10 ton retort. Green River shale was used and a maximum temperature spike of 900°C (1650°C) was reached for a 5 hour duration in a total retort operational time of 90 hours, see Table 7.

Experimental Results:

The 1018 steel surface region is shown in Fig. 66. The structure is very different from the structures observed in the LETC 10 ton retort for the 1018 steel specimens. The reasons for the difference are not known. The secondary electron images show the multi-layer region at low and higher magnifications. The outermost layer, as shown in peak analysis 1 is high in iron and contains some sulfur. In the micrograph it does not appear to be an iron oxide scale, but appears to be like the base metal, which is shown at the bottom of the micrograph. Some distance from the outer surface is a region of embedded high sulfur containing particles that have very little iron in them as evidenced by peak analysis 2 and the iron map. Their specific composition was not determined. Beneath this layer appears to be another iron region that contains some sulfur and is similar in appearance to the base metal. Finally, a line of mixed sulfides and iron oxide formed, Fig. 67. The sulfur map indicates that only a portion of the structure contains sulfur. It is assumed that the remaining portion of the structure in this region is iron oxide rather than iron. Determination of how and why such a complex, layered structure had formed was not possible. It is unlike any of the previously exposed 1018 specimens.

Fig 68 shows optical micrographs of bare and aluminized 316SS specimens after exposure in the retort. These are typical morphologies for all of the 300 series stainless steels tested. The uncoated specimen on the left of Fig. 68 shows a thin, protective Cr_2O_3 scale.

The aluminized coating shown in the right-hand figure was not affected by the retort environment.

Fig. 69 shows the scale formed on a bare 410 stainless steel specimen. It consists primarily of iron-chromium sulfide and indicates that a significant amount of corrosion had occurred. The 12% Cr in this alloy did not form a protective barrier scale and instead probably acted as a form of catalyst to promote the formation of the scale as the layer was quite thick.

The low chromium content alloys exposed in the retort were inadvertently not analyzed.

Discussion:

The behavior of the alloys in the L-2 retort exposure was generally different from that observed on the same steels in the LETC 10 ton retort exposures. This was particularily true for the 1018 steel and, to a lesser degree, for the 410SS. Since there was no control over the type of exposure the specimens had in the retort and little documentation of the local test conditions, an analysis of the differences is not possible. All that can be said is that the variation in the corrosion conditions in in-situ oil shale retorts can result in a variety of types and extents of high temperature corrosion.

RETORT L-3

Test Conditions:

A series of 11 alloys was tested in the large retort at the Lawrence Livermore National Laboratory. Green River shale was used. In one section of the retort low oil content shale (lean shale) was

retorted and in the other section high oil content shale (rich shale) was retorted. Specimens were placed in both sections. Only some of the specimens were recovered from the spent shale pile after the test. A high temperature spike of 1150°C was reached for a few hours in the retort in an operation which ran for a total of 130 hours for both sections. The rich shale section operated at a somewhat higher temperature than the lean shale section, but the specific temperature difference was not reported to LBL. It is, therefore, not know whether the 1150°C temperature spike was in the lean or rich shale section.

Experimental Results:

Fig. 70 shows the overall appearance of the 1018 steel exposed in the rich and lean shale sections of the retort. There was a major difference in the amount of corrosion that occurred on each specimen. Fig. 71 shows cross sections of the two specimens. Whether the difference in the amount of corrosion was due to the temperature difference in the two sections of the retort or to the difference in the corrosion environment in the rich and lean shale section is not known. The temperature difference was relatively small and both temperatures were far above the rapid corrosion temperature of the 1018 steel. Therefore, it is speculated that the corrosion environment was primarily the cause of the difference in the attack due to the chemical differences of the two shales.

Both scales had the same type of morphology and composition distribution, but to different degrees. Fig. 72 shows the scale on the 1018 from the rich shale exposure. The scale is primarily iron oxide, probably Fe_2O_3, with large and small voids. A thin layer of iron

sulfide occurs at the scale-shale interface and intermittently in the scale just above the scale-metal interface. No internal sulfidation was observed on the sulfur x-ray map.

Fig. 73 shows the lean shale scale SEM micrpgraph. There are a few large voids in the iron oxide scale, no sulfide at the scale-shale interface and a heavier band of iron sulfide immediately adjacent to the scale-metal interface, but still in the scale. The scale layer is also much thinner than was formed on the 1018 exposed to the rich shale, see Fig. 71. These differences indicate that the corrosion environment is somewhat different in the rich and lean shales.

The cross section of the 2 1/4Cr1Mo steel specimen is shown in Fig. 74. The secondary electron image shows a scale with two layers, separated by a zone of porous scale. The scale consists of an outer layer of iron oxide and an inner layer of iron sulfide with some $FeCrO_4$ spinel near the scale-metal interface. The heavy sulfide formation is unlike that which occurred in the other ferritic alloys, the no-chromium content 1018 and the 12% chromium 410SS, tested in this retort. The scale on the 2 1/4Cr1Mo steel in the rich shale was thinner at$\sim$250μm than the heavy scale on the 1018 steel in the rich shale, 570μm. It was also thinner than the scale on the 410SS in the rich shale which was $\sim$300μm.

The 410SS specimens exposed in retort L-3 also corroded extensively in spite of their 12% Cr content. Fig 75 shows cross sections of the scale formed on the specimens exposed in the rich and lean shales. The difference in the amount of attack is significant. The layered appearance of the scale formed in the rich shale section is

representative of the manner in which heavy scales formed on several alloys exposed to oil shale retort environments.

Fig. 76 shows a micrograph of the rich scale cross section. Two EDAX peak analyses and the Fe, Cr, S x-ray maps show the distribution of those elements. The Cr appears to be distributed generally throughout the scale as small enclaves of iron chromium sulfide, see EDAX peak analysis 1. A heavier layer of iron sulfide occurs at the top of the scale layer and at the scale-metal interface. Nowhere is there any evidence of Cr_2O_3.

Fig. 77 shows the thin, non-porous scale that formed on the 410SS placed in the lean shale section of retort L-3. The body of the scale, peak analysis 1, consists of iron-chromium sulfide and iron oxide. The composition and morphology of this scale is quite different from that observed on the 410SS from the rich shale section.

Fig. 78 shows the 310SS specimens exposed in the rich and lean sections of retort L-3. Essentially no corrosion occurred on either specimen, which was typical of all of the high chromium stainless steels and iron base alloys exposed in retort L-3.

Discussion:

It was not expected that their would be such a marked difference in the corrosion potential of two Green River shales as occurred in retort L-3. The difference in the retorting temperatures of the two sections of the retort was not the cause of the large difference in the scales formed on the 1018 and 410SS specimens as both temperatures were above the free scale formation temperatures of the alloys. Rather it

was compostition differences in the shales that caused the difference. A detailed chemical analysis of the shales was not available.

The difference in the nature and thickness of the scale on the 2 1/4 Cr-1Mo steel compared to the other ferritic steels tested in the retort appears to be a function of the chromium content of the alloy. Below the chromium content required to develop an effective barrier layer of Cr_2O_3, the amount of chromium present can actually enhance the formation of sulfide scale and, subsequently, iron oxide scale. The reason for this occurrance can be obtained from studying the stability diagram for Fe-Cr-S-O system.

It can only be concluded that alloy selection for use in retort components is a strong function of relatively small differences in the shale when selecting alloys with no or low chromium content. Alloys with chromium contents above 18% appear to be able to resist the corrosion potential of both types of shale, even when the temperature spike was as high as the 1150 C measured in this retort.

RETORTS CS 78, 79

Test Conditions:

Specimens were exposed in two controlled state retort (CSR) runs at LETC.This retort is a 13' long 3"ID steel tube with a 1" OD steel tube placed concentrically within the 3" ID tube. Shale is placed in the 1" annulus between the tubes. External heating is provided by a contigous series of 24 pairs of 6" long electrical heaters that are designed to retort the shale without the heat coming from combustion of pyrolized shale as occurs in in-situ retorts. In this manner, the

actual pyrolysis reaction could be studied in a cleaner manner. The electric furnaces surrounding segments of the 12 ft high tube were set to heat the shale to temperatures of 582°C (1080°F) to 780°C(1460°F).

In run CS78, 1018 carbon steel and 304SS were exposed to an Antrim shale retorting environment in a run which lasted 269 hours. Fig. 79 shows these specimens after exposure. Temperatures along the length of the CSR were 582°C (1080°F), 684°C (1265°F), 690°C (1275°F), and 696°C (1285°F). One specimen of each type was placed at each of these four temperature levels. The 1018 and 304SS specimens from the 684 C level were chosen for detailed analysis. In run CS79, low alloy steels of compositions 2 1/4Cr -1Mo, and 1 1/4Cr-1/2M were tested along with specimens of Incoloy 800 and 825 in a run which lasted 179 hours. The maximum temperature reached during retorting was 800°C (1472°F).

Experimental Results:

In run CS78, 304SS and 1018 carbon steel specimens were subjected to an Antrim shale retorting environment. The 304SS (Fig. 80) exhibited some internal attack (.001 in.) in the form of $(Fe,Cr)_{1-x}S$. The Cr concentration was highest in the corrosion layer next to the base metal, as shown by the EDAX peak analyses of Fig. 80. The alloy had a 1.5% reduction in metal thickness, and an external scale thickness of 0.05mm. The 1018 carbon steel was tested primarily to get an idea of the relative activities of oxygen at the scale-atmosphere interface by analyzing the types of iron oxides formed. No internal attack was observed on the 1018. A layer of iron oxide formed next to the base metal with a layer of FeS above it. Total reduction in metal thickness was 1.75%. Total scale thickness was 0.025mm. Visual

observations and x-ray diffraction analysis showed the oxide to be Fe_3O_4 with some sulfur in it.

In CS79 two Cr-Mo low alloy steels and Incoloy 800 and 825 samples were exposed to an Antrim shale retorting environment at a maximum temperature of 780°C (1460°F). All alloys exhibited moderate attack with <2% reduction in metal thickness. The Cr-Mo alloys showed little evidence of sulfidation as shown in the EDAX analyses in Fig. 81 for the 2 1/4Cr-1Mo alloy. The secondary electron image in the lower right corner of Fig. 81 is a blow-up of the center of the photo in the upper left of the same figure. The scale has separated from the base metal during mounting in bakelite, but it exhibits an interesting morphology. The total scale thickness was 0.2mm inches. EDAX peak analyses indicate very little S present in the inner 0.1mm. of the scale, and no S present in the outer portion. Note that the bottom of the inner scale has a rougher, more porous appearance than the remainder above it. This could indicate a different oxide structure or crystal orientation due to the fact that this portion was previously attached to the substrate. This inner scale appears to be an iron oxide with some Cr and S in it. The outer scale, also 0.1mm thick, appears to be a Cr and S free Fe_3O_4 layer, as determined by x-ray diffraction analysis.

A noticeable lack of S in the scale was also indicated in the analysis of 1 1/4Cr-1/2Mo steel in Fig. 82. The EDAX analyses show a small amount of Cr and S in the scale next to the substrate and even less of these two elements farther away. X-ray maps for Fe and Cr are also shown in Fig. 82. Note no heavy Cr concentration anywhere in the

scale; rather the Cr seems to be evenly distributed, indicating that the Fe_3O_4 has some Cr in it.

The Incoloy 800 and 825 exhibited similar scaling characteristics to each other. The retorting temperature of 780°C (1460°F) and the high Ni content of these alloys (30 - 40%) resulted in an $(Fe,Ni)_{1-x}S$ phase in addition to $(Fe,Cr)_{1-x}S$. Fig. 83 shows an SEM photo of Incoloy 800. The alloy had a mixed Fe-Cr-S and Fe-Ni-S scale morphology, with most of the sulfide concentrated in the outer edge of the scale. This is shown by the x-ray map for sulfur.

Discussion:

Although the specimens in this run CS78, were exposed to the same type of shale as those in the 10 ton retort run S-54, two important differences existed: (1) The peak temperature of exposure was markedly lower (675°C and 780°C compared to 900° - 1100°C in simulated in-situ retort tests) and (2) based on the dominating presence of Fe and Fe-Cr oxides, the P_{O_2} at the metal surfaces during retorting was higher than in the in-situ retort tests. This second difference was illustrated by the scales formed on the 1018 carbon steel specimens run in the CSR. X-ray analysis showed that the surface scale consisted of alternate layers of Fe_3O_4 and FeS, thus indicating P_{O_2} of $>10^{-20}$ atm at 675°C and P_{S_2} of $<10^{-10}$ atm at the same temperature based on equilibrium stability phase diagrams.

The 304SS specimen showed a scale morphology similar to that of the stainless steels in the S-54 retort run. The surface scale consisted of $(Fe,Cr)_{1-x}S$ next to the base metal and a layer of FeS with

some Cr in it at the scale-shale interface. Assuming a reaction described by Equation [3] on page 36 at 675°C, value of P_{S_2} $=10^{-12}$ atm was calculated for the reaction. A very light amount of internal CrS attack was detected by EDAX analysis, and the CrS_2 did have some Fe in it (Fig. 80). No definite Cr_2O_3 layer was found. This suggests the following hypothesis:

1. the Cr_2O_3 layer initially formed could have been transformed into the $(Fe, Cr)_{1-x}S$; or
2. the formation of Fe_3O_4 on the outermost surface competed with the Cr_2O_3 for oxygen ions and starved the chromia, allowing $(Fe,Cr)_{1-x}S$ to grow underneath.

The alloy steels tested in run CS79 consisted of 1 1/4Cr-1/2Mo, and 2 1/4Cr-1Mo. The Cr-Mo steels showed only moderate reduction in metal thickness (<1%), and their scales had very little S in them. The scales consisted of Fe-Cr oxides near the metal surface topped with Fe_3O_4 (Figs. 81 and 82). Fe_3O_4 formation at the operating temperature of 780°C requires a P_{O_2} of approximately 10^{-17} atm or greater. A thermodynamic equilibrium stability diagram indicates that the absence of any sulfide scale is an indication of a P_{S_2} $<10^{-15}$ atm during the retorting operation.

The Incoloy, iron-nickel-chromium alloys exposed in the same run did show noticeable sulfide scale formation (Fig. 83), and a small amount of internal sulfide attack. Note in the x-ray concentration maps in Fig. 83 tht Ni is concentrated in the alloy just below the metal-scale interface, whereas the Cr is concentrated more in the outer scale. There is some Cr in the internally sulfidized region also.

This sulfide presence suggests a P_{S_2} $>10^{-15}$ atm which is not in agreement with the P_{S_2} speculated for the Cr-Mo steels above.

Two possible explanations for this discrepancy are:

1. The relatively small amount of Cr diffusing to the surfaces of the Cr-Mo steels was transformed into Cr_2O_3 and then $FeCr_2O_4$ before the sulfide had a chance to form, whereas the much higher concentrations of Ni and Cr in the Incoloys encouraged initial formation of sulfides.
2. Note especially in Fig. 81 that the surface scale had separated from the 2 1/4Cr-1Mo alloy. This occurred during cross sectioning. It is possible that any noticeable sulfide scale may have been mechanically removed during cross sectioning. Note from the EDAX peak in Fig. 81 that some S does exist in the lower portion of the scale, but not at the top surface. So, a sulfide was, perhaps, once present on the surface.

GEOKINETICS HORIZONTAL IN-SITU RETORT

A test exposure of 6 specimens each of 11 of the alloys listed in table 6 (1 1/4Cr-1/2mo steel, 309SS, and Incoloy 825 were not tested) was made in an actual in-situ retort at the Geokinetics Corporation facility south of Vernal Utah. Three specimens of each alloy to be tested, 1.27cm square by varying thicknesses, were interspersed between alumina washers along two 304 stainless steel rods 27 inches long; one is shown in Fig.84. The two rods were attached to long mild steel rods

that extended to the surface. The top of one specimen holder rod was 31.5 ft. below the ground surface and the other rod was 39.5 ft. below the surface. The assemblies were placed in 1" dis. thermowell mild steel pipes and attached above the ground level to a handle as shown in Fig. 85.

The test exposure conditions were not controlled during the retort operating duration of four months. Unfortunately, the corrosion conditions were so severe that neither rod was recovered after the retort run. Exactly what happened and where along the length of the assembly it occurred could not be determined. Only short pieces of the rod holding the specimen holder rod could be recovered after the test. Distortion of the rod or catastrophic oxidation of it or both could have been the cause of the failure to recover the specimen holder. No further effort was made to expose specimens in a Geokinetics in-situ retort.

LBL LABORATORY CRUCIBLE TESTS

A series of oil shale exposure tests were carried out in a small laboratory crucible at LBL. The small mullite crucible held 15 gm of shale into which individual, small specimens of alloys were immersed wholly or partially. The crucible was heated in a furnace with an argon gas cover over the ground shale. Higher, more controlled temperatures could be achieved in the crucible tests than were reached in the larger scale simulated in-situ retorts at LETC and LLNL. The higher test temperatures used represented those which normally occur in actual below ground retorts where the shale surrounding the retort insulates it to a greater degree than occurs in the above ground

simulated in-situ retorts used for all of the other corrosion tests in this program. The more controlled temperatures were required to be able to establish the basis for the occurrence of observed corrosion products on the specimens.

A series of tests was performed on 304 stainless steel at 1000°C to determine whether periodic replenishment of the crucible with 15 grams of fresh shale during 48 hour exposures would better maintain the corrosivity of the small amount of shale in the crucible. Runs were completed replacing the shale twice (after each 16 hrs.) once (after 24 hrs) and leaving the initial shale for 48 total hours. Results showed the maximum attack occurred when the initial shale was left in the crucible for 48 hours because this time period allowed more extensive interaction between the samples and the reactive gases from the shale to occur. The 16 and 24 hour replacement periods allowed the reactive gases to clear the crucible when the shale was replaced, reducing the corrosivity.

Fig. 86 shows 304SS after a 48 hour non-replenished shale run. There is an outer scale of primarily chromium sulfide with a thin chromium oxide layer between the outer scale and the substrate metal. There are also areas of internal sulfidation primarily along grain boundaries resulting from the inability of the chromium oxide layer to act as a diffusion barrier to sulfur. This breakdown of the Cr_2O_3 protective scale duplicates the behavior of austenitic stainless steels in in-situ retort exposures at LETC. The ability of the laboratory crucible to simulate the corrosion conditions that occur in large scale retorts was demonstrated.

The effect of chromium content in steel alloys exposed to oil shale retorting conditions were determined using the small laboratory crucible at a test temperature of 1000°C for 48 hour exposures. 15gm of fresh, finely ground Anvil points, Green River shale with a 1.7% sulfur content was used in each test of a 1.3cm x 1cm x 0.3cm size specimen. The steels that were tested were 1018 mild steel, 2 1/4Cr-1Mo steel, 5Cr-1/2Mo steel, 9Cr-1Mo steel, and 304 and 310 austenitic stainless steels.

Fig. 87 shows a cross section of the mild steel with x-ray maps for iron and sulfur. The structure above the solid region of iron is iron oxide scale. The sulfur present is in small MnS inclusions that are normally present in the as-rolled steel. No sulfide formation was observed either externally or internally in this steel which contains no chromium. Of the six steels tested in this series, the 1018 underwent the greatest amount of corrosion.

Fig. 88 shows the corrosion product that formed on the 2 1/4Cr-1Mo steel. An entirely different corrosion process from that on the 1018 steel took place on this steel. The heavy, outer scale was primarily iron sulfide with a small amount of chromium in it. Internal sulfidation also occurred, forming primarily iron sulfide with some possible chromium sulfide. Some MnS inclusions in the as-rolled steel can also be seen. There is possibly some chromium oxide at the scale-metal interface, but it could also be chromium sulfide. The presence of the small amount of chromium, not enough to form a protective oxide layer, appeared to catalyze the formation of sulfides,primarily iron sulfide. The amount of scale which formed, however, was less than that

which formed on the 1018 steel.

Fig. 89 is a cross section of the 5Cr-1/2Mo steel exposed in the same oil shale environment as the previous two specimens. Yet another pattern of corrosion products occurred at this level of chromium. A thin, external, interrupted layer of iron oxide formed with no sulfur in it. Along the scale metal interface line a partial layer of chromium oxide appears as darker gray in the secondary electron image, upper left photo in Fig.89. Some chromium oxide extends upward into the thin iron oxide layer. Starting beneath the chromium oxide layer are regions of internal sulfidation. No sulfide formation occurred from the bottom of the interrupted chromium oxide band upward to the external surface. It can be seen by comparing Fig. 88 and 89 that much less corosion occurred on the 5 Cr containing steel compared to the steel containing 2 1/4 Cr.

The next steel in the test series was the 9Cr-1Mo steel; it is shown in Fig. 90. In this steel, essentially no free scale formed during the 48 hour exposure. Even at only 9%Cr, a continuous appearing Cr_2O_3 scale formed on the surface with no evidence of any iron corrosion products above it. A rather extensive network of internal Cr_2O_3 formed, which is known to occur at intermediate chromium contents in austenitic stainless steels. The Cr_2O_3 forms in a semi-chromium depleted zone beneath a surface Cr_2O_3 barrier scale. In the case of the 9Cr content steel, the zone of ideal Cr content to form internal Cr_2O_3 was quite large. There was essentially no sulfide formation in the specimen, either externally or internally.

The cross section of the scale formed on the 304SS was the same as that described earlier. However, a less corrosive shale used in this test series resulted in markedly less corrosion in the 304SS specimen than is shown in Fig. 86. The 310SS formed a scale shown in Fig. 91. A substantial surface barrier scale of Cr_2O_3 had formed, but some sulfur was present in the scale. There was considerable internal oxidation of the 310SS, but no apparent penetration of sulfur as had occurred in the 304SS, Fig. 86.

Discussion:

In the six alloys tested under the same oil shale exposure conditions in the crucible tests, a different corrosion behavior occurred for each alloy. The occurrence of the various oxides and sulfides that formed on each alloy can be explained reasonably well using the appropriate thermodynamic equilibrium stability diagrams. The occurrence of corrosion products in one form or another is primarily due to shifts in the compound formation lines on the stability diagram because of partial depletion of the reacting elements as they form corrosion products. The formation of iron sulfide scale on the 2 1/4Cr-1Mo steel rather than the iron oxide scale that formed on the 0%Cr, 1018 steel may be due to some subtle effect of the relatively small amount of either Cr or Mo present in the 2 1/4Cr 1Mo alloy promoting sulfide formation by some catalytic type mechanism.

The crucible tests at 1000°C showed a variation in scale formation for each alloy tested. The test results were similar to those observed in many specimens in the large,simulated in-situ retort tests. However, the presence of a layer of finely powdered shale in

comparatively intimate and constant contact with the specimen surfaces resulted in a more uniform layered corrosion product formation than was observed in the in-situ retort exposures. The variety of corrosion products on a single specimen that occurred in the large retort exposures was also markedly reduced. These differences strengthen the thought that very different corrosion environments existed locally in actual retorts where the contact between the shale and the metal specimens varied considerably.

ABOVE GROUND RETORT EXPOSURES

The CS78 and 79 retort tests described above can be considered as being carried out near or at above-ground retorting conditions as the temperatures reached are in the range of the higher pyrolysis temperatures used in above-ground retorts. Additional tests were carried out to investigate the behavior of alloys exposed to shale at above ground retorting conditions. A 3in. dia., 2ft. long stainless steel retort, externally heated by a furnace, was used for one series of tests at LBL. A series of specimens was also exposed in a full scale experimental retort in Colorado.

LBL 3in. Diameter Retort:

Fig. 92 is a photograph of the LBL retort unit with the furnace open, showing the alumina tube into which a sealed stainless steel retort, 3in. dia x 2 ft long is placed. The setup shown was developed for other types of oil shale retort studies and was lent to this project to run the alloy exposure tests.

The following alloys were tested in 1.27cm square by 0.6cm thick size specimens:

1018 steel	410SS	1018 alonized
2 1/4Cr-1Mo	304SS	304SS alonized
5Cr-1/2Mo	321SS	
9Cr-1Mo	310SS	

The bare alloy specimens' surfaces were ground to 240 grit and placed in the retort in layers. Four samples of each alloy were placed in each layer with several inches of shale placed between each layer. All of the samples were placed in the center portion of the retort as sharp thermal gradients occurred at the ends. After the retort was loaded, its top, open-end was welded closed. The retort was placed inside of the alumina tube and the clam shell furnace closed around it. Thermocouples were placed along the outside surface of the retort.

Temperatures between 550°C and 560°C (1025°F) were maintained from 4" from either end of the retort for the 48 hour test duration. After the exposure the furnace was turned off and the retort allowed to cool for several hours before the welded top was cut off and the specimens retrieved.

The type and extent of the corrosion which occurred on the specimens was expected. At the test temperature of only 550°C, essentially no corrosion occurred on the steels which contained 5% or more chromium and on the two aluminized steels. Only the 1018 steel had any observable corrosion product on it and it measured <20 mils/year. It appeared similar to the scale shown on the 1018 steel in Fig. 79. The 2 1/4Cr-1/2Mo steel had <10mils/year corrosion rate.

Large Scale Above-ground Retort:

Low alloy and stainless steels of various chromium contents were exposed to the oxidizing, sulfidizing environment of a large scale, experimental, above-ground retorting facility. Tests were run in various regions of the retort ranging in temperature from 100°- 600°C for a period of approximately 500 hours. 1018 carbon steel was the only material to corrode significantly in the low temperatures of the above-ground retort, at a rate of 56 mils/yr. Moreover, the regions of the retort where attack was heaviest were those regions in which the retorting components are typically refractory lined. 304 and 310 stainless steels exhibited essentially no thickness loss and little noticeable corrosion. It is significant to compare the relatively long duration of the low operation temperature, above ground retort tests (500 hrs) to the high operation temperature, laboratory crucible and 10-ton simulated in-situ retort tests (48 -80 hrs). There is very little attack on metal surfaces at the lower temperatures utilized in the above-ground retorts even though the sulfur content of the shale is the same.

Corrosion in Shale Oil:

A limited number of tests were performed to determine the potential of raw, retorted shale oil to corrode the piping steels used to carry them away from the retort. 5 steels were partially and totally immersed in a stirred 2 liter container of shale oil retorted from Green River shale. The alloys were: 1018 carbon steel, 2 1/4Cr-1Mo, 5Cr-1/2Mo, 9Cr-1Mo, and 304 stainless steel. The samples were approximately 1" square by 0.125" thick. They were exposed for 100

hours at 200°C, a representative but high side temperature of shale oil in piping at a retort site.

None of the alloys had any measureable amount of corrosion at the end of the 100 hr exposure and the tests were stopped at that time. The 5CR-1/2Mo steel did develop a black smudge on its surface that could be removed by a light rub with tissue. All of the other alloys remained in their light, as-ground surface condition. It was concluded that none of the steels tested would corrode at anywhere near a 20mils/yr rate at any temperature that they might see in a shale oil piping system

GENERAL CONCLUSIONS

1. At temperatures above 1000°C in in-situ and modified in-situ (MIS) type oil shale retorts, Antrim and Green River oil shales can cause catastrophic failure of all possible candidate iron base alloys.
2. The operation temperatures of above-ground oil shale retorts, 550°C, are below those that cause corrosion of iron-base alloys at rates exceeding 20 mpy.
3. There are significant differences in the corrosivity of Antrim and Green River oil shales and shales of various Fisher Assay oil content in in-situ type retorting environments. In general, high sulfur Antrim shale is more corrosive than lower sulfur Green River shale and high oil content Green River shale is more corrosive than lower oil content Green River shale.

4. Thermodynamic equilibrium stability diagrams can be used to estimate the partial pressures of sulfur and oxygen in in-situ oil shale retorting environments by relating the corrosion scale products formed to the appropriate regions on the diagrams for the measured temperatures of operation.

5. Alumina is a more effective corrosion barrier than chromia in in-situ oil shale retorting environments. The use of aluminized coatings on steels can markedly increase their ability to withstand the corrosive environments of in-situ retorts.

6. Laboratory crucible tests using small quantities of pulverized oil shale can cause the same types of corrosion products to occur on steels that occur in large scale retorts at the same elevated temperatures.

7. Raw shale oil causes less than 20 mils/yr corrosion on all iron base alloys at typical transport temperatures.

8. While the basic corrosion trends were similar, some differences occurred in the type and/or degree of corrosion observed in specimens exposed in LETC and LLNL simulated in-situ oil shale retorts that could not be readily explained.

REFERENCES

1. Martel, R. and Harak, A., "Preliminary Results from Retorting Michigan Antrim Shale," LERC/TPR-711, Laramie Energy Technology Center, Laramie, WY, July 1977.

2. Synthetic Fuels Data Handbook, Cameron Engineers, Inc., 1315 S. Clarkson Street, Denver, CO 80210.

3. Foerster,T. and Levy, A., "Corrosion of Metals in Coal Char Environments," Proceedings of NACE Conference on High Temperature Corrosion, San Diego, Calif, March 1981.

4. Burnham, A., "Sulfur Reactions in Oil Shale Processing," Proceedings of NACE Conference on Corrosion-Erosion-Wear of Materials in Emerging Fossil Energy Systems, Berkeley, Calif., January 1982.

5. "Oil Shale Tract C-b; Modifications to Detailed Development Plan," submitted by Ashland Oil, Inc., Lessee and Occidental Oil Shale, Inc., Operator of the C-b Shale Oil Venture, February 1977.

6. Loucks, R., "Occidental Vertical Modified In-Situ Process for the Recovery of Oil from Oil Shale," Summary Report for the period November 1, 1976 to October 31, 1977, Contract No. EF-77-A-04-3873.

7. "Rio Banco Oil Shale Project, revised Detailed Development Plan," submitted by Gulf Oil Corp. and Standard Oil Co. (Indiana), Volume 1, May 1977.

8. "Rio Banco Oil Shale Project, Revised Detailed Development Plan," submitted by Gulf Oil Corp. and Standard Oil Co. (Indiana), Volume 2, May 1977.

9. Gordon, B., Worrell, W., Nagarajan, V., "Thermodynamic Predictions of the Behavior of Fe-Cr-Al Alloys in Coal Gasifier Environments," Oxidation of Metals, Volume 13, No.1, pp. 13-23, February 1979.

10. Douglass, D., "In-Situ Oil Shale Retort-Thermocouple Well Failure Analysis," Sand 79-0742, Sandia Laboratories, Albyquerque, NM, May 1979.

11. Jacob, K. T., Rao, D. B., Nelson, G. G., "Phase Relations in the Fe-Cr-S System and the Sulfidation of an Austenitic Stainless Steel," NASA Technical Memorandum, 78, 465, December 1977.

ACKNOWLEDGEMENT

Several students participated in the oil shale retort corrosion program. Their contributions are appreciated. Particular thanks is due Elliot Slamovich who helped in compiling and structuring the data and figures generated by all of the earlier student participants into the final report. The students were:

Bob Bellman
Cathy Coulman
Ed Elliott
Ehsen Ettehadieh
Jacqui Glanville
Quan Nguyen
Jennifer Okano
Edmundo Ossio
Elliott Slamovich
Bob Stanley
Matt Trask

TABLE 1

COMPOSITION OF GREEN RIVER AND ANTRIM SHALES

COMPOSITION	COLORADO GREEN RIVER SHALE	MICHIGAN ANTRIM SHALE
shale feed:		
oil content,gal/ton	22.5	9.7
water content, gal/ton	5.3	7.9
hydrogen, wt-pct	1.7	1.3
total carbon, wt-pct	15.3	8.6
sulfur, wt-pct	0.5	3.5
nitrogen, wt-pct	0.3	0.3
carbon dioxide, wt-pct	17.8	1.2
mineral carbonate, wt-pct	24.2	1.7
Spent Shale:		
water content, wt-pct	0.4	0.3
hydrogen, wt-pct	0.3	0.1
total carbon, wt-pct	5.9	2.9
sulfur, wt-pct	0.4	1.8
nitrogen, wt-pct	0.1	0.2
carbon dioxide, wt-pct	14.4	0.7
mineral carbonate, wt-pct	19.7	0.9

TABLE 2

DISTRIBUTION OF SULFUR IN GREEN RIVER OIL SHALE [2]

							AVERAGE
Oil yield of shale, gal/ton.	10.5	26.7	36.3	57.1	61.8	75.0	
Total sulfur in raw shale, percent	.62	.56	.73	1.96	1.99	1.85	
Distribution of total sulfur into types, percent:							
Organic sulfur	27	27	37	19	21	24	26
Pyritic sulfur	71	73	63	79	77	72	72
Sulfate sulfur	2	trace	trace	2	2	4	2
TOTAL	100	100	100	100	100	100	100
Distribution of total sulfur in assay products, percent:							
Oil	5	11	8	7	9	11	8
Gas	2	10	19	18	23	6	13
Spent shale	93	79	73	75	68	83	79
TOTAL	100	100	100	100	100	100	100

TABLE 3

CHEMICAL COMPOSITION OF THE INORGANIC PORTION OF VARIOUS GRADES OF GREEN RIVER SHALE AND OF THE SPENT SHALE PRODUCTS[2]

Chemical Constituent	Very Low-Grade Shale (10.5 gal/ton)	Medium-Grade Shale (26.7 gal/ton)	High-Grade Shale (36.3 gal/ton)	Very High-Grade Shale (61.8 gal/ton)
Raw Shale				
SiO_2	40.9	26.1	26.5	26.4
Fe_2O_3	4.3	2.6	2.9	3.1
Al_2O_3	9.4	6.5	6.3	7.0
CaO	11.0	17.5	14.2	8.3
MgO	5.4	5.3	5.6	4.5
SO_3	0.1	0.6	1.2	1.4
Na_2O	1.8	2.6	2.7	1.9
K_2O	3.4	1.0	1.9	1.0
Spent Shale:				
SiO_2	53.27	41.90	42.36	49.19
Fe_2O_3	5.64	4.10	4.74	5.87
Al_2O_3	12.28	10.58	10.46	13.13
CaO	14.82	28.11	23.54	15.40
MgO	7.00	8.53	9.30	8.35

TABLE 4

POWDER DIFFRACTION ANALYSIS OF OUTER SCALE OF 310SS THERMOCOUPLE SHEATH
d - values for standard compounds

310SS Sheath Scale	9-273 Hex CrS	Cr_2O_3	$FeCr_2O_4$	$Fe_{1-x}S$	$(FeNi)S_8$	$Fe_8Ni_8S_{16}$	$FeCr_2S_4$
		3.633s			5.78w		
						3.31w	3.35s
	3.08w						
3.06w							
					3.03s		3.01vs
	2.99s					2.99m	
				2.98s			
2.97w							
			2.95m				
						2.93m	
					2.90m		
2.67m		2.67m					
	2.65vs			2.65vs			
						2.62s	
2.53s							
			2.52vs				
					2.51vw		2.50s
		2.48vs					
					2.30w		
						2.25w	
2.09vs		2.09w					
	2.07vs		2.07s	2.07vs			
						2.04vs	2.04m
					1.93m		1.92s
		1.81m					
1.80s						1.80w	
					1.78vs		1.77vs
1.72m	1.72vs			1.72m			
						1.71m	
			1.69m				
		1.67vs					
1.62m	1.62s						
				1.61m			
			1.60vs			1.59w	
							1.58m
					1.53w		
1.49s	1.49w			1.49w			
		1.47w	1.46vs				
							1.44s
1.33w	1.33vs						
			1.31w		1.31w		
	1.30w	1.29w					
1.28w							
			1.26m		1.26w		

vs - very strong peak
s - strong peak
m - medium peak
w - weak peak

TABLE 5

POWDER DIFFRACTION ANALYSIS OF SCALE OF MILD STEEL PIPE

X-RAY d SPACINGS (Å)

Outside of A	Outside of B	4-0755 γ-Fe_2O_3 iron oxide	13-534 α-Fe_2O_3 iron oxide
		1.09 (19)	
			1.310 (20)
1.4495 (35)			
1.4784 (50)	1.4784 (50)	1.48 (53)	1.452 (35)
1.6091 (35)			1.484 (35)
1.6195	1.6117 (35)	1.61 (33)	
1.6873 (60)	1.6879 (60)		
1.7446	1.7084 (10)	1.70 (12)	1.690 (60)
1.8329 (40)	1.8329 (40)		1.838 (40)
1.9632			
2.0256			
2.1252 (25)	2.0878 (25)	2.08 (24)	
2.1943 (40)	2.1943 (40)		2.201 (30)
2.2962 (20)			
		2.32 (6)	
2.3901 (5)	2.4086 (5)	2.41 (1)	
2.5060 (100)	2.5196 (100)	2.52 (100)	2.510 (50)
2.6804 (100)	2.6804 (100)		2.690 (100)
		2.78 (19)	
2.8820			
2.9664 (35)	2.9482 (40)	2.95 (34)	
3.3236			
3.6596 (25)	3.6449 (25)		3.660 (25)
		3.73 (5)	
4.0733			

TABLE 6

STEEL COMPOSITIONS EXPOSED IN SIMULATED IN-SITU RETORTS

Alloy Designation	Typical Composition in Wt%									
	Cr	Ni	Mo	Mn	Si	C	Al	Ti	Other	Fe
1018*	-	-	-	1.2	-	0.30	-	-	-	BAL
1 1/4Cr 1/2Mo*	1.25	-	0.5	0.5	0.5	0.15	-	-	-	BAL
2 1/4Cr 1Mo*	2.25	-	1.0	0.5	0.5	0.15	-	-	-	BAL
5Cr 1/2Mo	5.0	-	0.5	0.5	0.5	0.15	-	-	-	BAL
9Cr 1Mo	9.0	-	1.0	0.5	0.5	0.15	-	-	-	BAL
410*	12.0	-	-	1.0	1.0	0.15	-	-	-	BAL
304*	18.0	8.0	-	2.0	1.0	0.08	-	-	-	BAL
309	23.0	15.0	-	0.54	0.74	0.11	-	-	-	BAL
310*	25.0	20.0	-	2.0	1.0	0.06	-	-	-	BAL
316*	16.0	10.0	2.5	2.0	1.0	0.08	-	-	-	BAL
321*	17.0	9.0	-	2.0	1.0	0.08	-	0.2	0.35Cu	BAL
347*	17.0	9.0	-	2.0	1.0	0.08	-	-	0.80Cb	BAL
Incoloy 800	20.6	30.8	-	0.80	0.33	0.03	0.32	0.42	0.14Cb	BAL
Incoloy 825	21.5	42.0	3.0	0.5	0.2	0.3	0.1	0.9	2.20Cu	BAL

*tested bare and aluminized

TABLE 7

LARGE SIMULATED IN-SITU RETORT EXPOSURES SUMMARY

Retort Run No.	Retort Type & Location	Low Alloy and Stainless Steels exposed	Type of Shale	Max Temp °C	Operation Time,Hrs
S-49	10 ton above ground LETC	304, 1018	Antrim	980	72
S-54	"	410, 309, 310, 316, 321, 347	Antrim	1040	85
S-57	"	410, 310, 347, bare & aluminized	Antrim	875	90
S-59	"	1018, 304, 309, 310, 316, 321, 347, 410, 1 1/4 Cr 1/2 Mo, 2 1/4 Cr 1Mo, bare & aluminized	Green River	825	68
S-60	"	1018, 304, 309, 310, 316, 321, 347, 410, 1 1/4Cr 1/2Mo, 2 1/4Cr 1Mo, Incoloy 800, 825	Green River	925	64
S-61	"	1018, 304, 310, 2 1/4Cr 1Mo	Green River	650	93
S-67	"	1018, 304, 310, 321	Moroccan "M" Zone	1100	18
L2	3' Diax20' high LLNL	1018, 304, 310, 316, 321, 347 410, 1 1/4Cr 1/2Mo, 2 1/4Cr 1Mo, bare & Aluminized	Green River	900	90
L3	"	1018, 304, 309, 310, 316, 321, 347, 410, 1 1/4Cr 1/2Mo, 2 1/4Cr 1Mo, Incoloy 800, 825	Green River	1150	130

(continued)

Table 7 - Large Simulated In-Situ Retort Exposures Summary (continued)

CS-78	Controlled State LETC	1018, 304	Antrim	700	269
CS-79	"	1 1/4Cr 1/2Mo, 2 1/4Cr 1Mo, Incoloy 800, 825	Antrim	800	179
LETC Site 9	Mod, In-situ Underground Wyoming	1018, 304, 310, 2 1/4Cr 1Mo	Green River	--	---
Geo-Kinetics	True In-Situ Underground Utah	1018, 304, 310, 321, 1 1/4Cr 1/2Mo, 2 1/4Cr1Mo Incoloy 800	Green River	>1100	---

TABLE 8

ELEMENTAL ANALYSIS OF ANTRIM SHALE

Major Elements Present	Concentration in Antrim Shale (wt/o)
H	0.95
Na	0.25
K	1.97
Mg	0.95
Ca	1.39
Ti	0.20
Fe	3.53
Al	6.97
C	6.35
Si	24.84
N	1.60
O	47.20
S	3.17
Cl	.22

From W. N. Musser, Dow Chemical Company, #FR310-January 1976

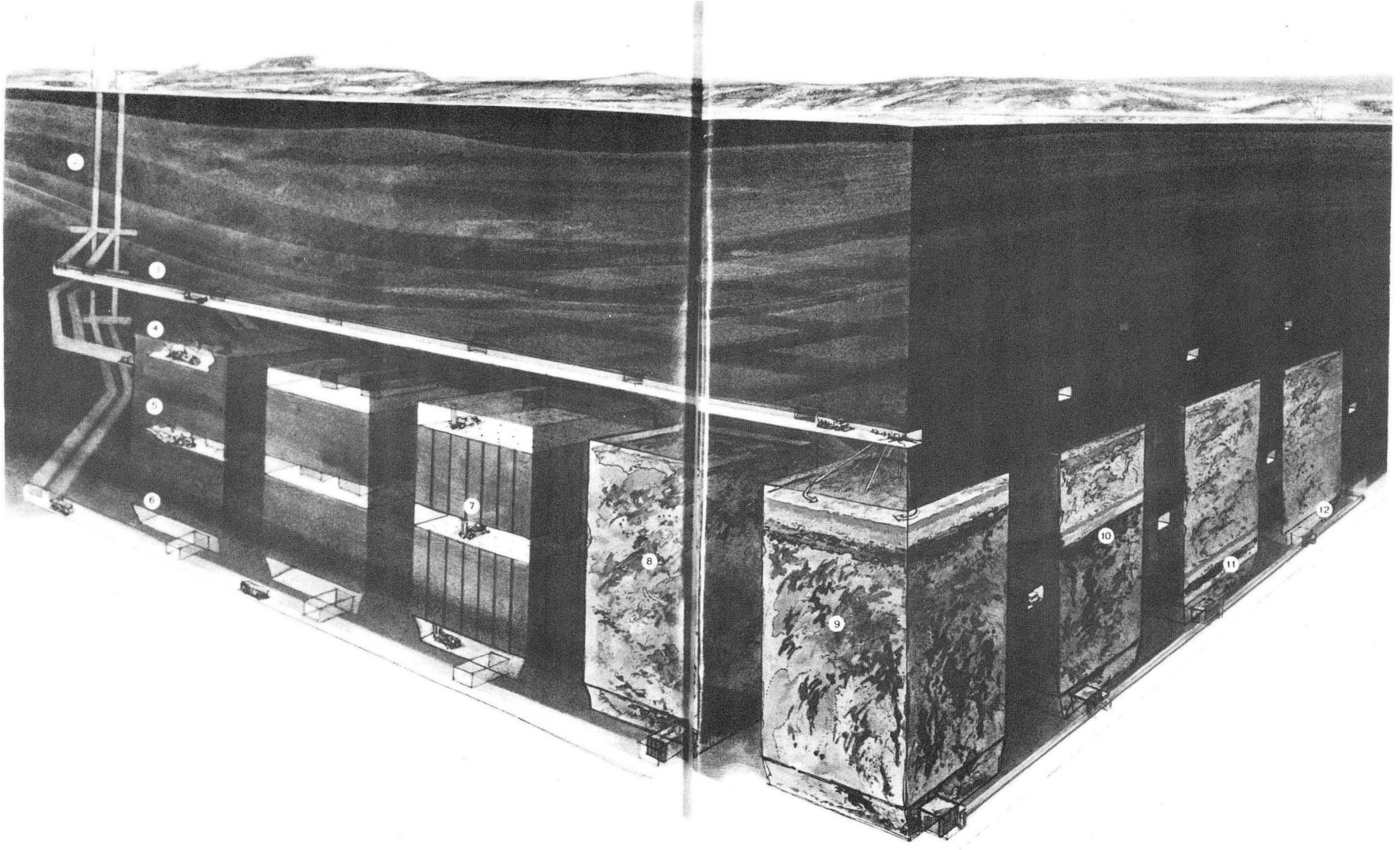

CBB 818-7322

Fig. 1 Idealized cross section of modified in-situ oil shale retort field

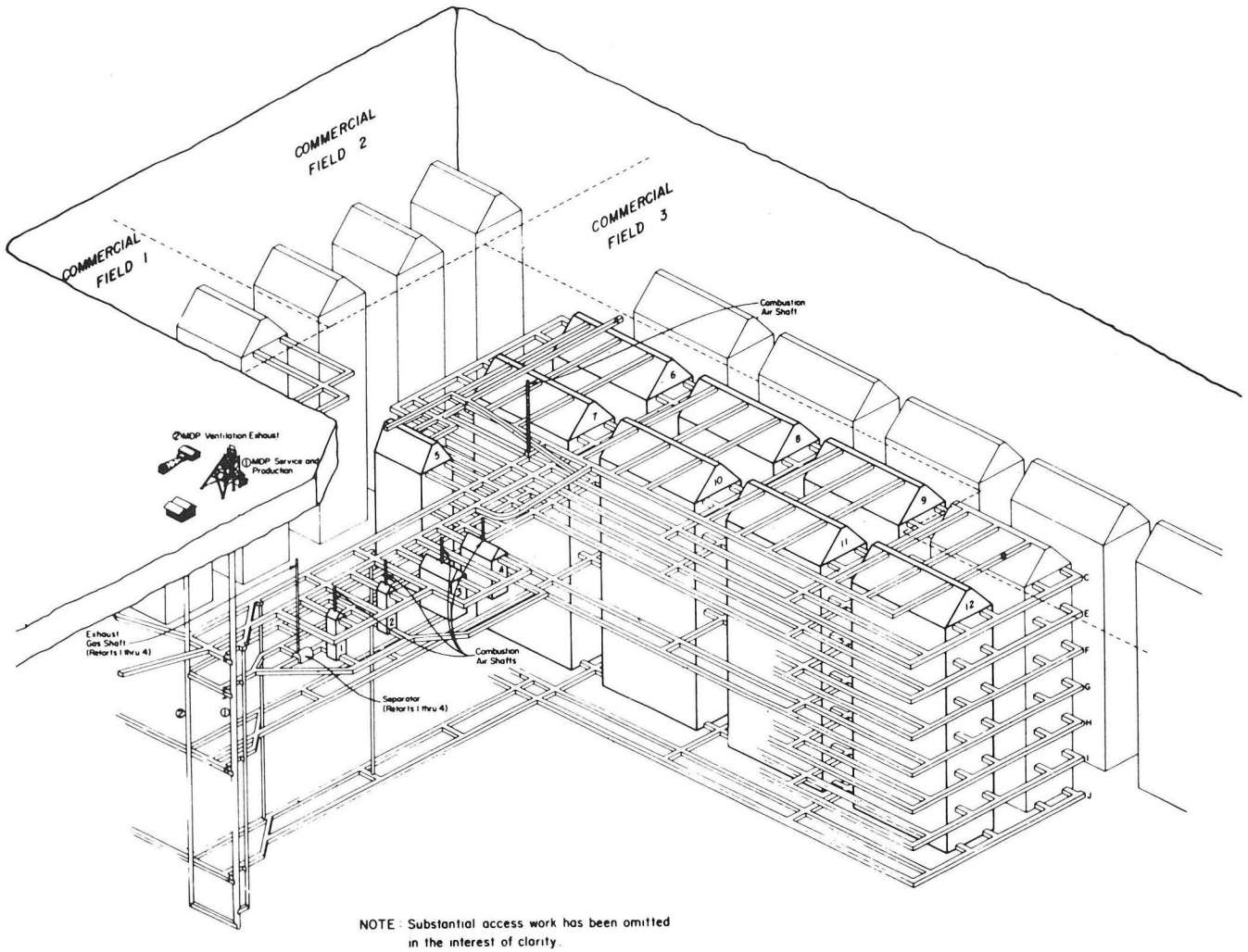

MODULAR DEVELOPMENT PHASE - SCHEMATIC ACCESS LAYOUT

XBL 833-8523

Fig. 2 Depiction of mining operations required to develop an in-situ retort field

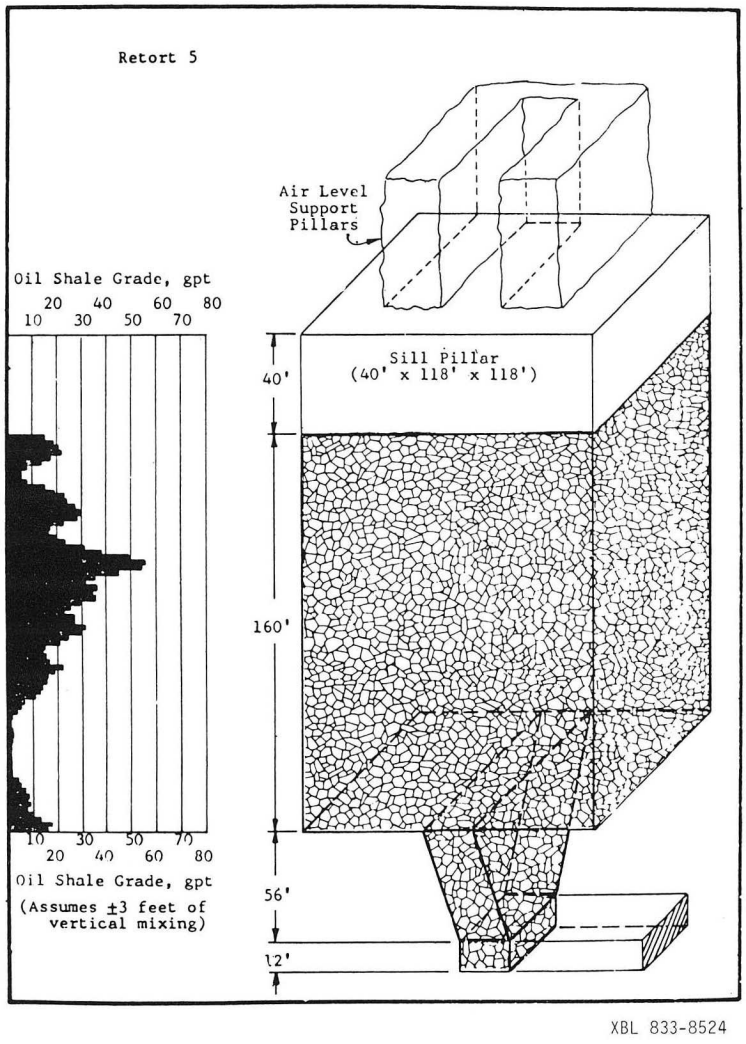

Fig. 3 Schematic of vertical rubblized retort

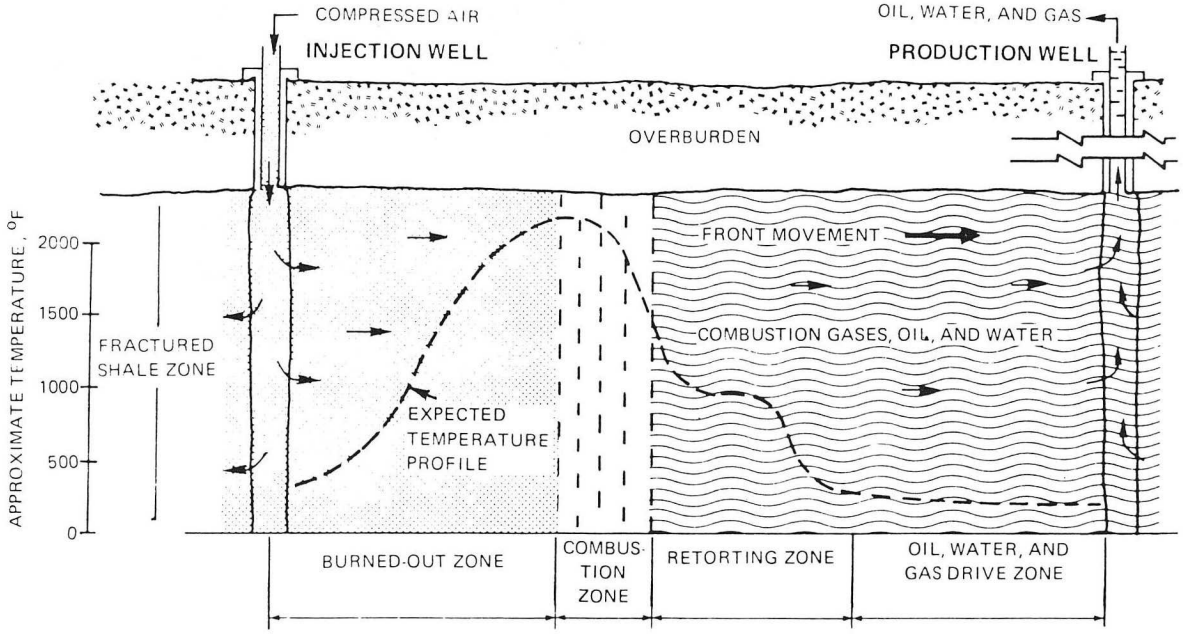

Fig. 4 Schematic of horizontal true in-situ retort

XBL 7911-12702

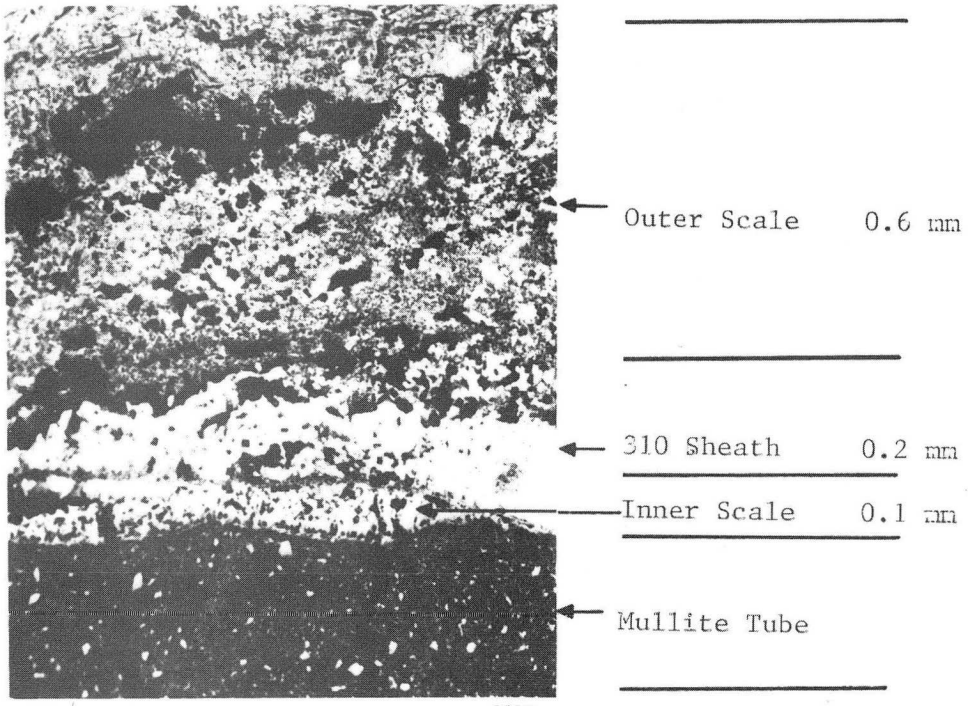

Fig. 5 Multiple scale cross section of 310SS thermocouple sheath

XBB 785-5072A

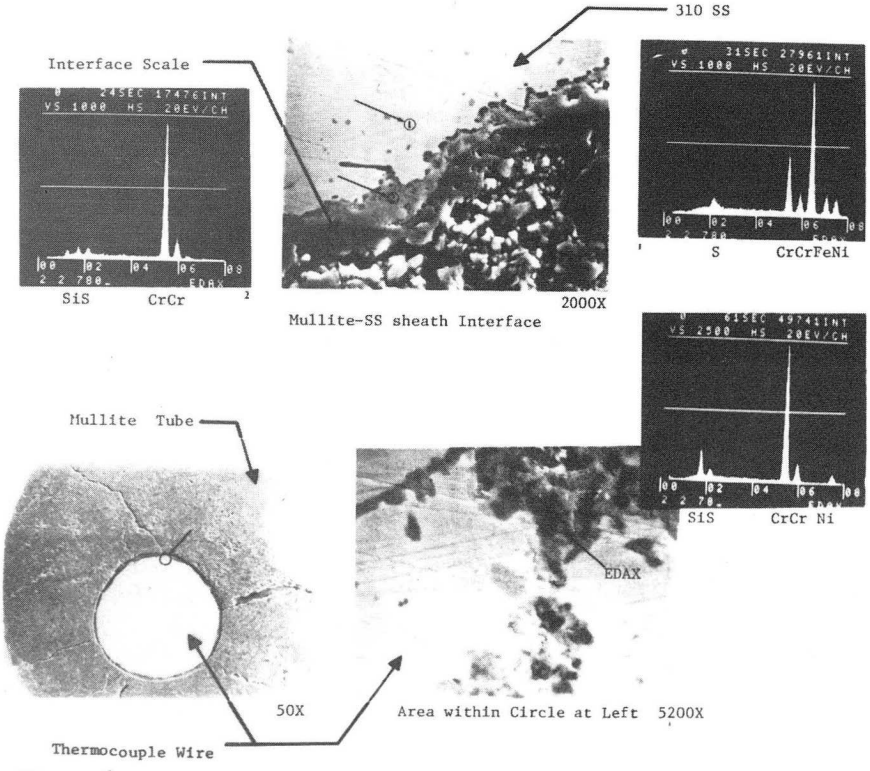

Fig. 6 310SS sheath-mullite tube interface area

XBB 784-4214A

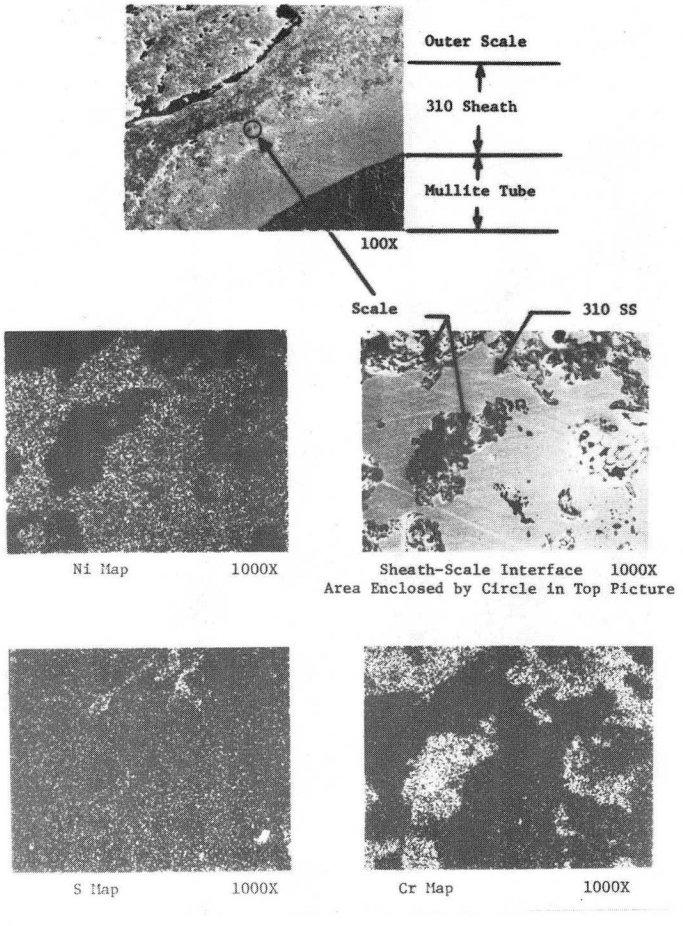

Fig. 7 310SS sheath-scale interface area

XBB 784-4216A

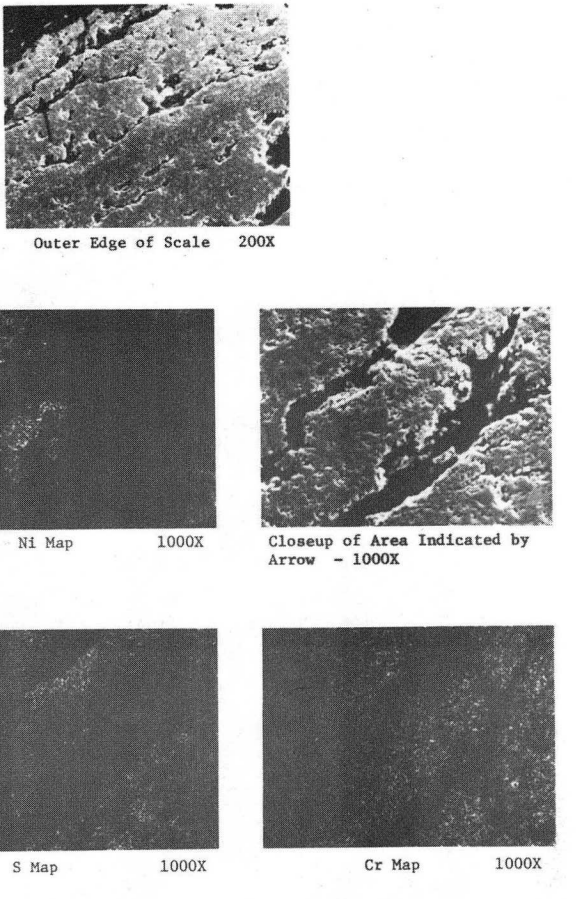

Fig. 8 Outer sacle on 310SS sheath

XBB 784-4215A

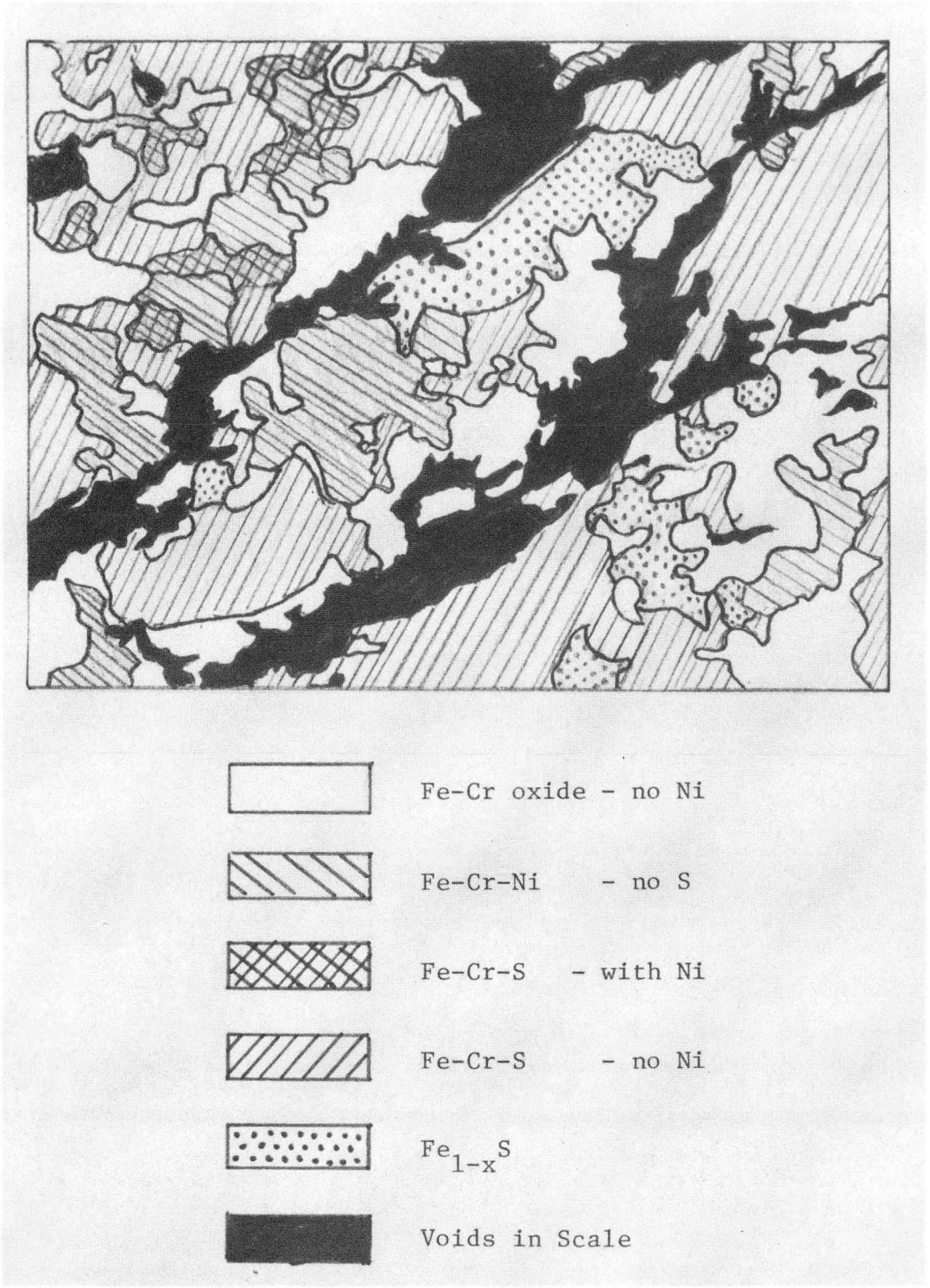

CBB 780-13091

Fig. 9 Tracing of close-up area in figure 8

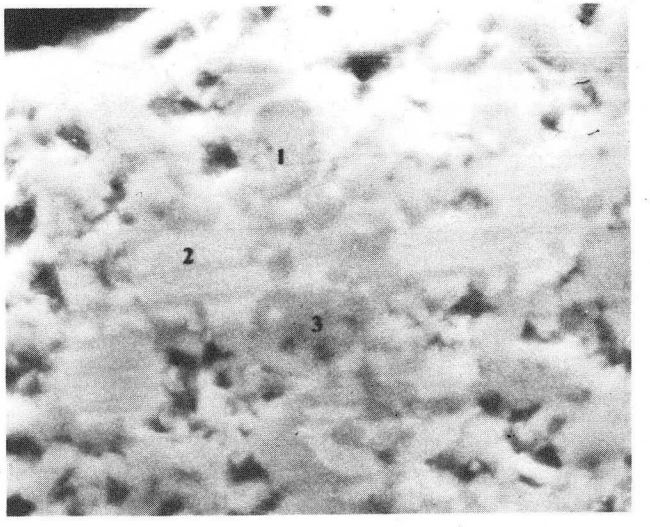

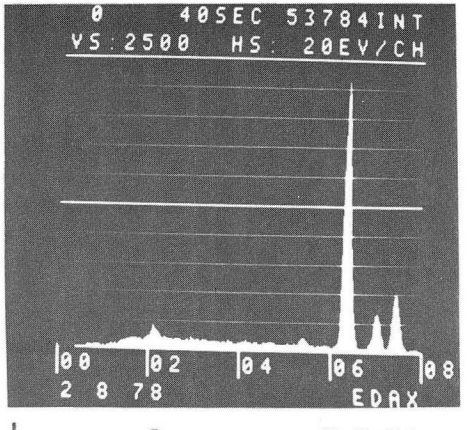

1 S FeFeNi

Fe-Ni Alloy

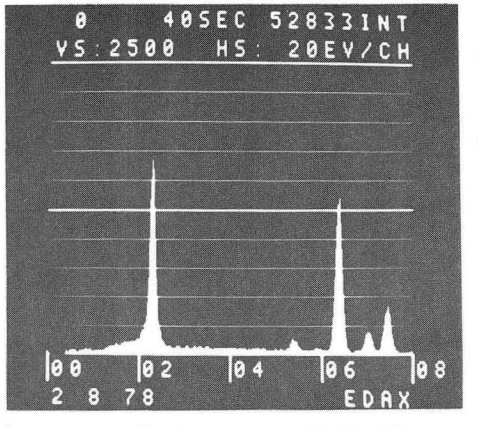

2 S FeFeNi

$Fe_{1-x}S$ with Ni

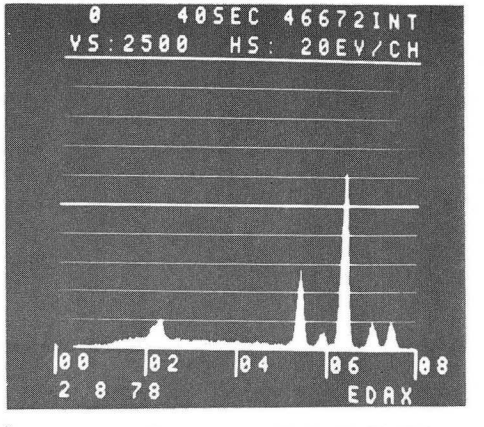

3 S CrCrFeFeNi

310 SS with S

XBB 784-4213A

Fig. 10 Outer scale on 310SS sheath; multi-phase region at high magnification

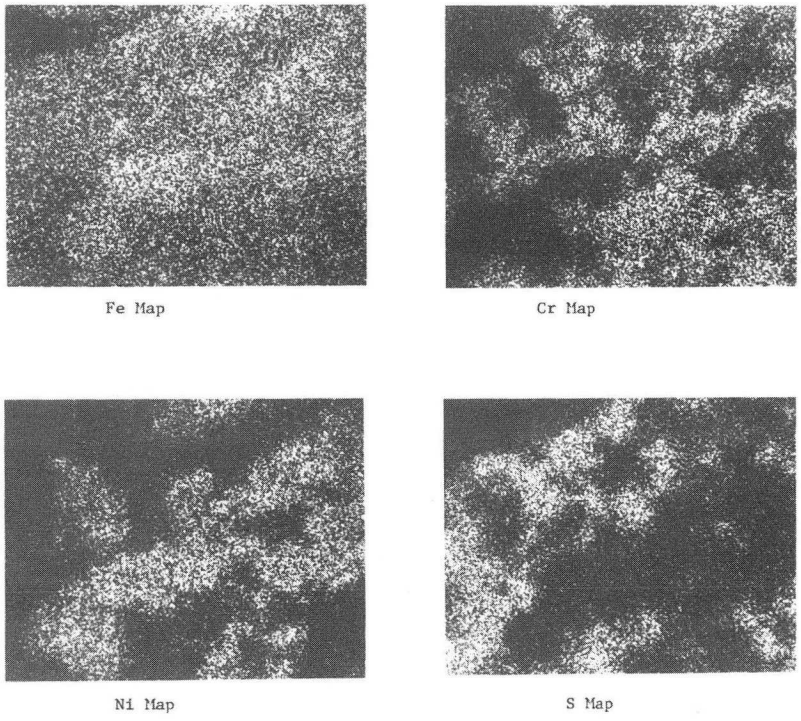

Fig. 11 310SS outer scale; multi-phase region x-ray maps

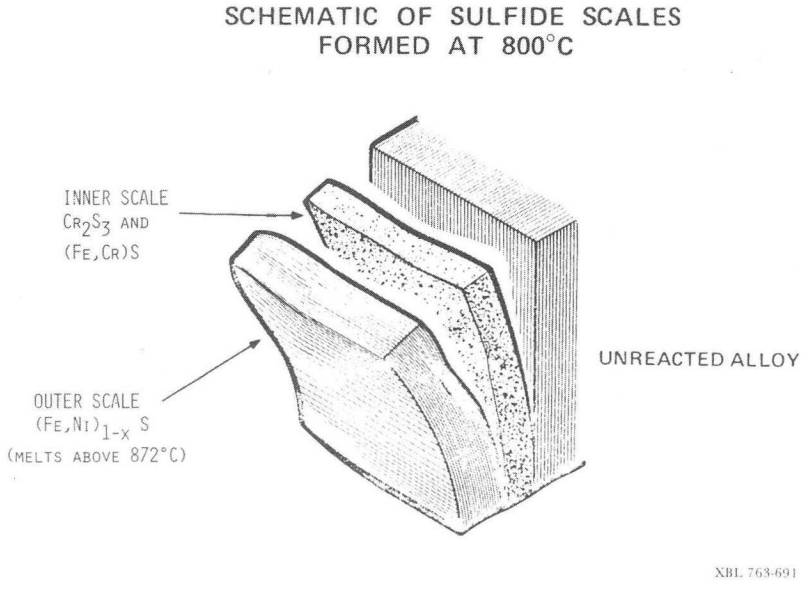

Fig. 12 Schematic of sulfide scales formed at 800°C

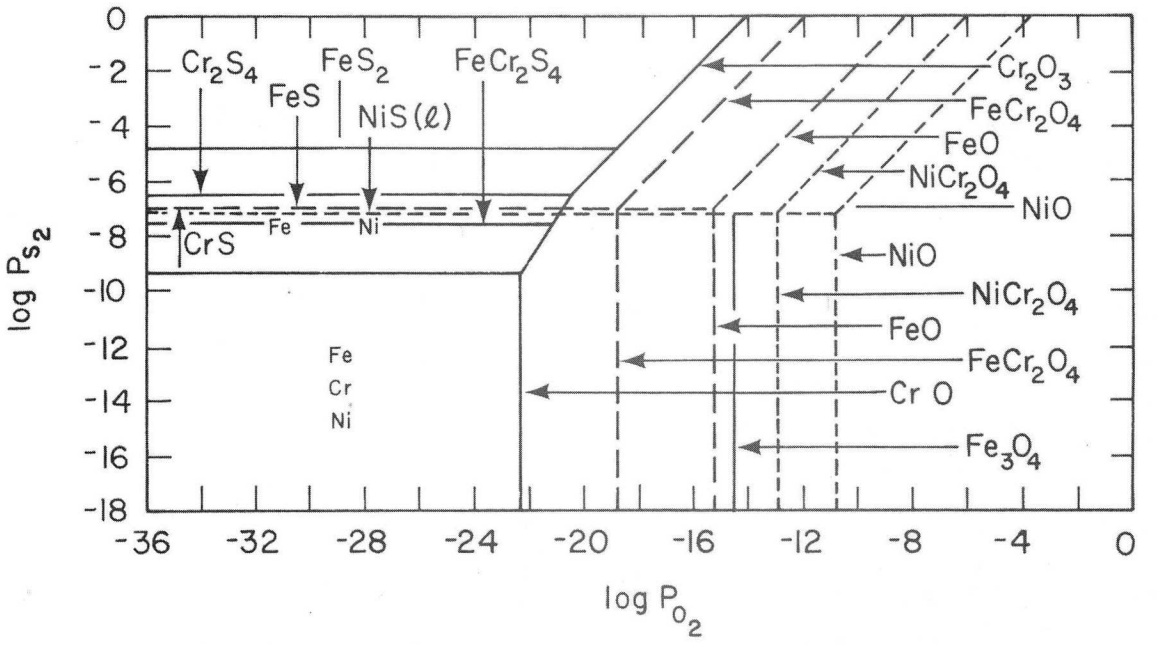

XBL 791-188

Fig. 13 Thermodynamic equilibrium stability diagram for Fe-Cr-Ni at 980°C

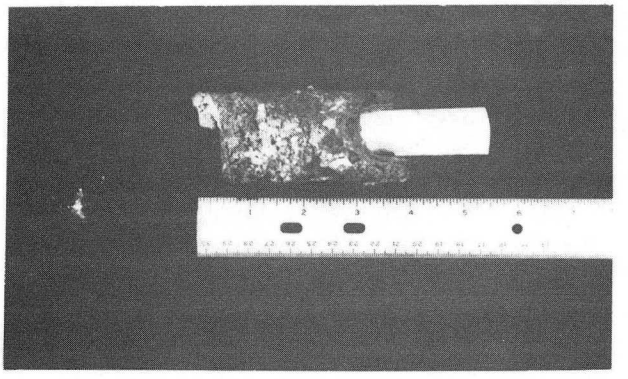

SPECIMEN A

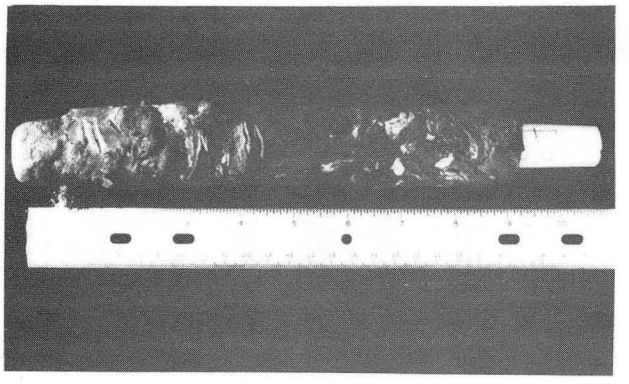

SPECIMEN B

XBB 795-7101

Fig. 14 After-service appearance of thermowell casings

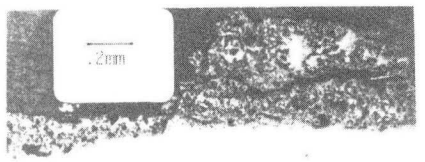

2A

Outer Edge

Inside Edge

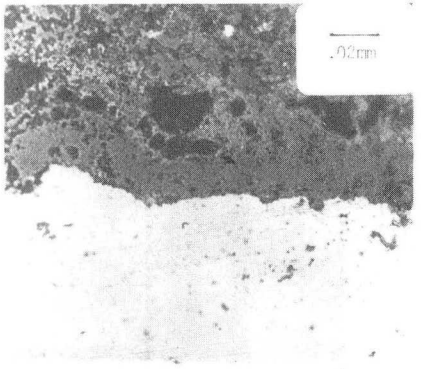

2B

Outer Scale

Base Metal

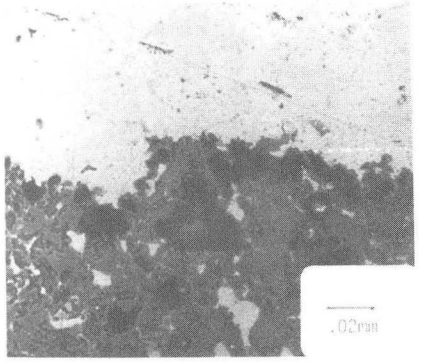

2C

Base Metal

Inner Scale

Fig. 15 Optical micrographs of specimen B

XBB 795-7091

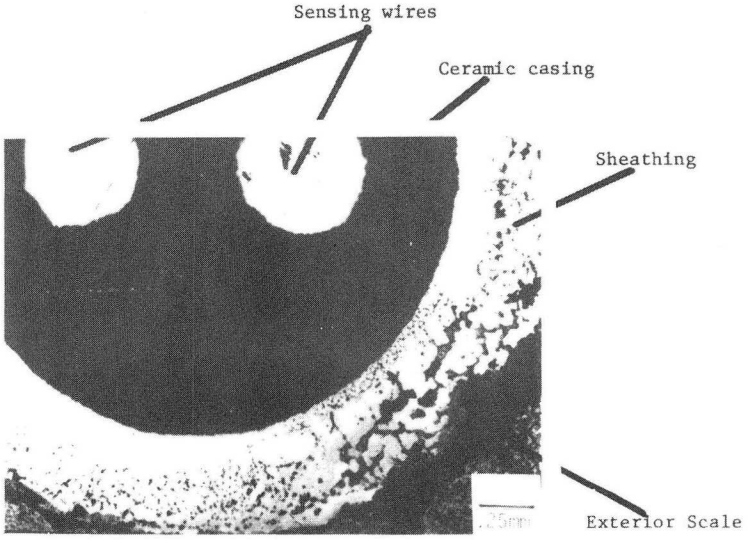

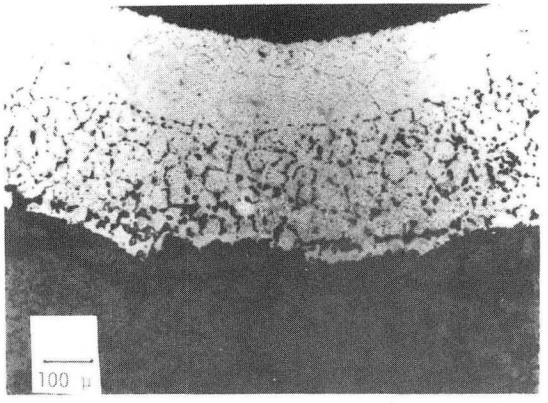

Fig. 16 Optical micrograph of thermocouple assembly cross section

XBB 795-7092

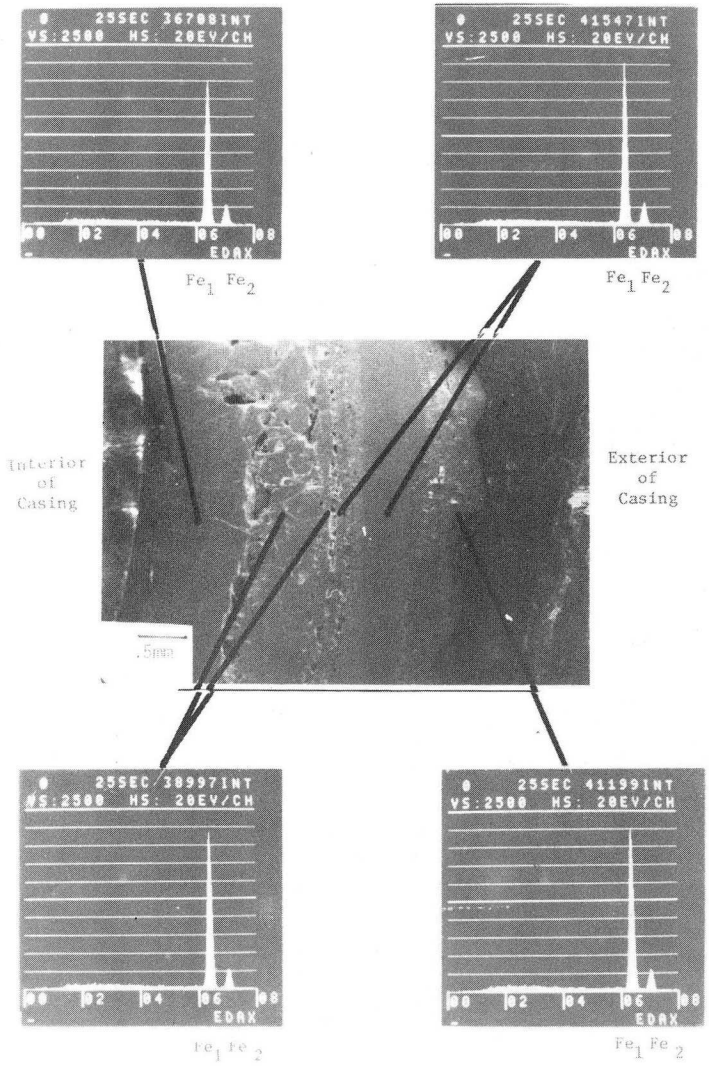

XBB 795-7094

Fig. 17 SEM micrograph of specimen B cross section

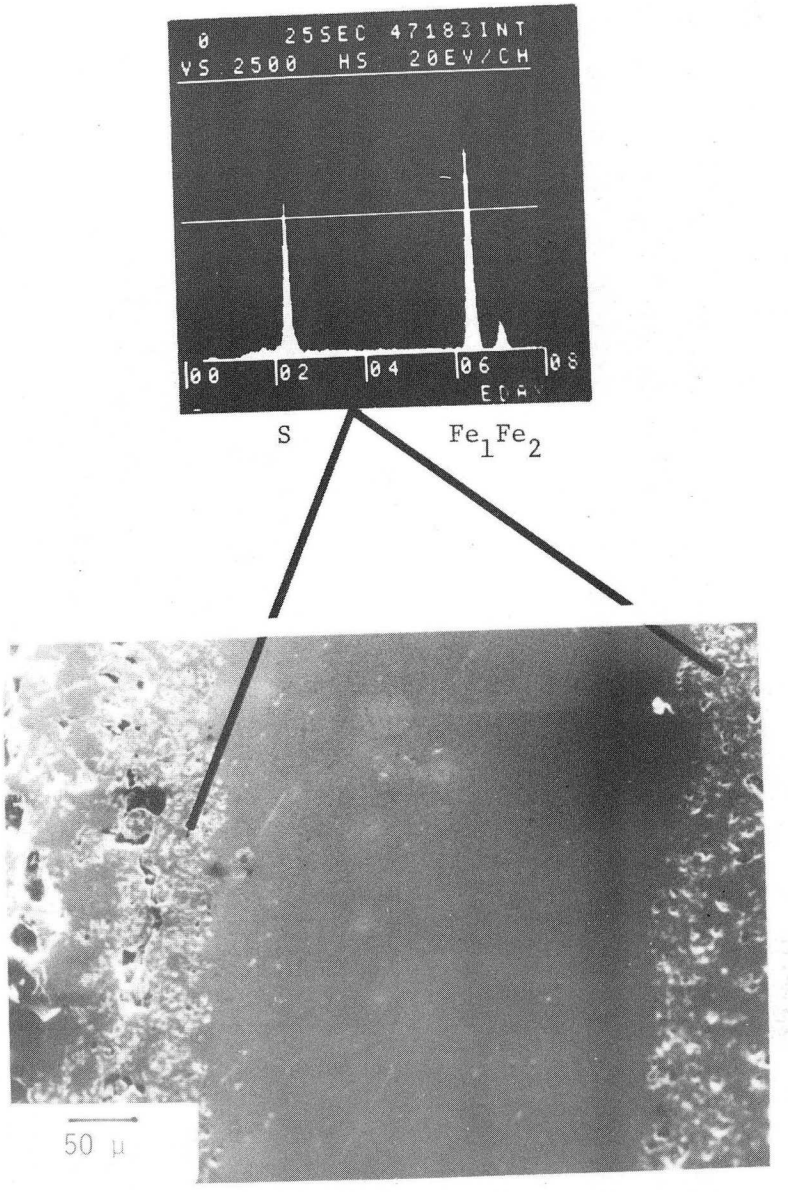

Fig. 18 Evidence of internal sulfidation of specimen B

XBB 795-7100

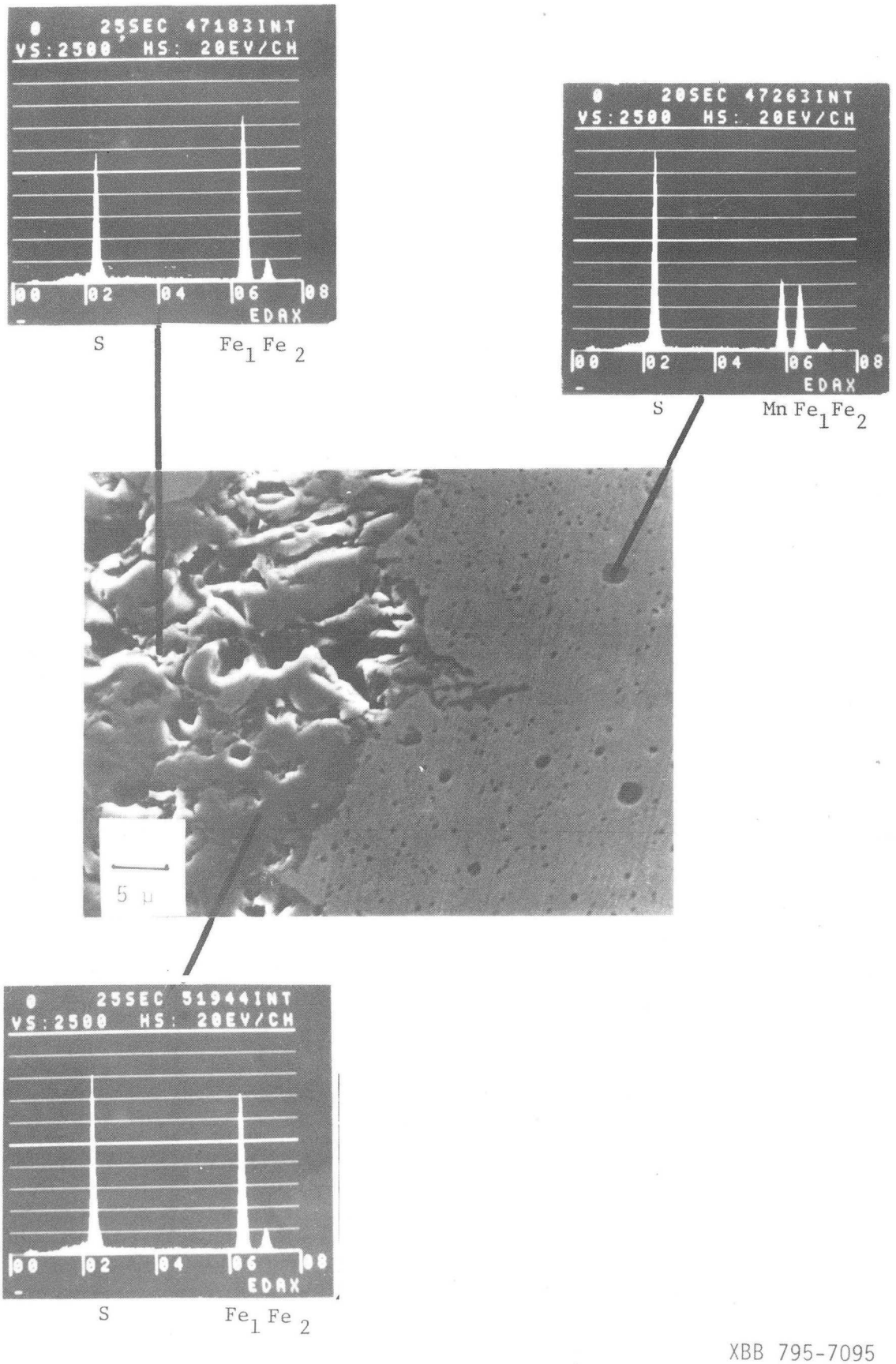

XBB 795-7095

Internal attack in base metal (Specimen B).

Fig. 19 High magnification micrograph of sulfide layer

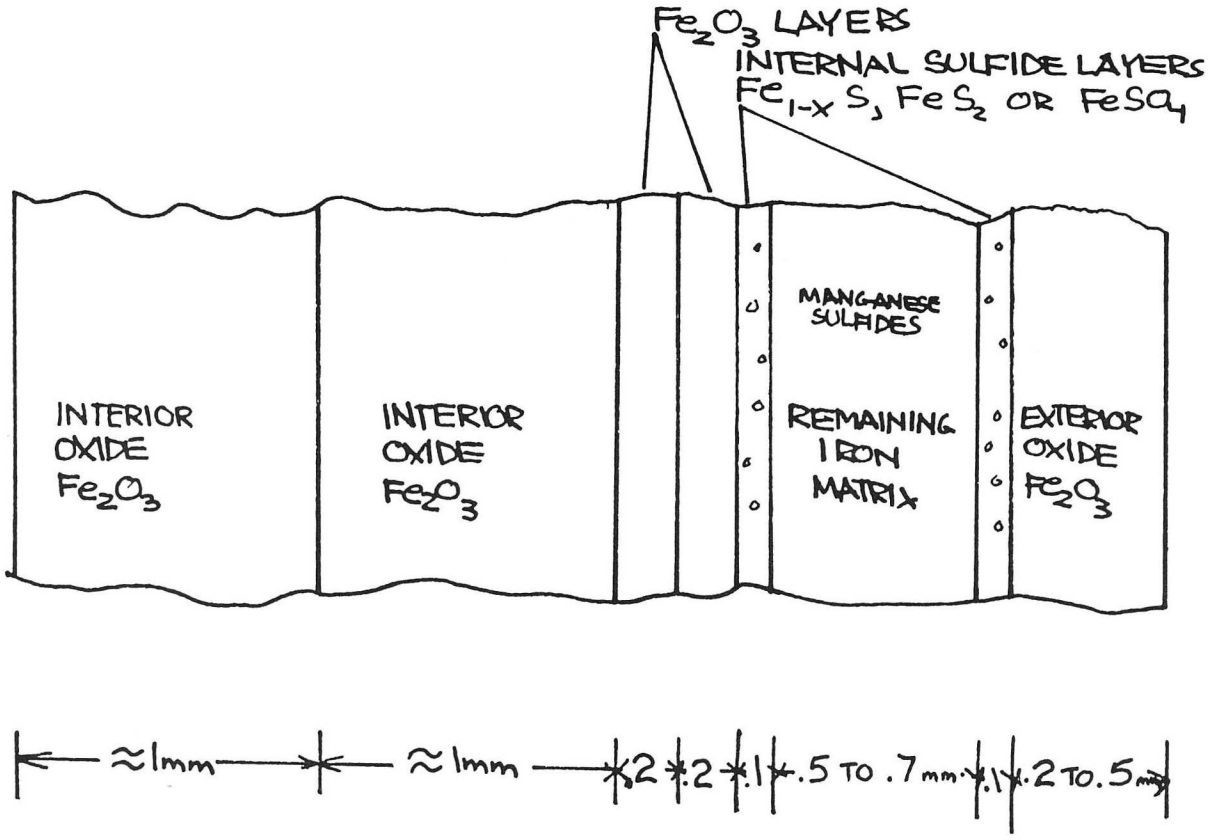

XBL 801-7712

Fig. 20 Sketch of cross section of scales on mild steel thermowell casing

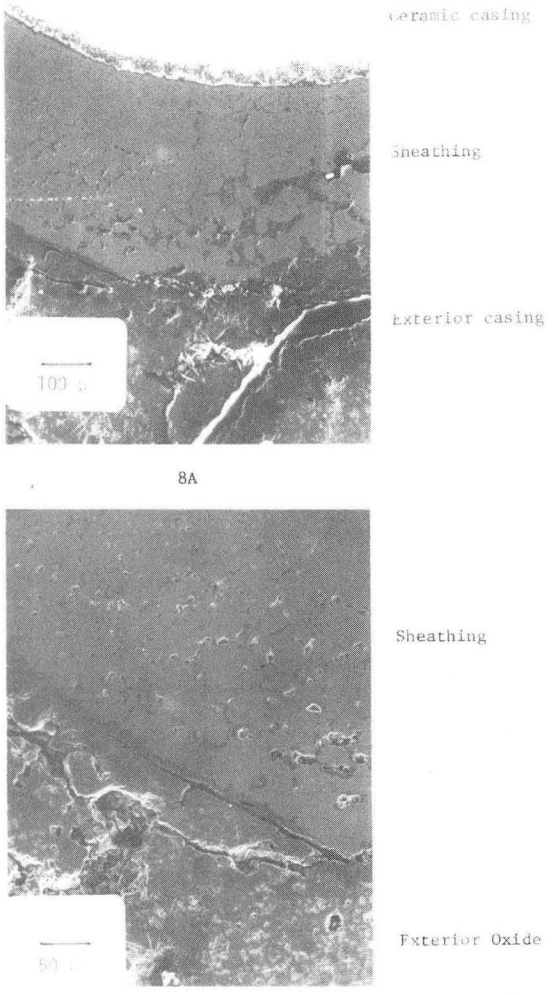

Fig. 21 SEM micrograph of specimen A thermocouple cross section

XBB 795-7093

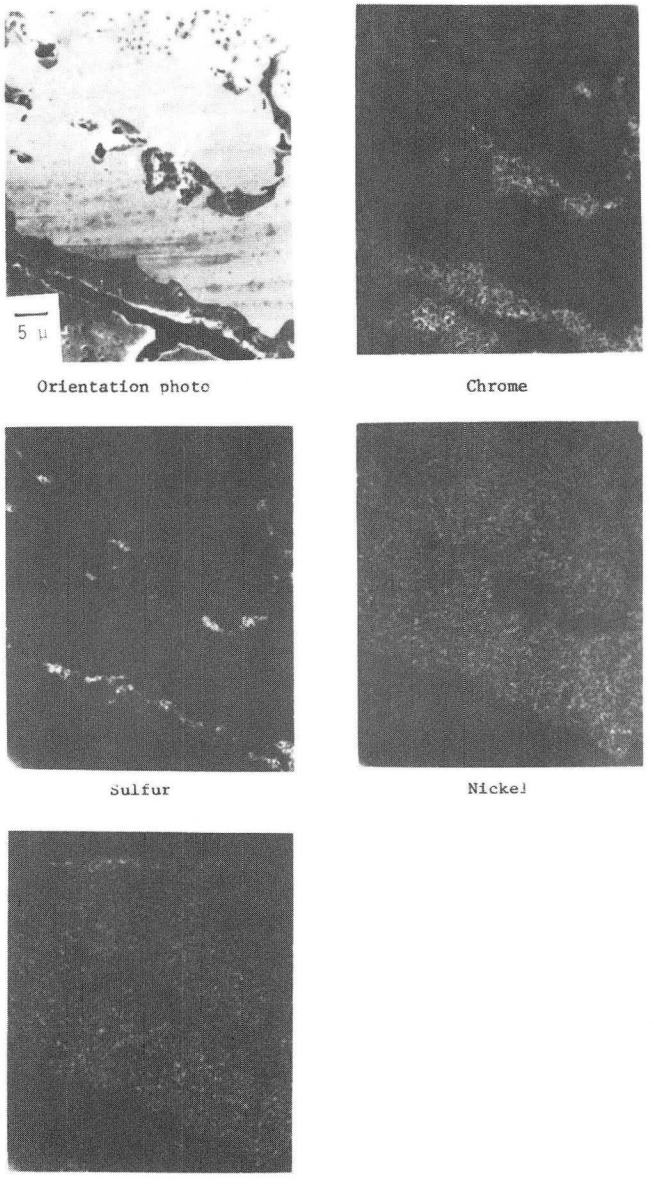

Fig. 22 Scale-metal interface area of stainless steel sheath

XBB 795-7099

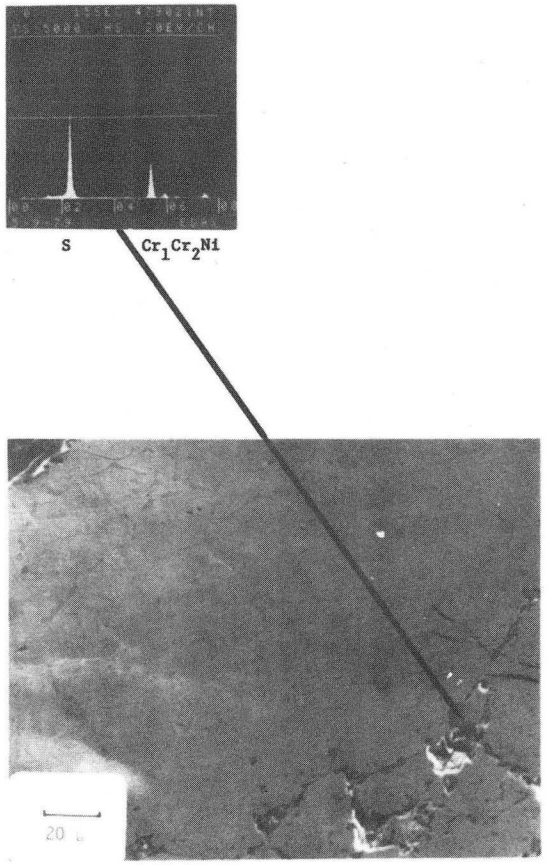

XBB 795-7102

Fig. 23 Area of sheath where the grain boundary attack changes

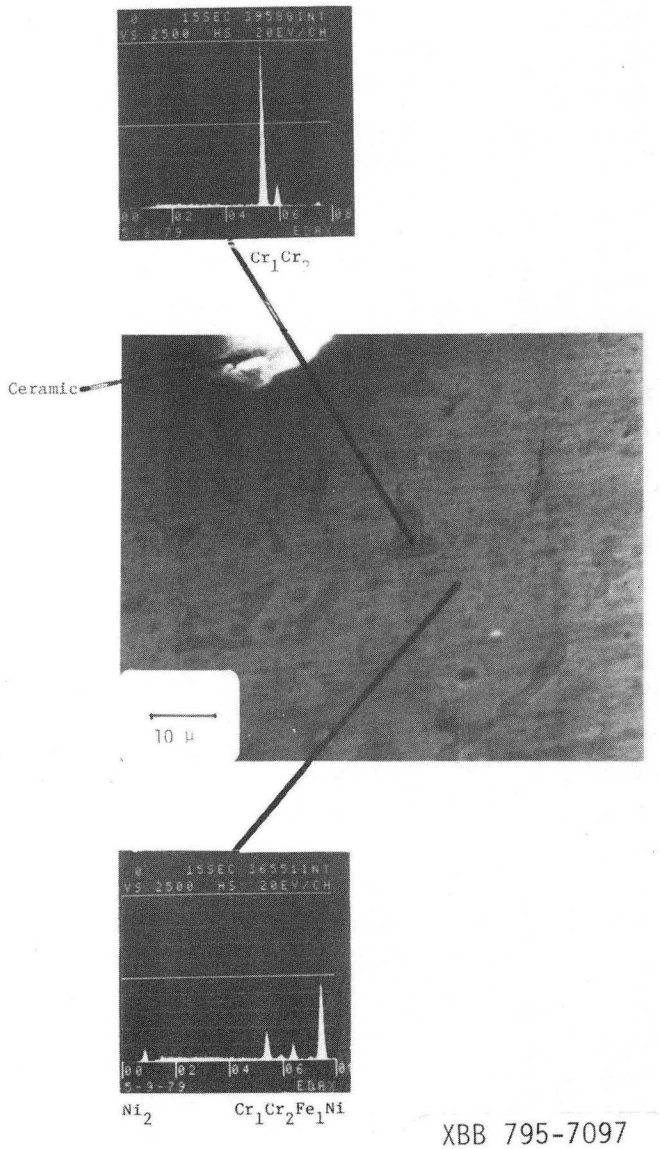

XBB 795-7097

Fig. 24 High magnification EDAX analysis of inclusions

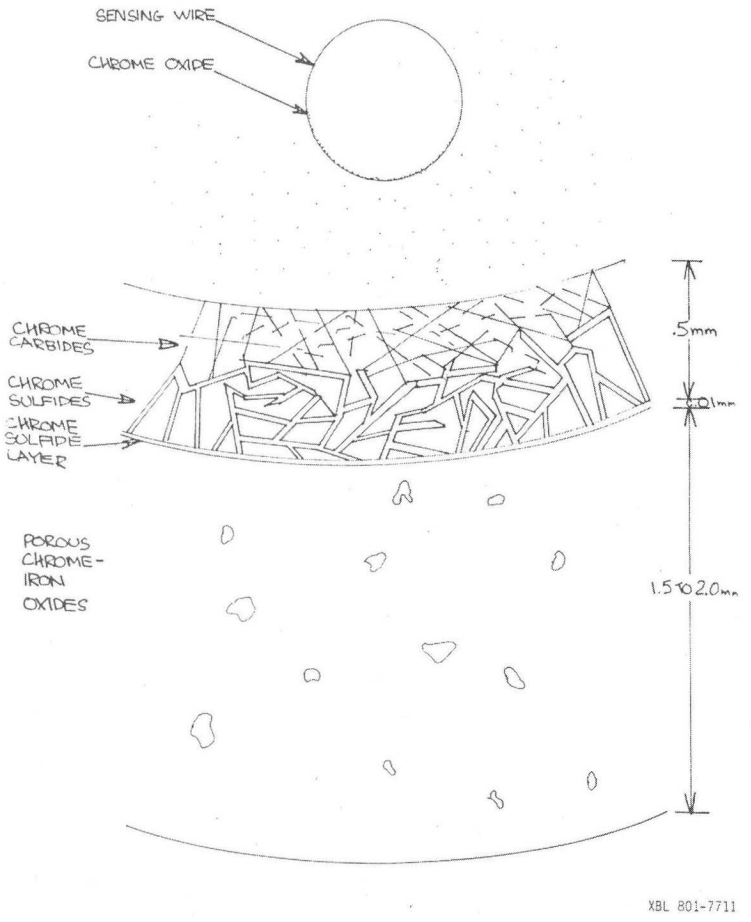

Fig. 25 Sketch of cross section of scales on and in stainless steel sheath

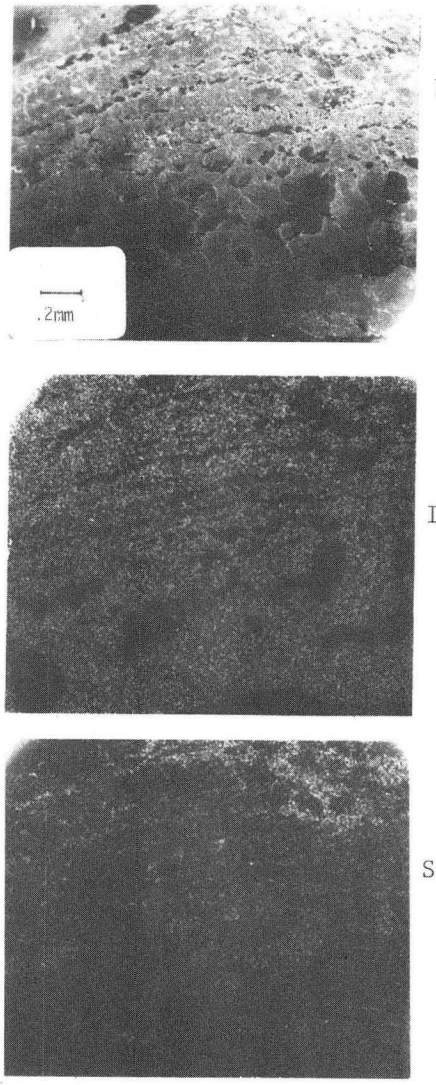

Fig. 26 SEM micrograph and x-ray maps of specimen A scale

XBB 775-7098

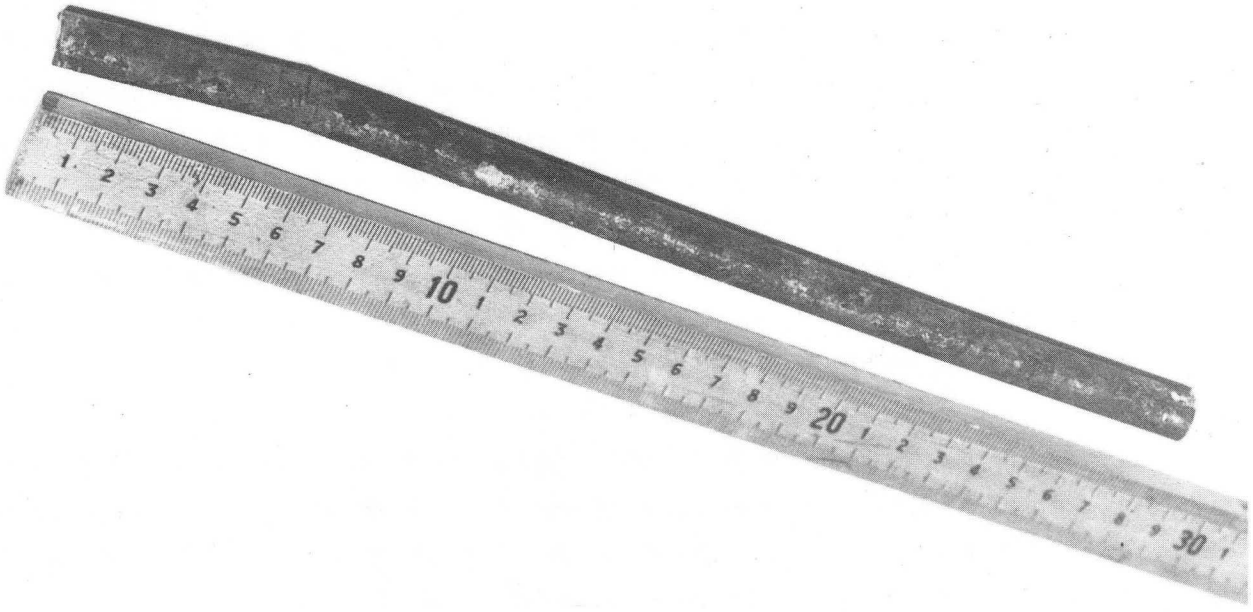

Fig. 27 321SS sheath from down-hole heating element

CBB 780-13710

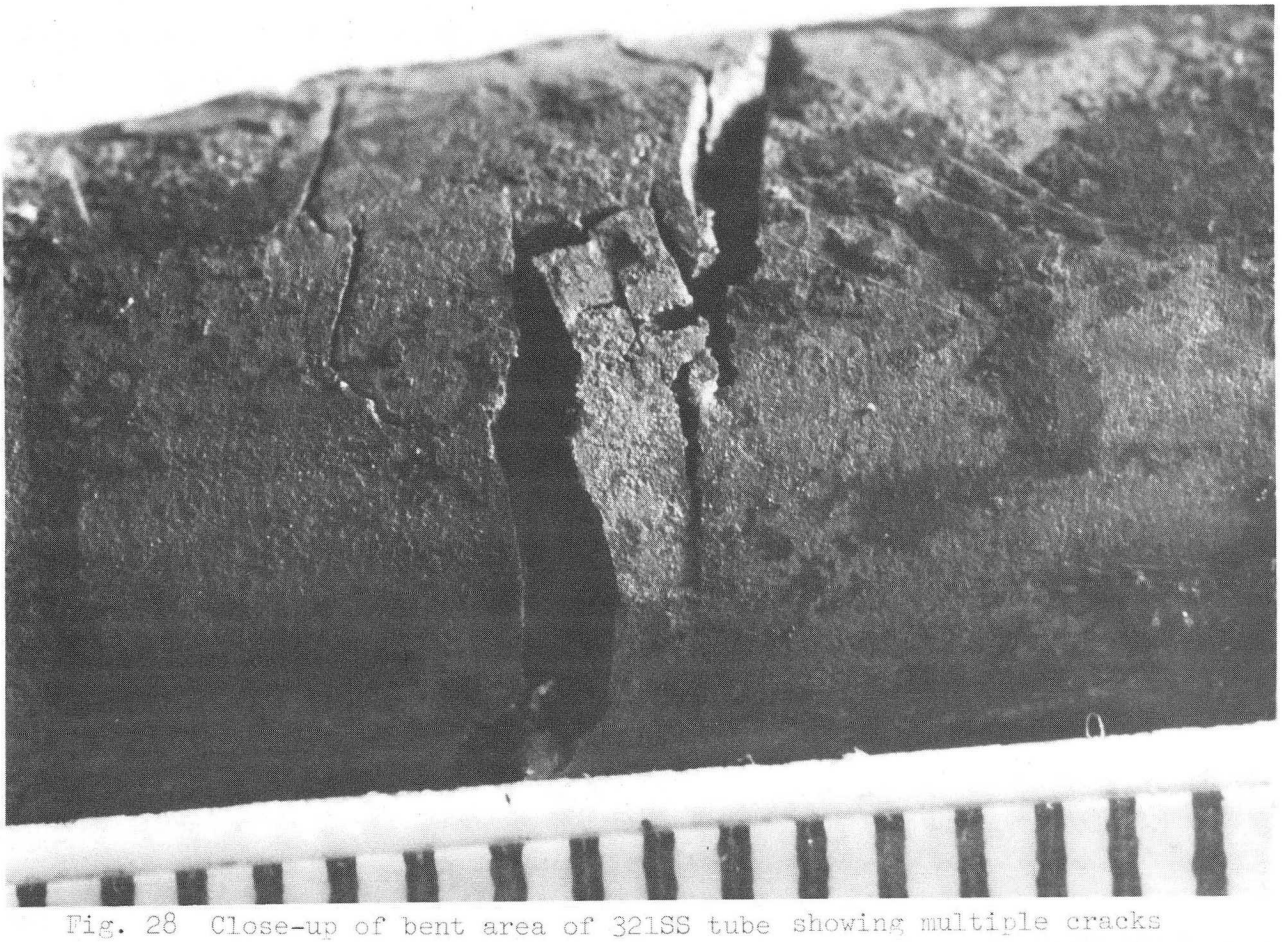

Fig. 28 Close-up of bent area of 321SS tube showing multiple cracks

CBB 780-13714

Fig. 29 304SS fin from burner stop

CBB 780-13712

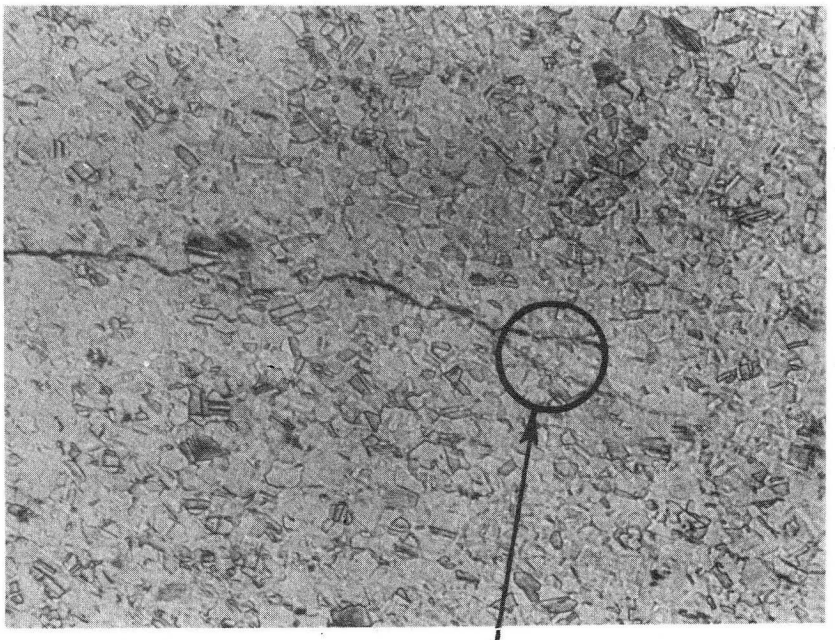

100X

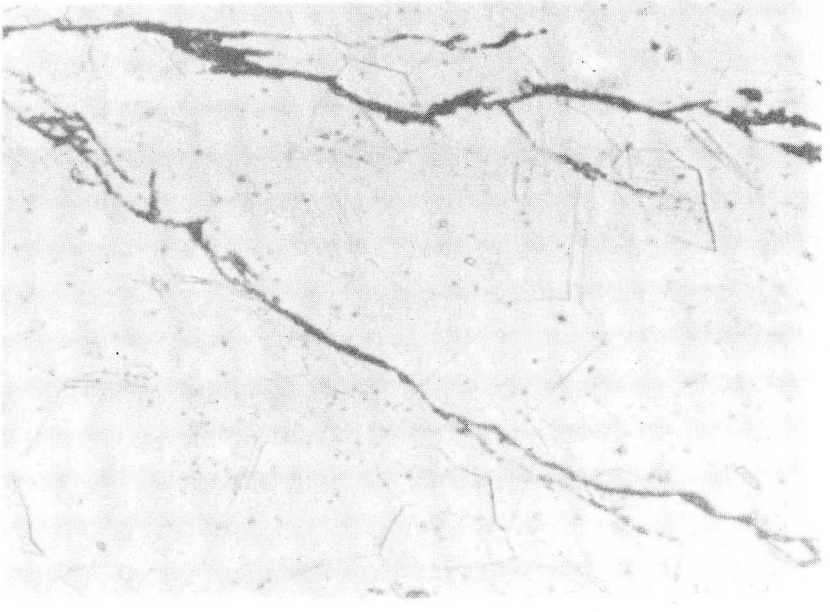

Blowup of Circled Area

1000X
XBB 780-15376

Fig. 30 Crack tip area of 321SS barrier sheath

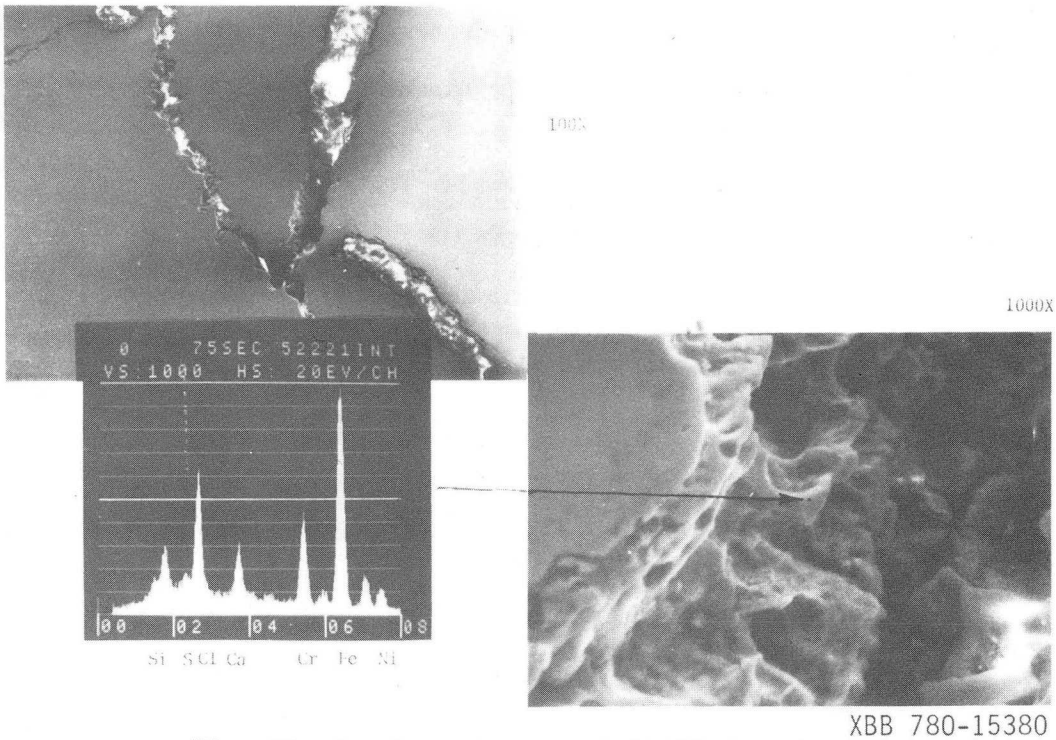

Fig. 31 Crack root area of 321SS sheath

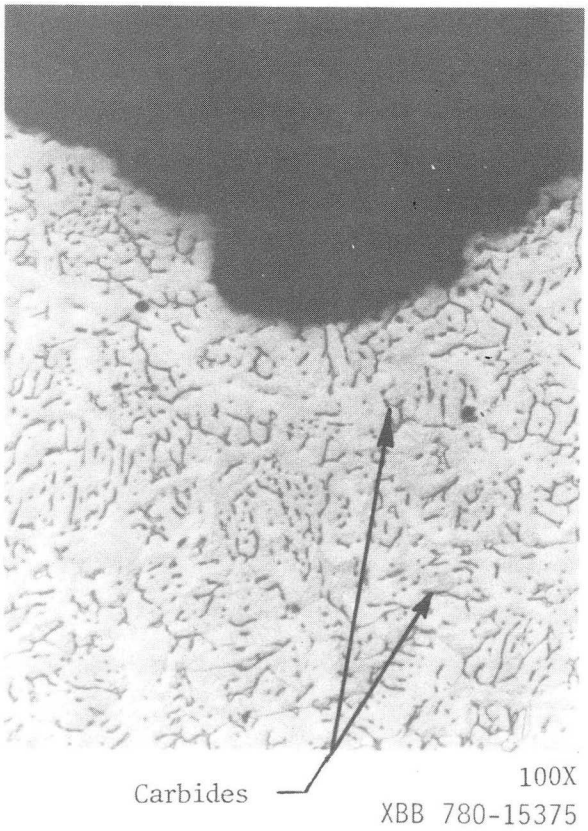

Fig. 32 304SS burner stop fin cross section

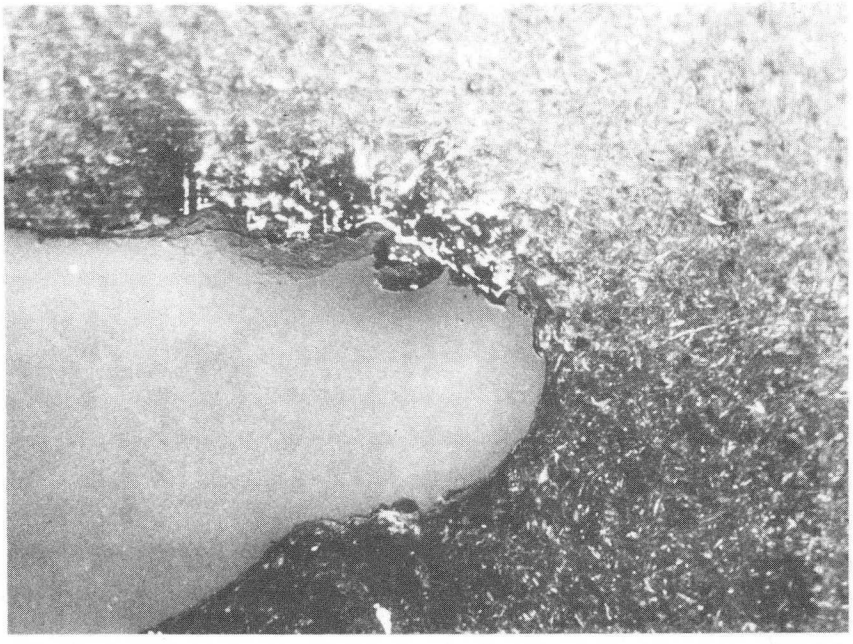

20X

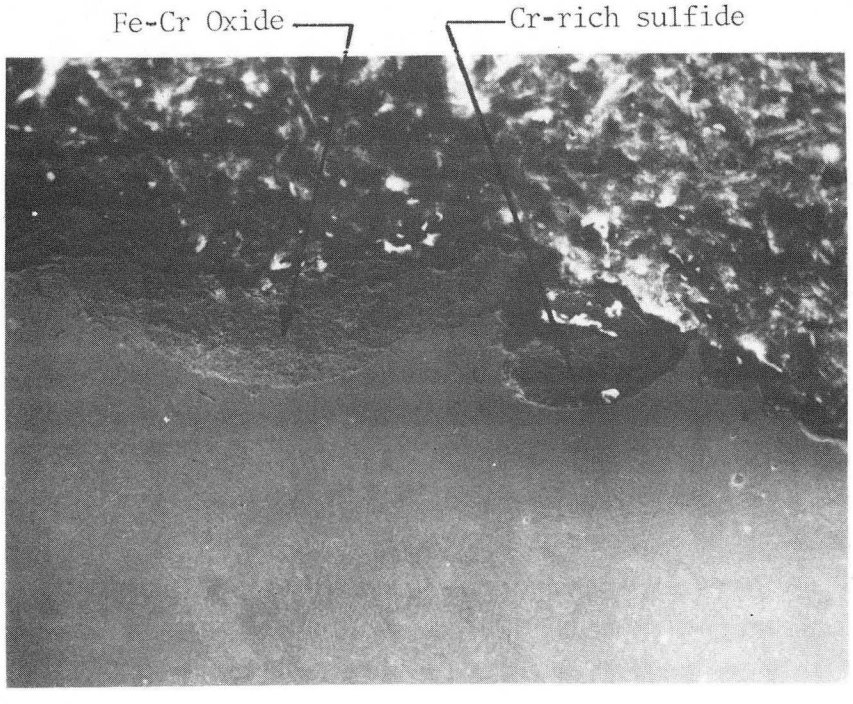

50X
XBB 780-15377

Fig. 33 SEM cross section of burner stop fin

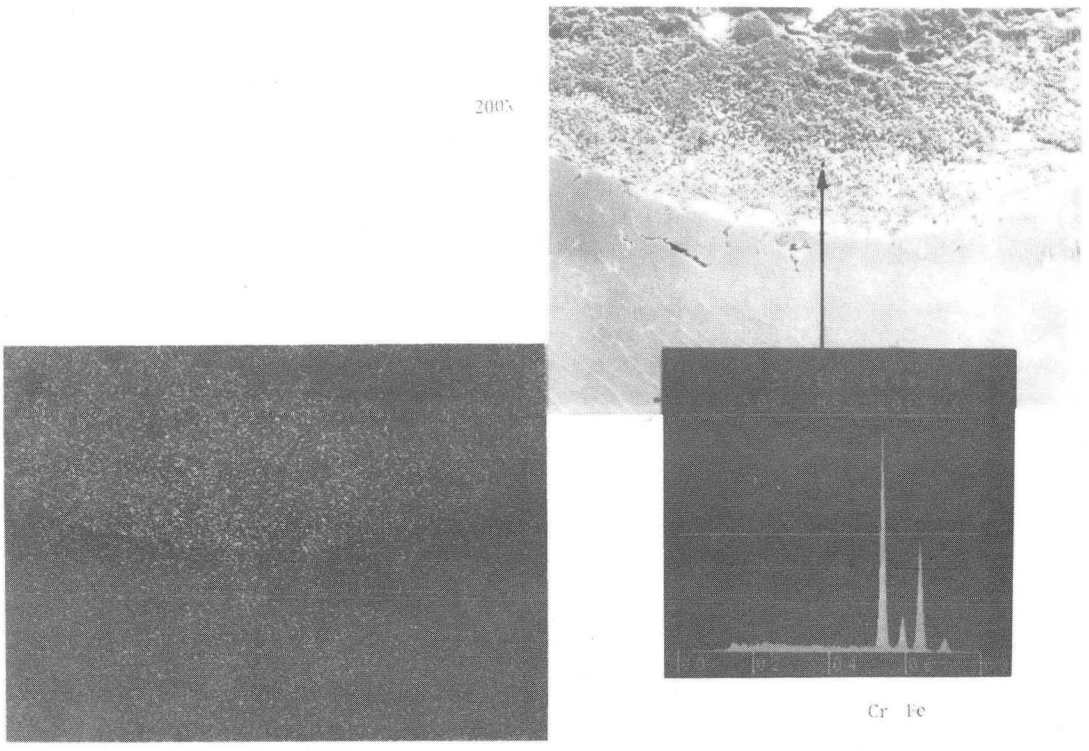

XBB 780-15378

Fig. 34 Fe-Cr-O spinel scale area

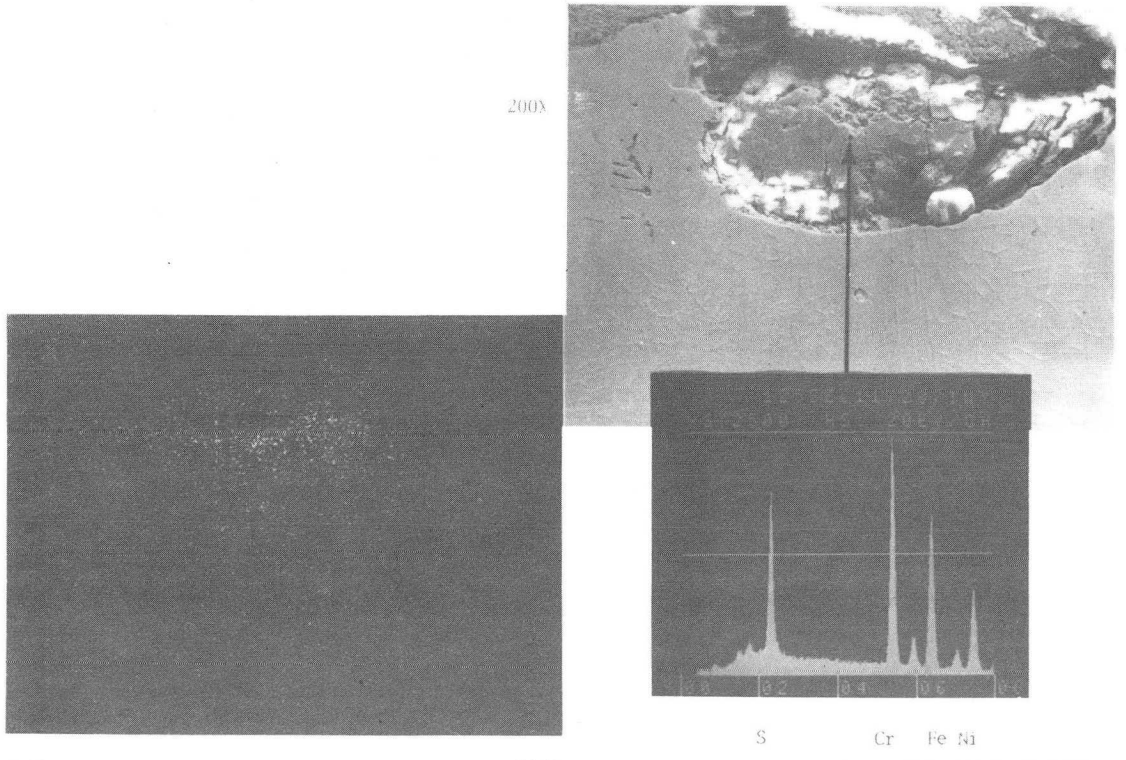

XBB 780-15379

Fig. 35 Fe-Cr-S spinel scale area

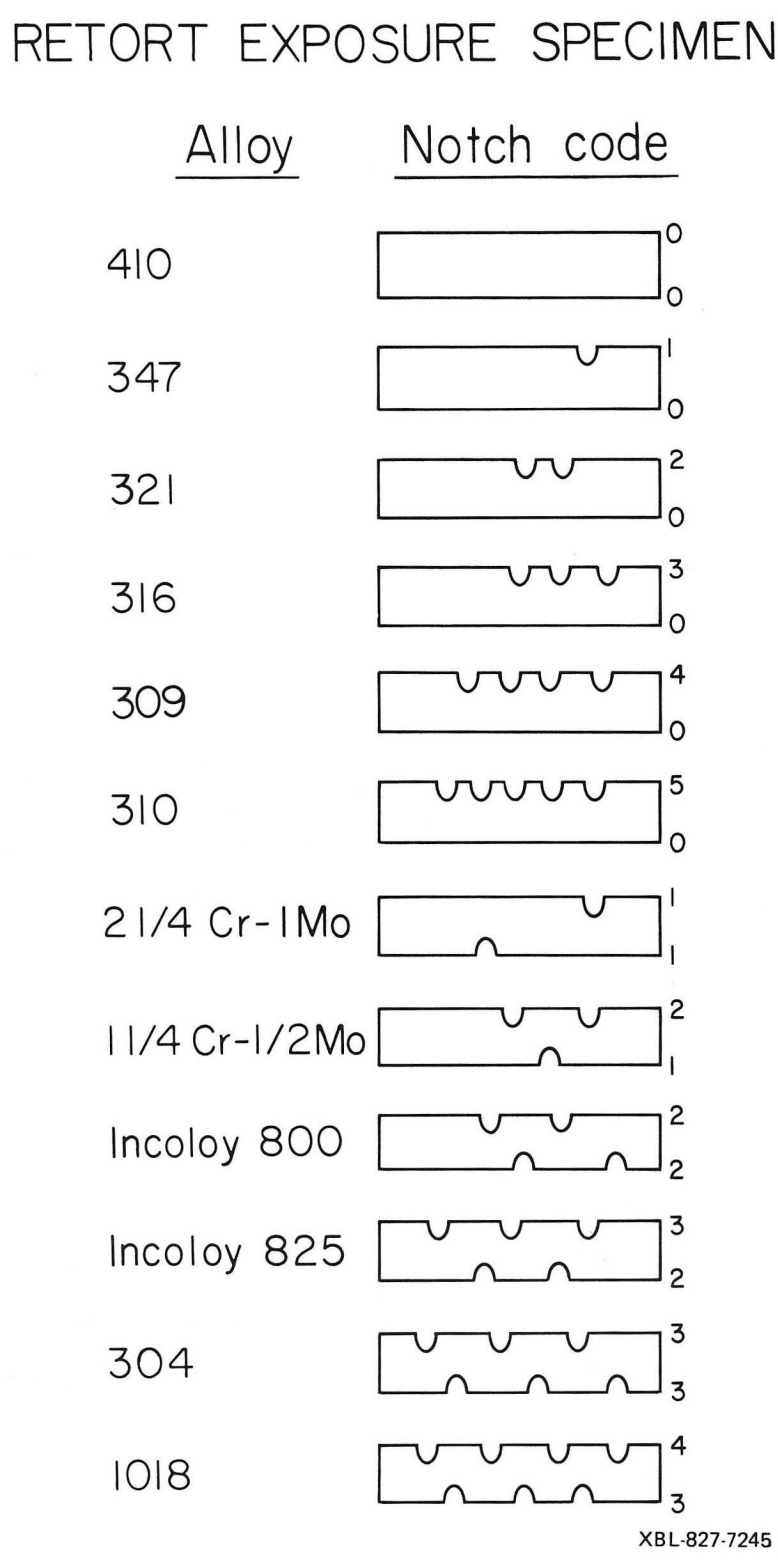

Fig. 36 Notched patterns of alloys tested

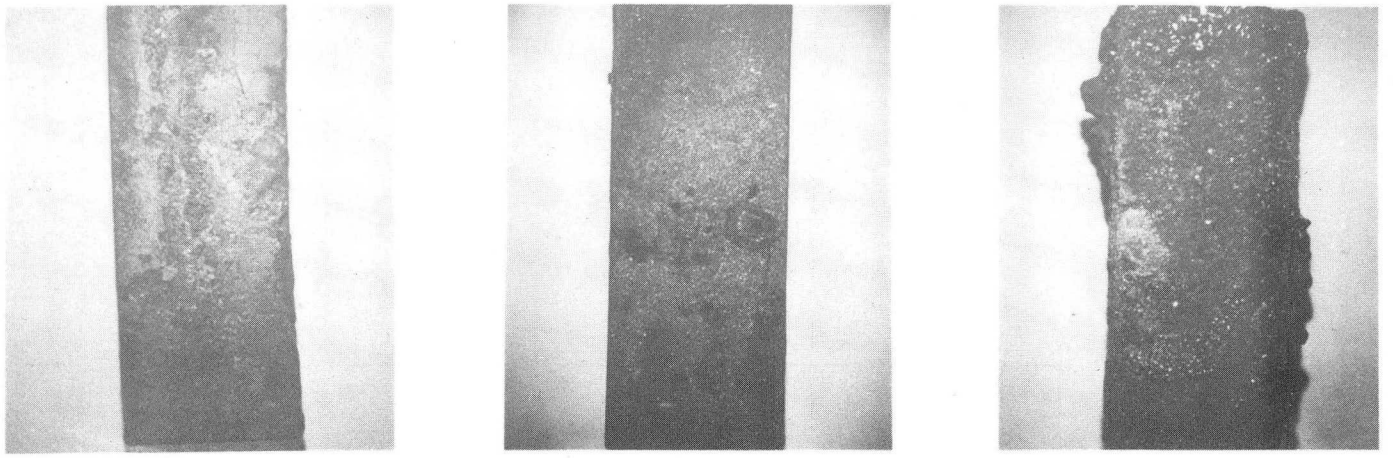

304 #1 304 #2 1018 #3

1018 #4 1018 #5 1018 #6

XBB 783-3232A

Fig. 37 Appearance of specimens exposed in retort S-49

1018 ANTRIM SHALE SPECIMEN

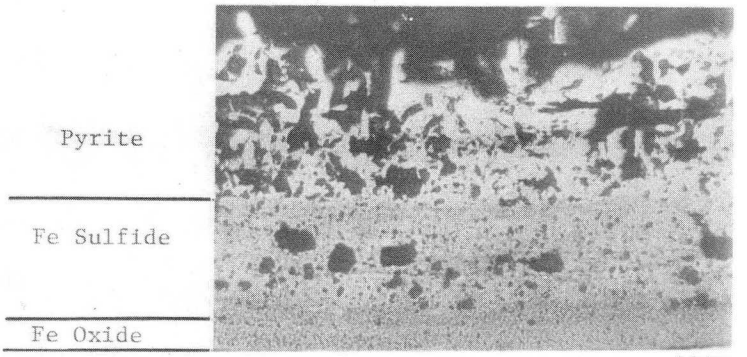

Scale Above substrate

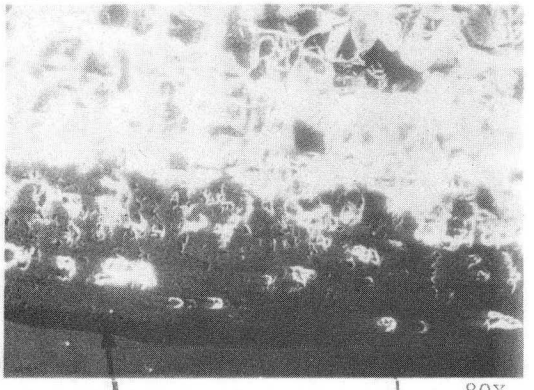

Dark Fe Oxide Layer

S Map

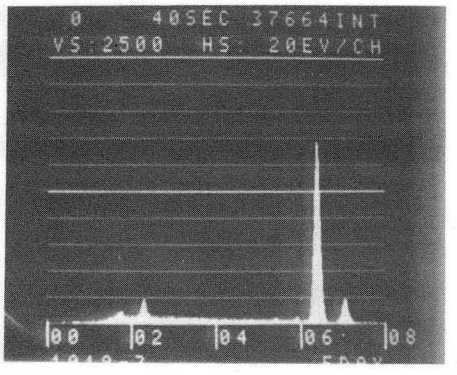

EDAX inside FeO Layer

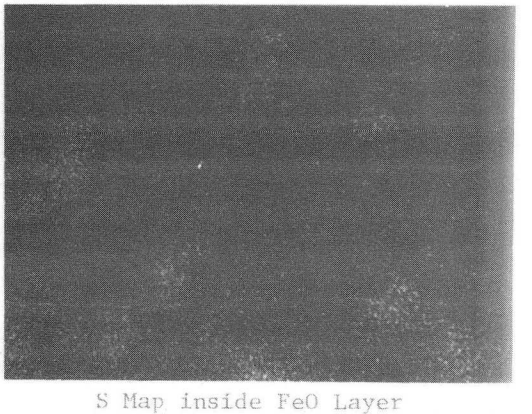

S Map inside FeO Layer

XBB 783-3231A

Fig. 38 Micrographs, peak analyses and x-ray maps of 1018 steel

304 ANTRIM SHALE SPECIMEN

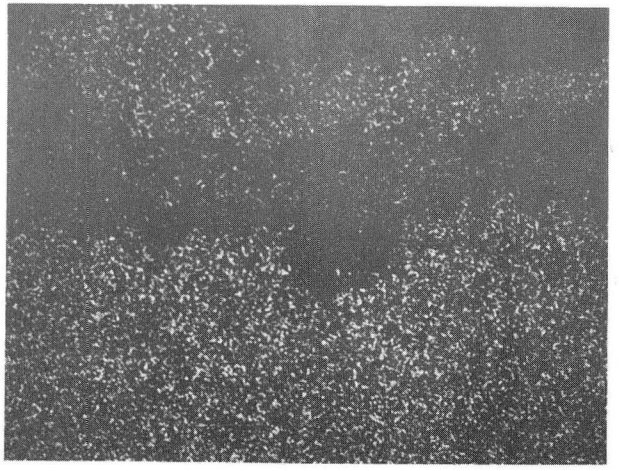

Fe Map at 1000X

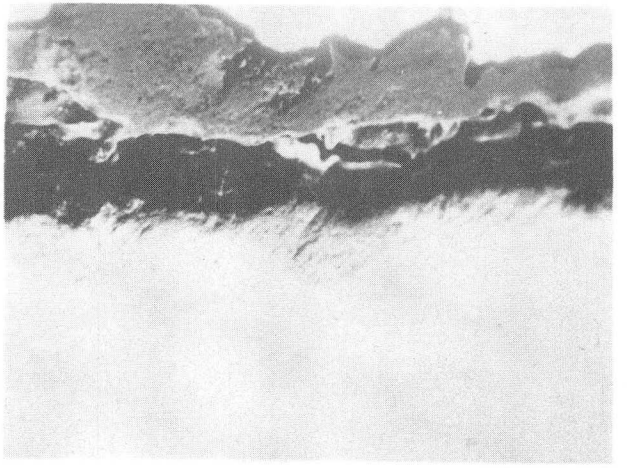

1000X

Cr Map at 1000X

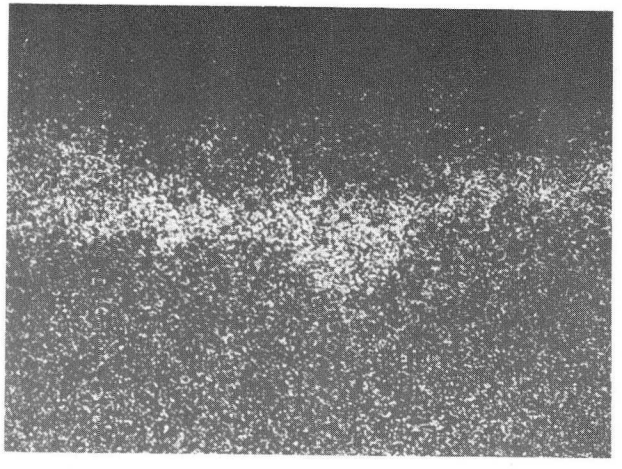

S Map at 1000X

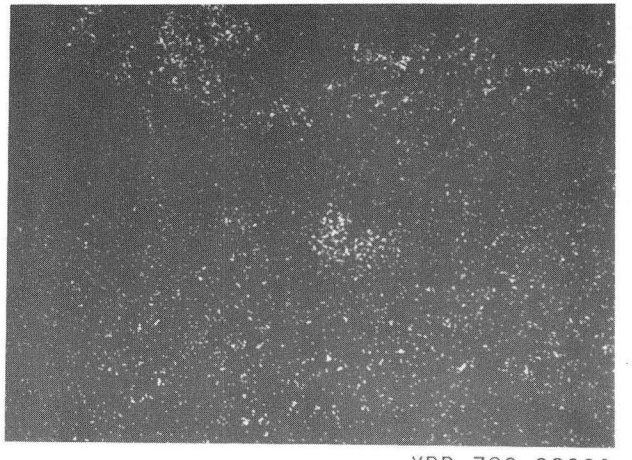

XBB 783-3233A

Fig. 39 Micrograph and x-ray maps of 304SS

304 ANTRIM SHALE SPECIMEN

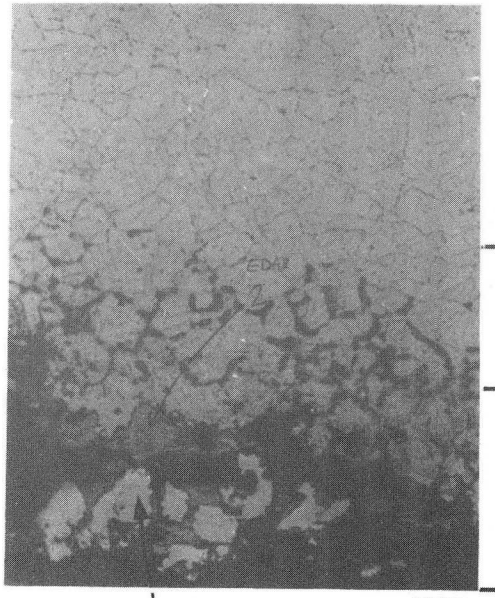

Carbides

Sulfides

.01 in.

Fe/Cr and Fe/Ni
Compounds

200X

1

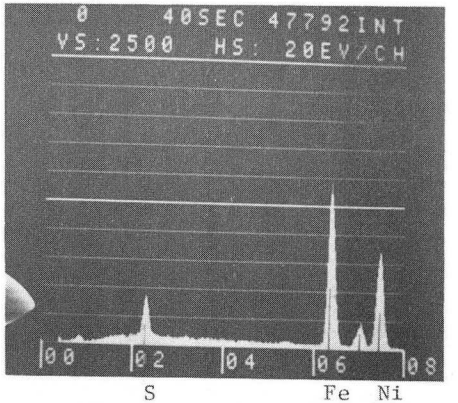

EDAX of Area 1

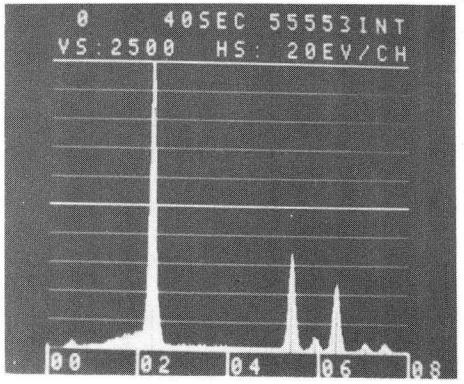

EDAX of Area 2

Blowup of
Surface Scale
860X

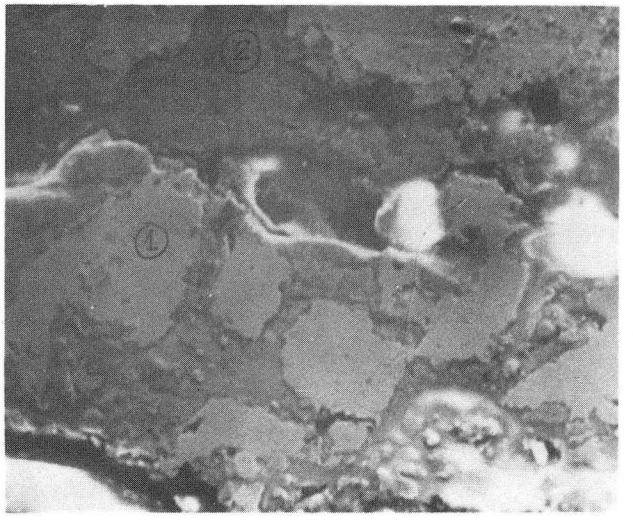

XBB 783-3237A

Fig. 40 Micrographs and peak analyses of 304SS

304 ANTRIM SHALE SPECIMEN

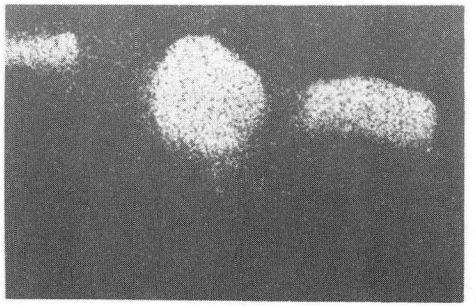

Si Map at 2000X

EDAX of Area 3

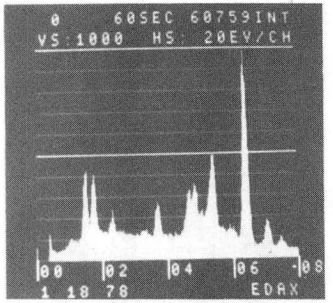

Al Si Ca Ce CrFe Ni

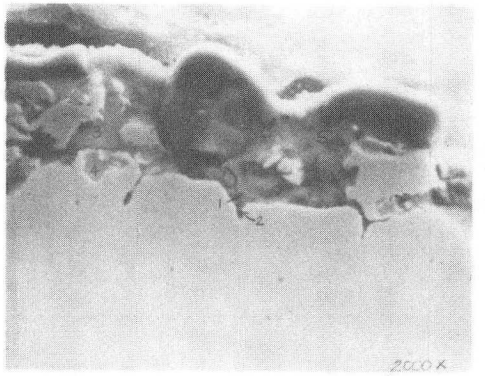

EDAX of Area 5

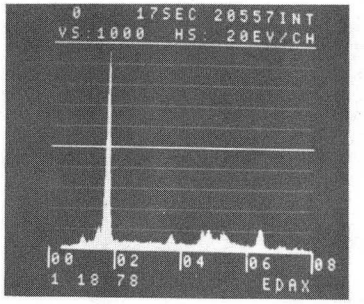

Si

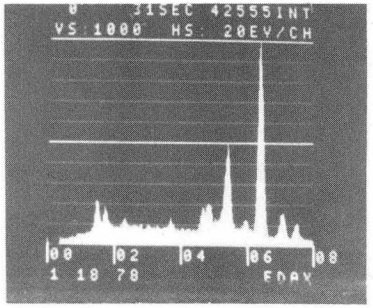

EDAX of Area 4

Al Si Ce CrFe Ni

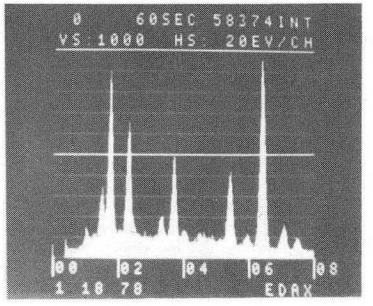

EDAX of Area 1

Al SiS K Ca Cr Fe Ni

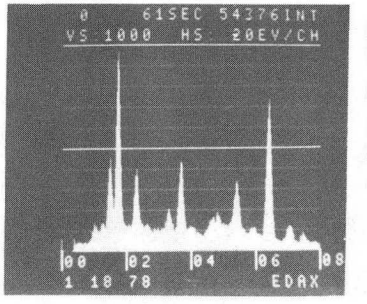

EDAX of Area 2

AlSiS KCa Cr Fe Ni

XBB 738-3236A

Fig. 41 Local area of scale on 304SS showing entrapped Si compound from shale

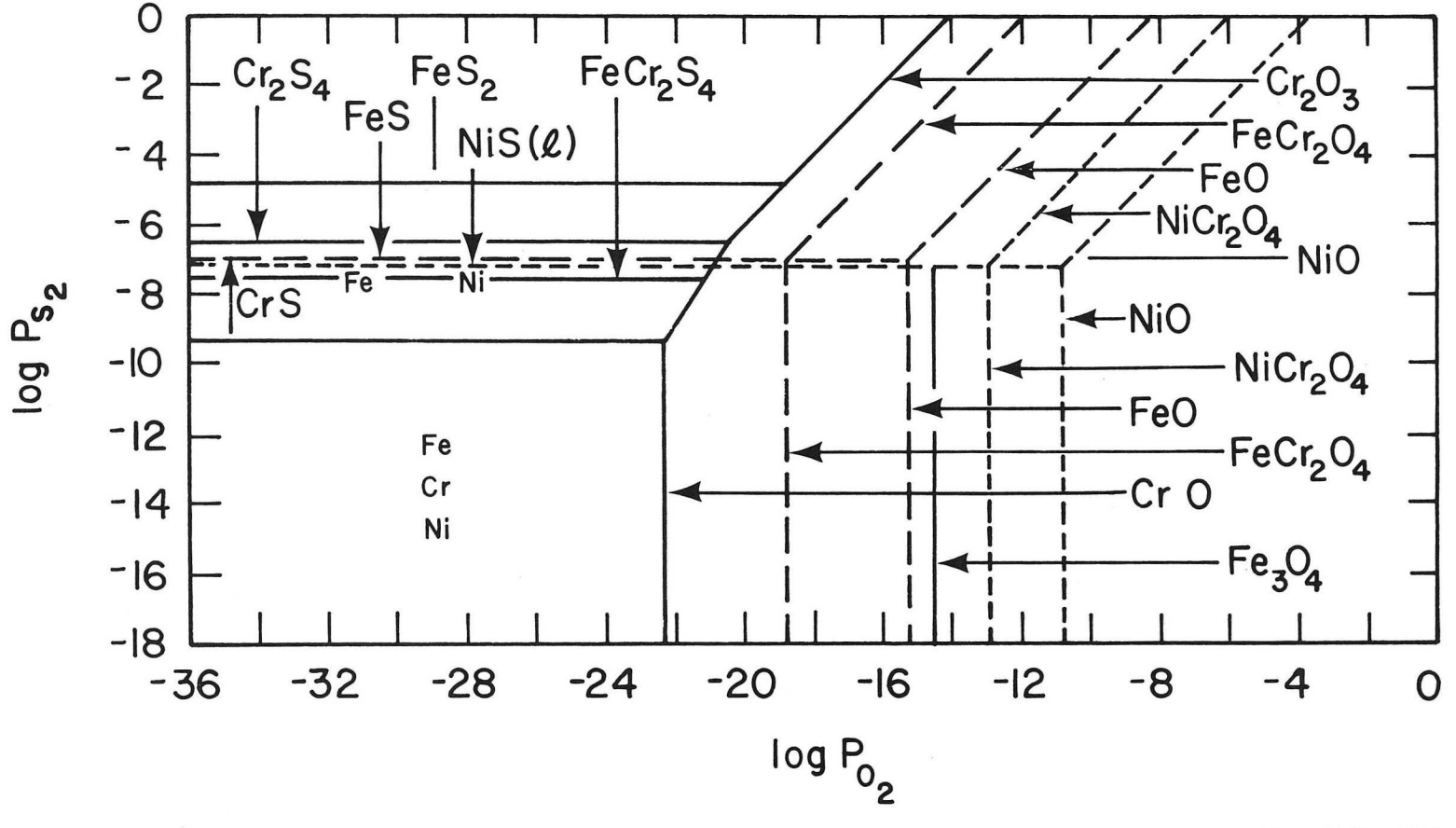

XBL 791-188

Fig. 42 Thermodynamic equilibrium stability diagram for Fe-Cr-Ni

CBB 789-12361

Fig. 43. 11-ton simulated in-situ retort at [illegible]

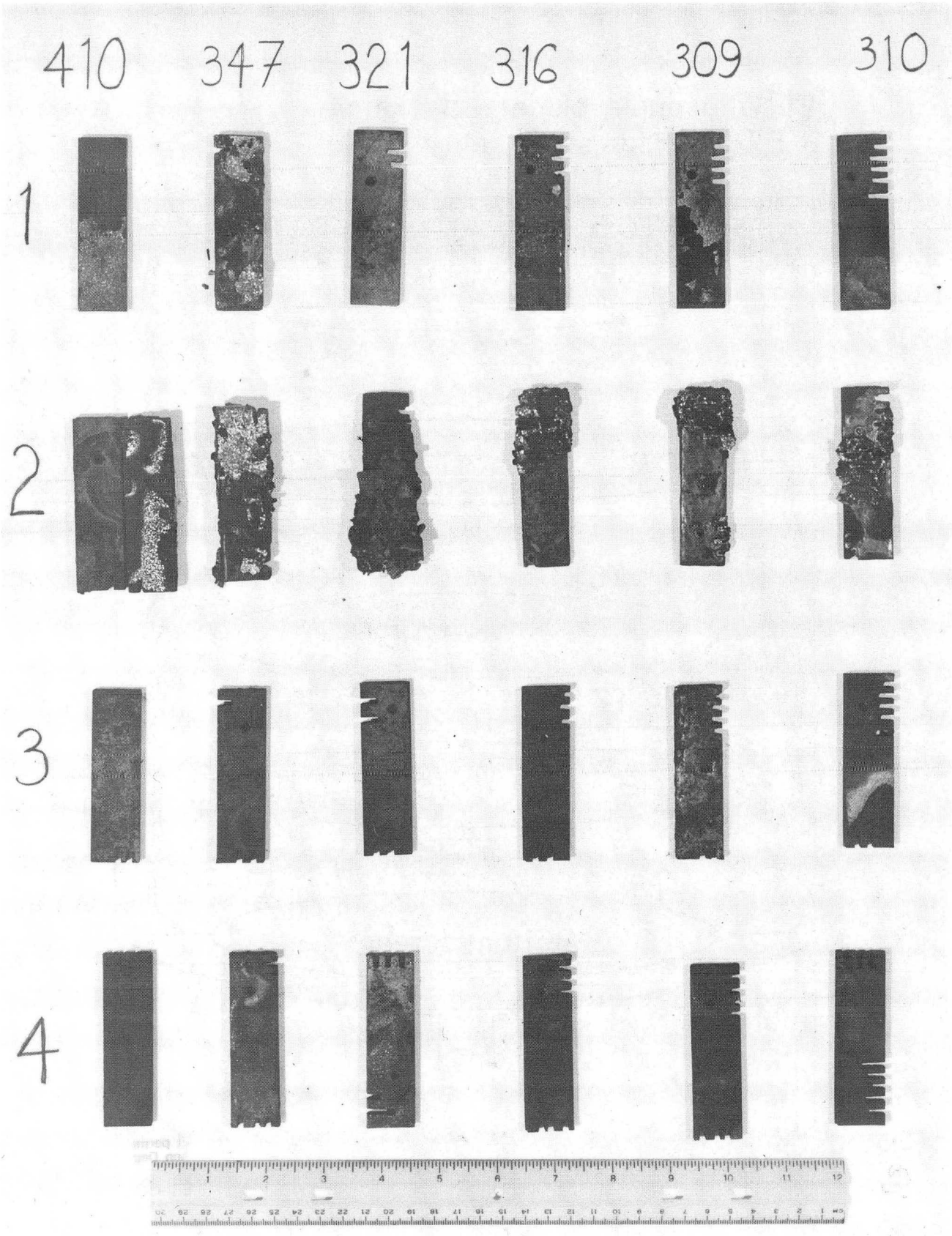

CBB 786-6950

Fig. 44 Appearance of stainless steel specimens from retort S-54

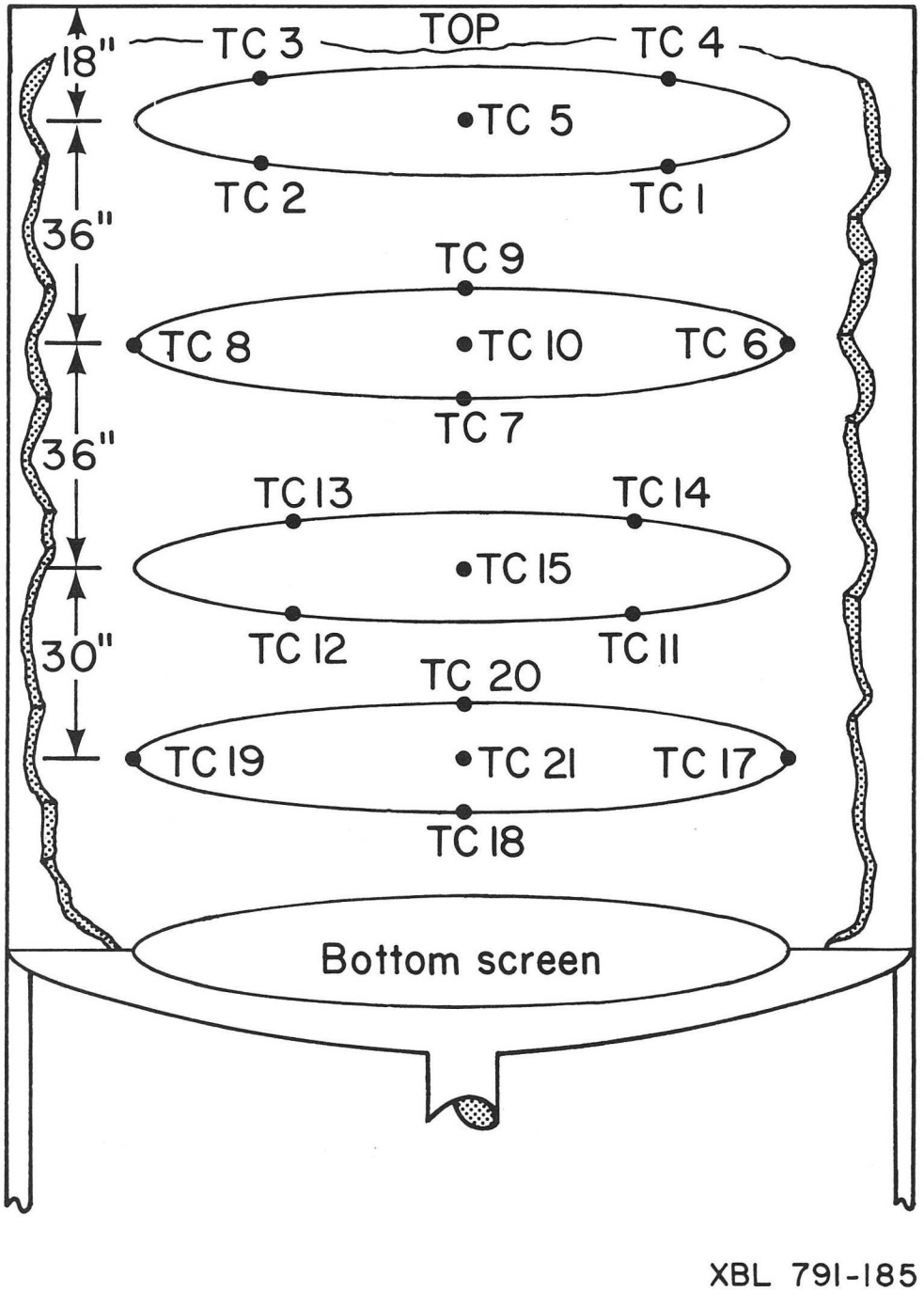

Fig. 45 Thermocouple locations in LETC 10 ton retort

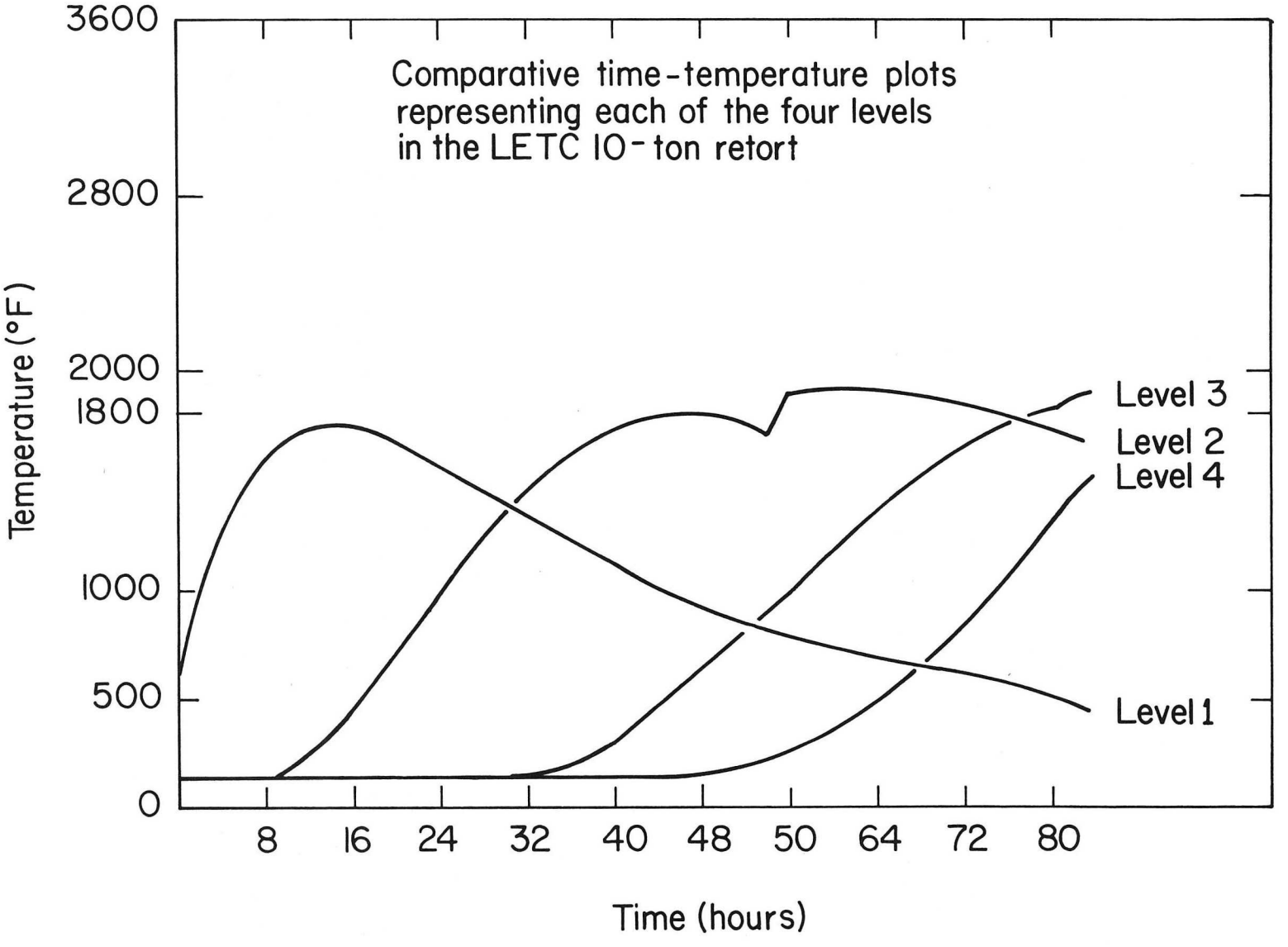

Fig. 46 Time-temperature curves for all four levels in retort S-54

Fig. 47 410SS specimen from level 2

CBB 786-7938

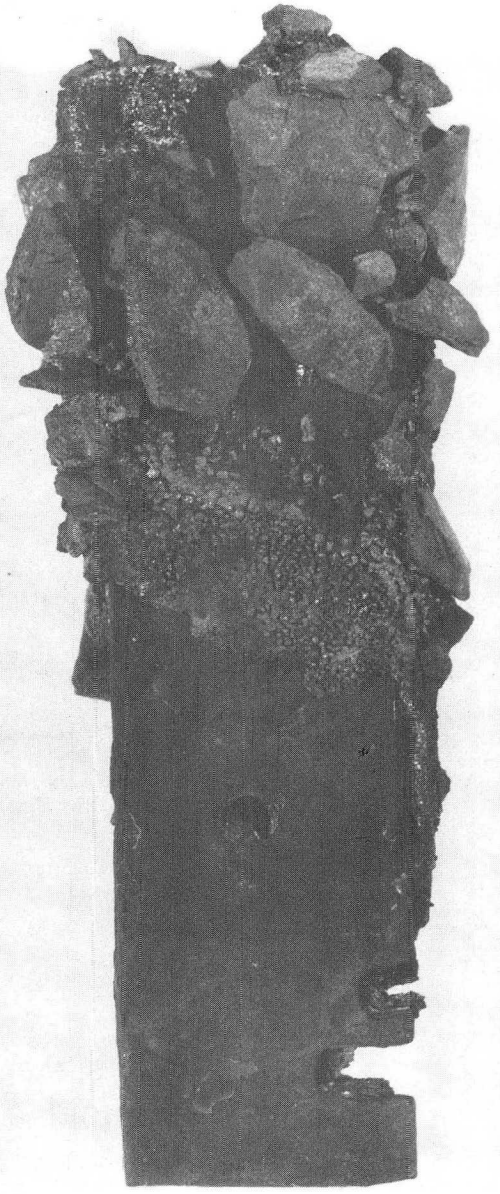

Fig. 48 321SS specimen from level 2

CBB 786-7928

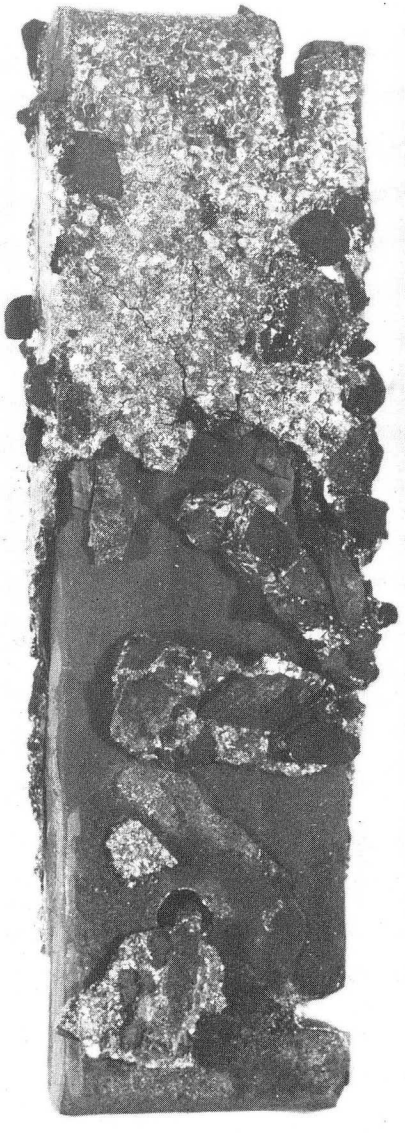

Fig. 49 347SS specimen from level 2

CBB 786-7940

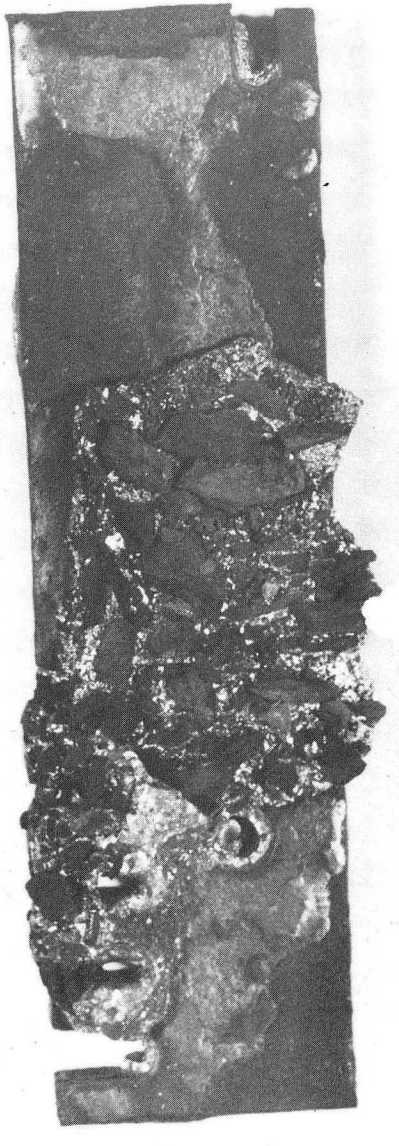

Fig. 50 310SS specimen from level 2

CBB 786-7922

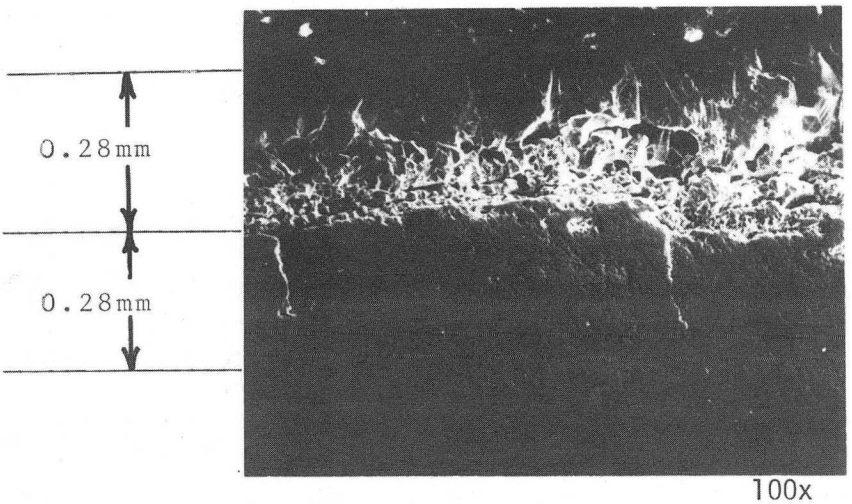

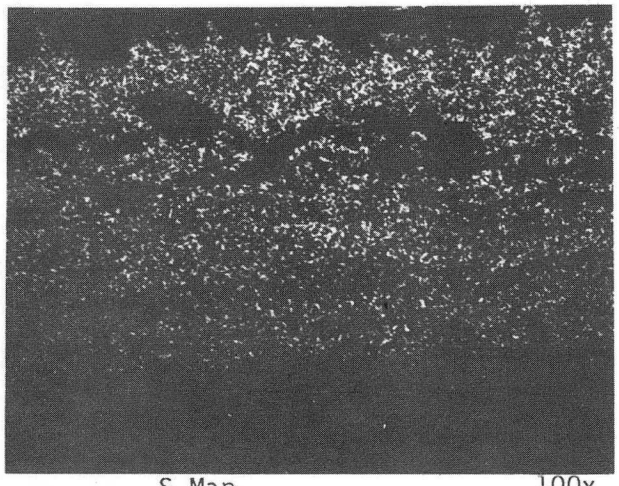

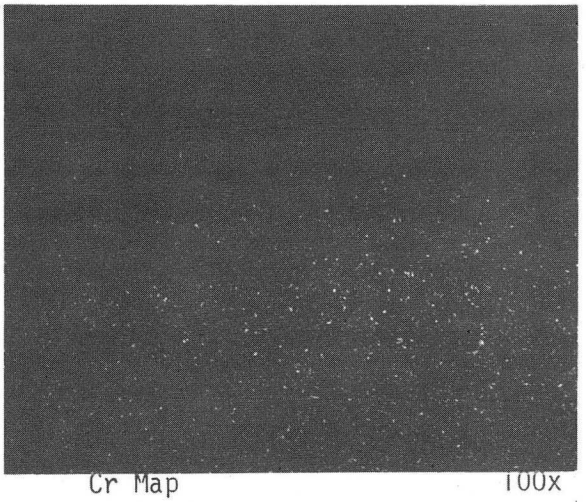

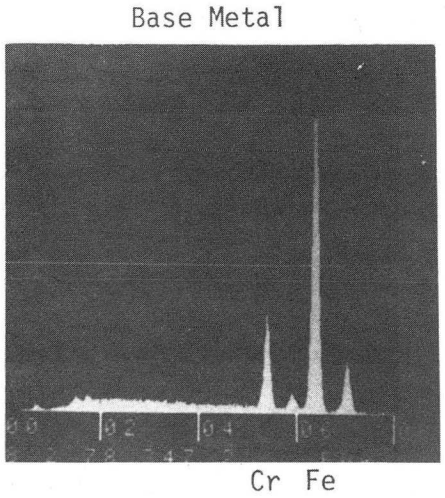

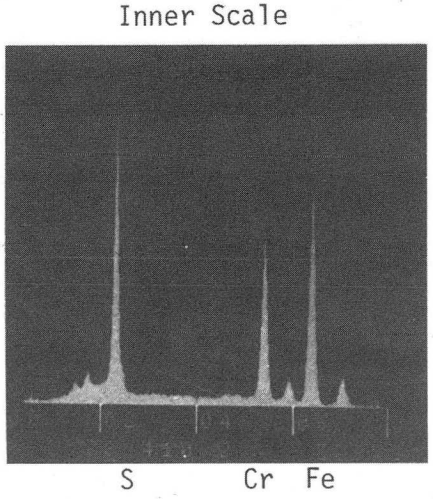

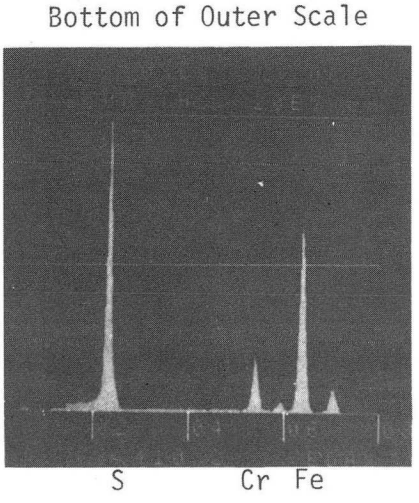

Fig. 51 Micrograph, x-ray maps and peak analyses of 410SS, level 2

XBB 789-12298A

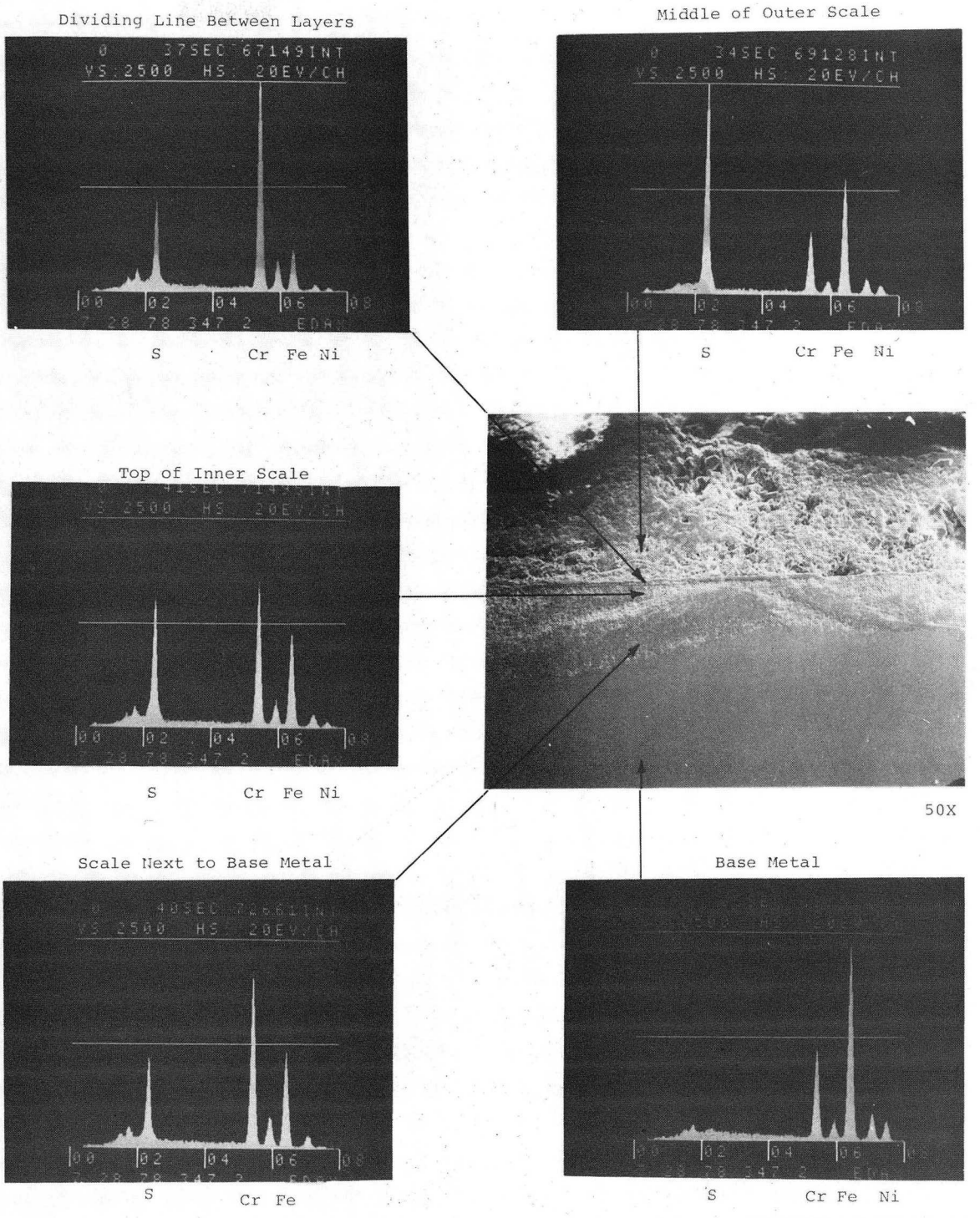

Fig. 52 Micrograph and peak analyses of 347SS, level 2

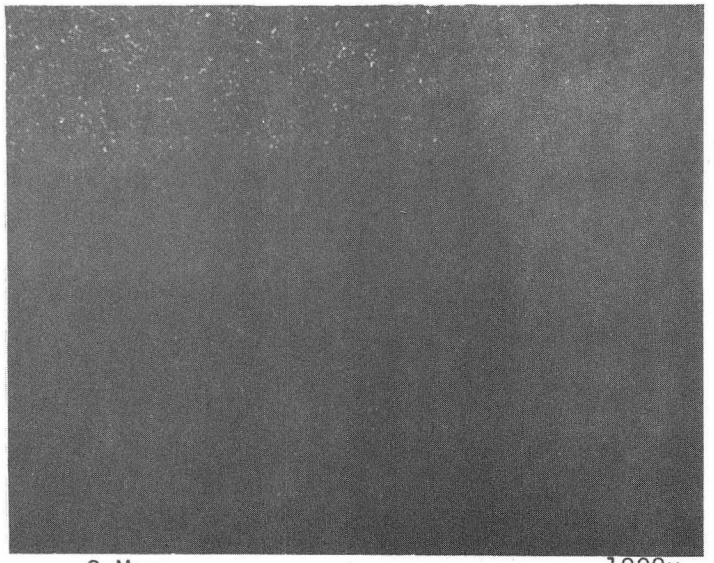

S Map 1000x

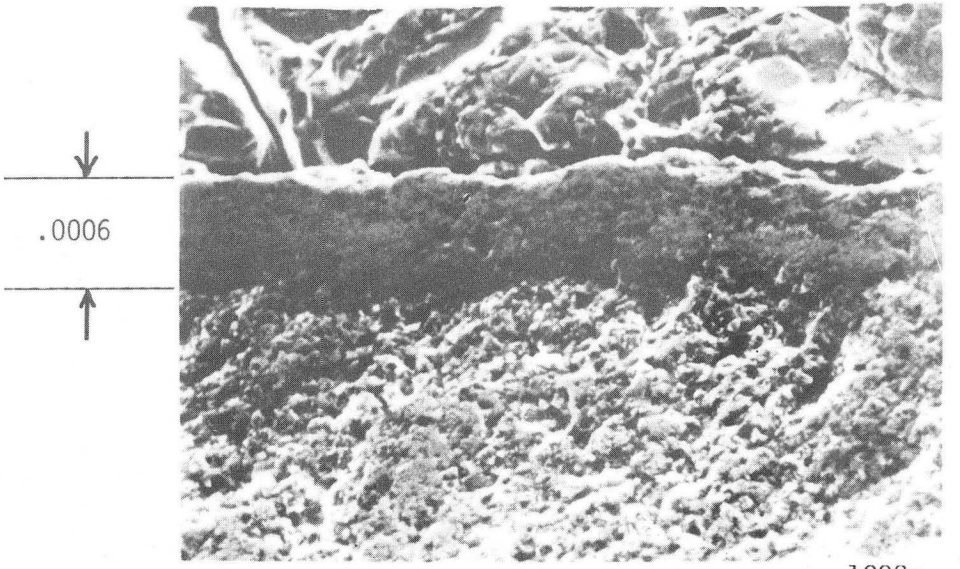

1000x

Cr Map 1000x

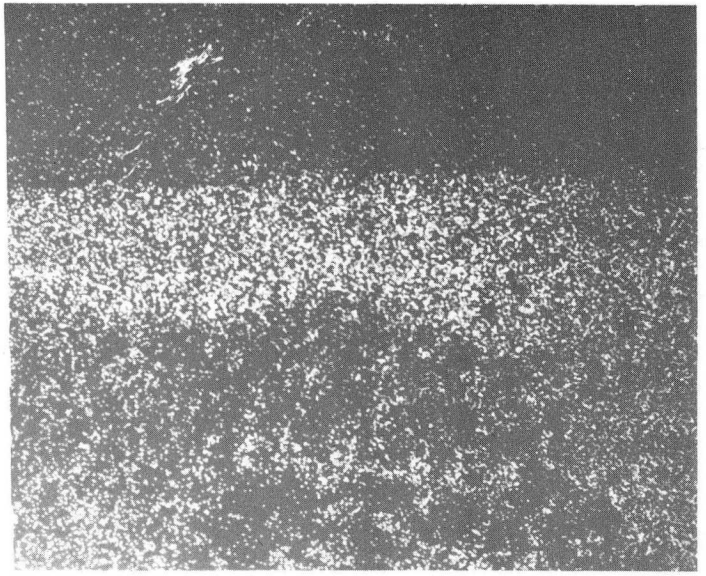

Fe Map 1000x

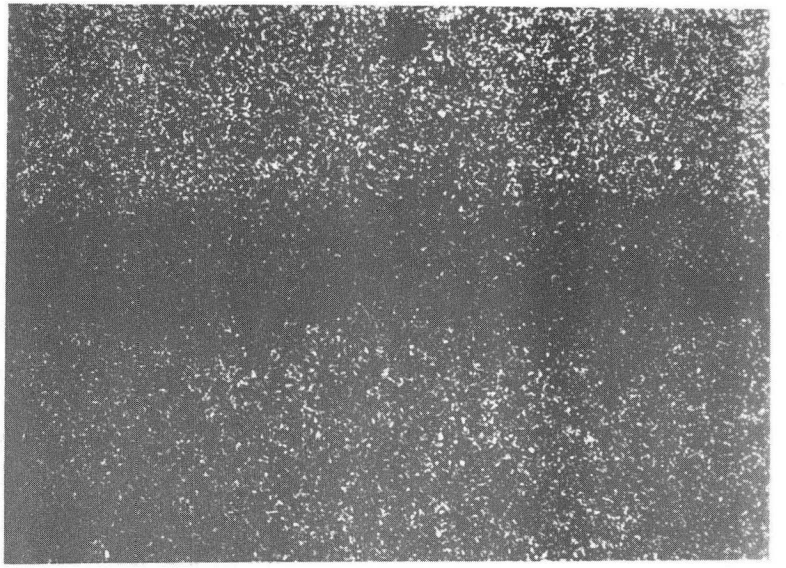

XBB 789-12299A

Fig. 53 High magnification micrograph and x-ray maps of 347SS, level 2

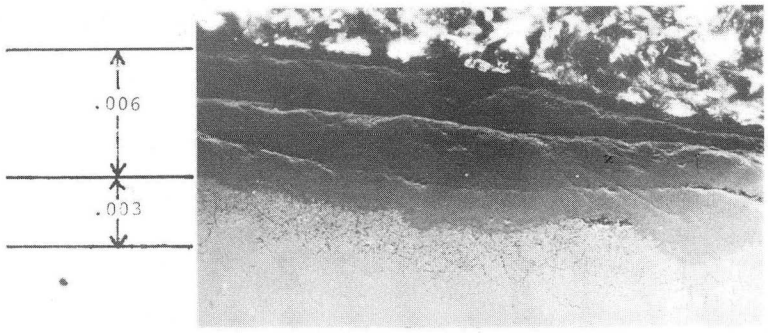

200X

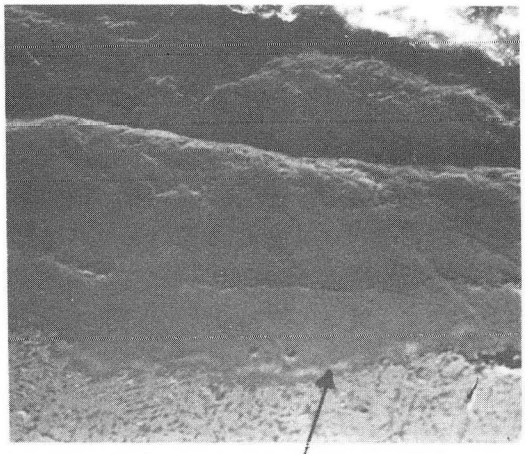

Cr Oxide Layer

500X

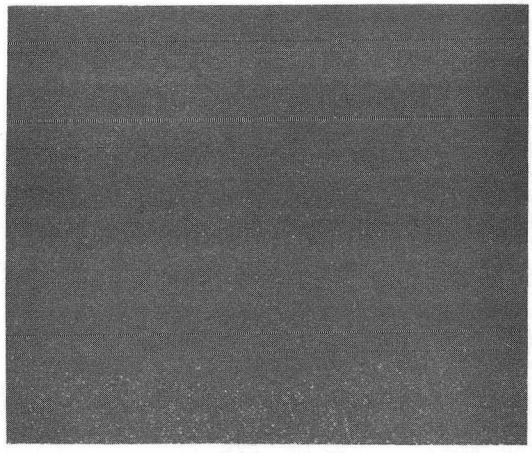

Fe Map 500X

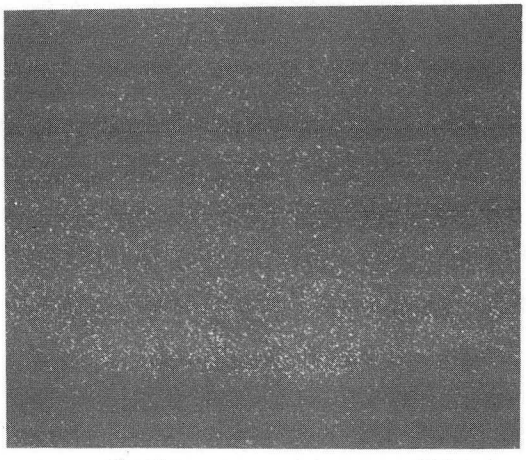

Cr Map 500X

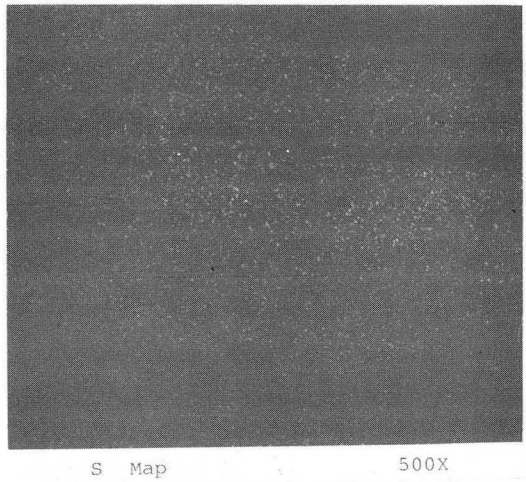

S Map 500X

XBB 789-12302A

Fig. 54 Micrograph and x-ray maps of 310SS, level 2

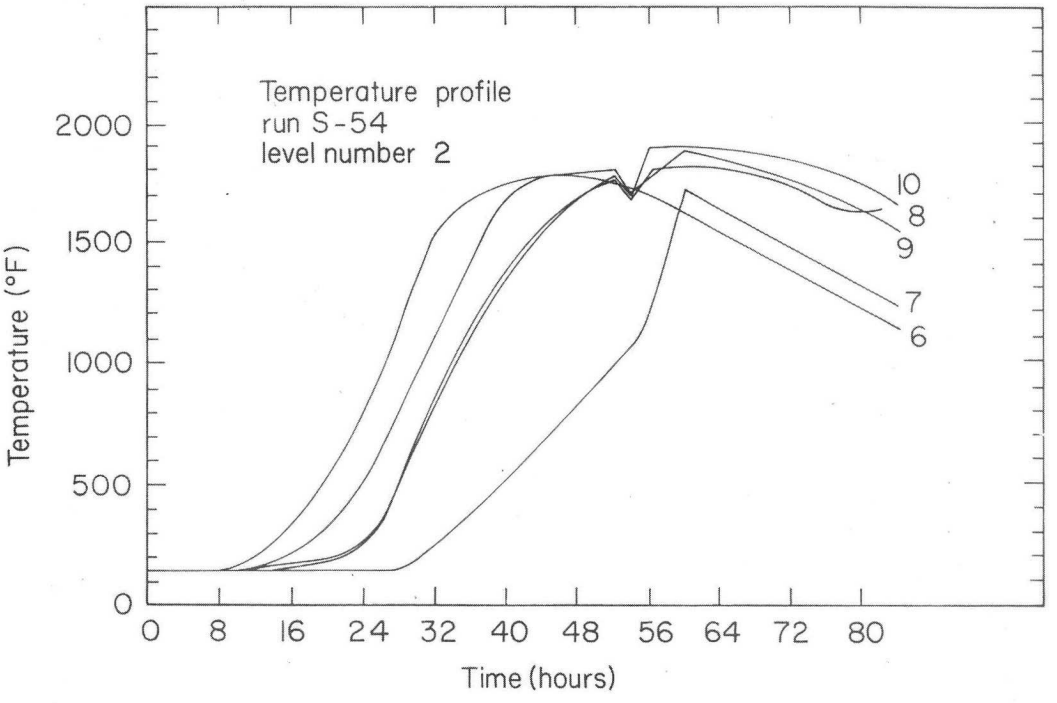

Fig. 55 Thermocouple readings at level 2 in retort S-54

XBL 791-187

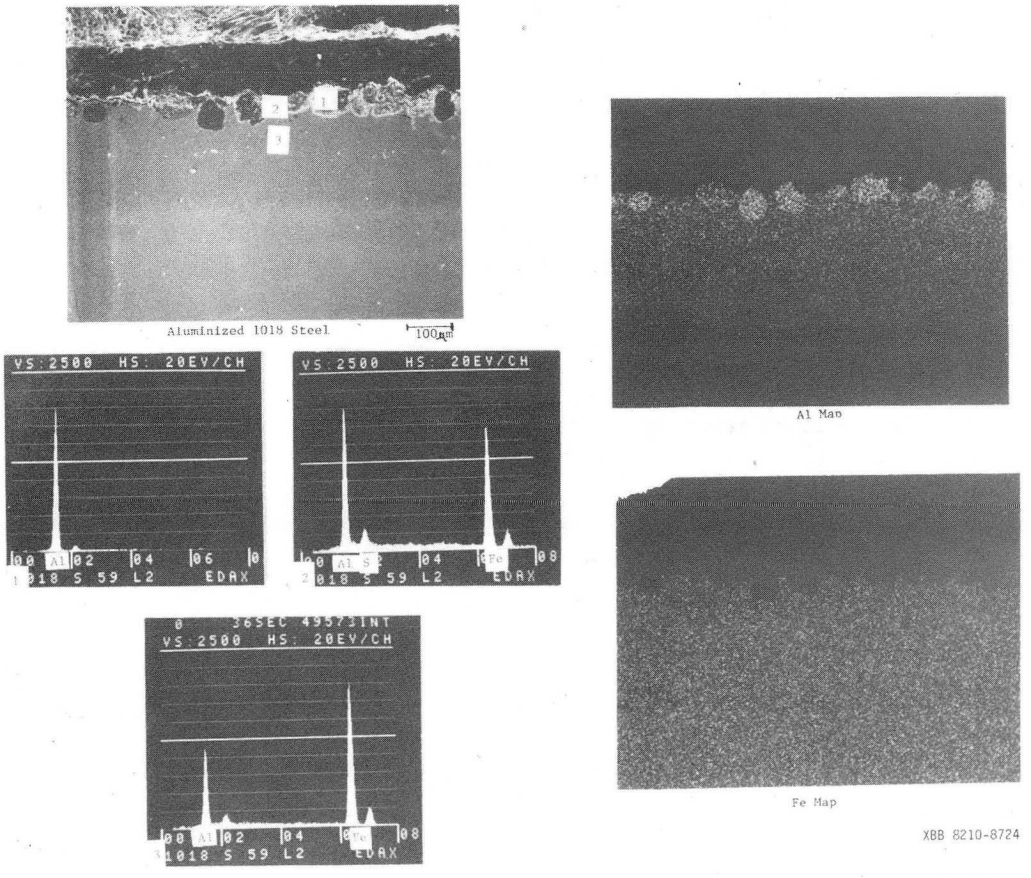

Fig. 56 Aluminized 1018 steel cross section from retort S-59

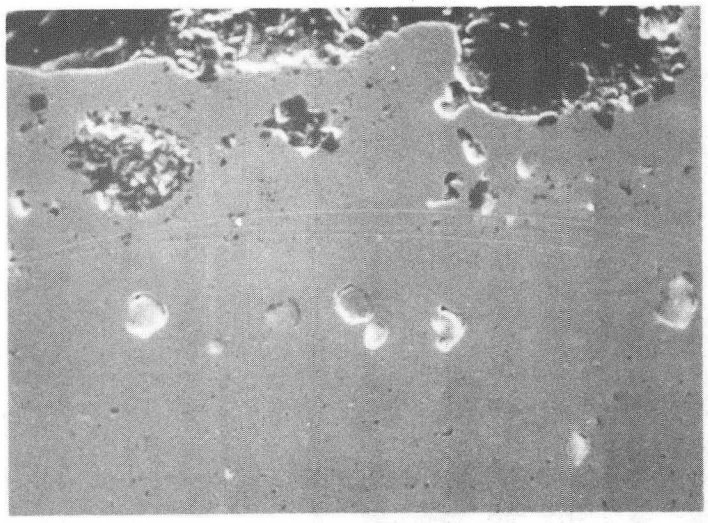

Aluminized 310SS

20μm

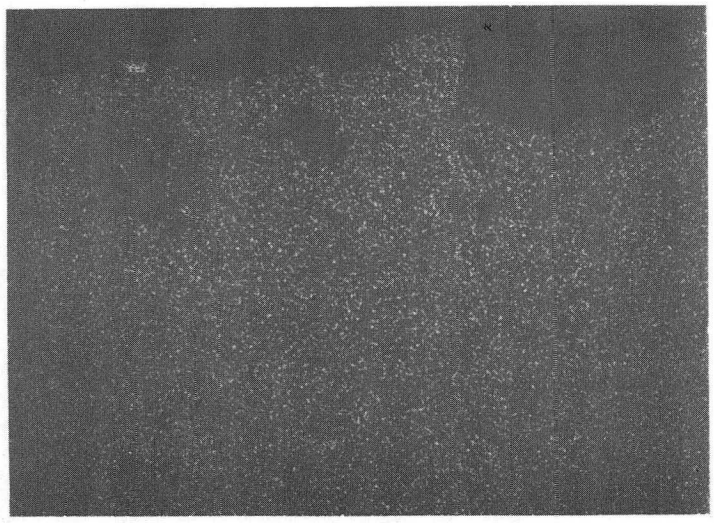

Fe Map

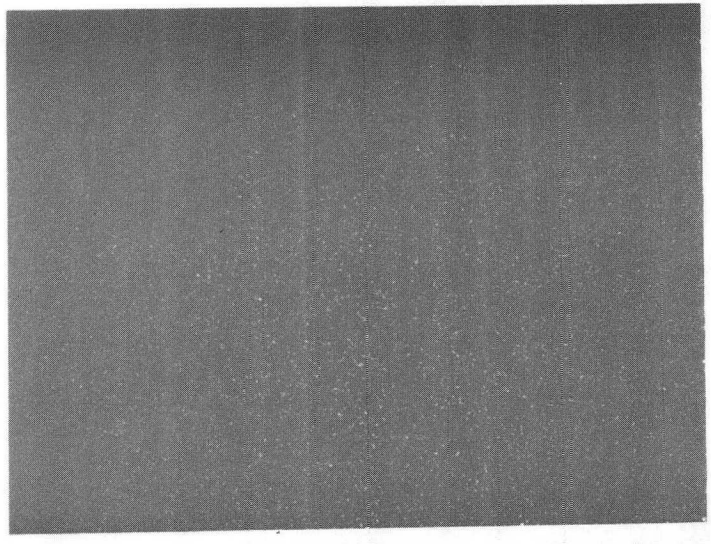

Cr Map

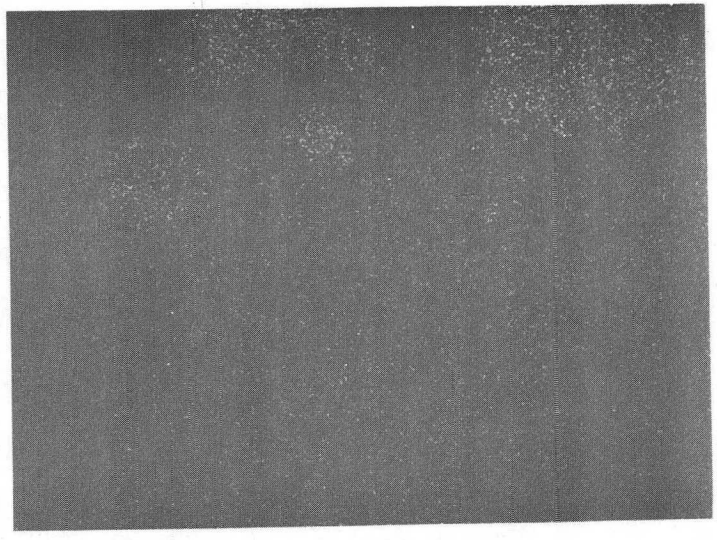

Al Map

XBB 8210-8725

Fig. 57 Aluminized 310SS cross section from retort S-59

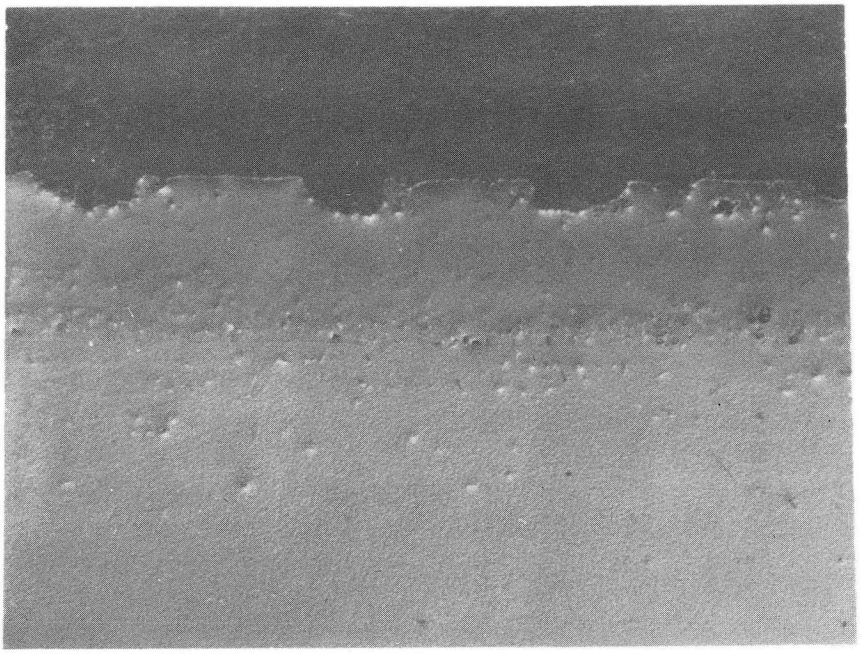

Aluminized 316SS

50μm

Fig. 58 Optical aluminized 316SS cross section from retort S-59

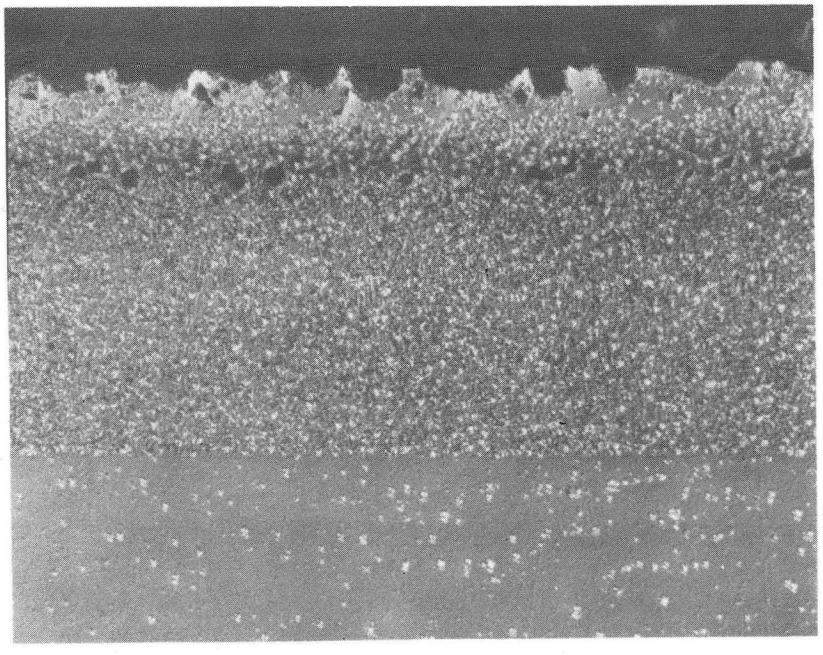

Aluminized 347SS

200μm

XBB 8210-8726

Fig. 59 Optical aluminized 347SS cross section from retort S-59

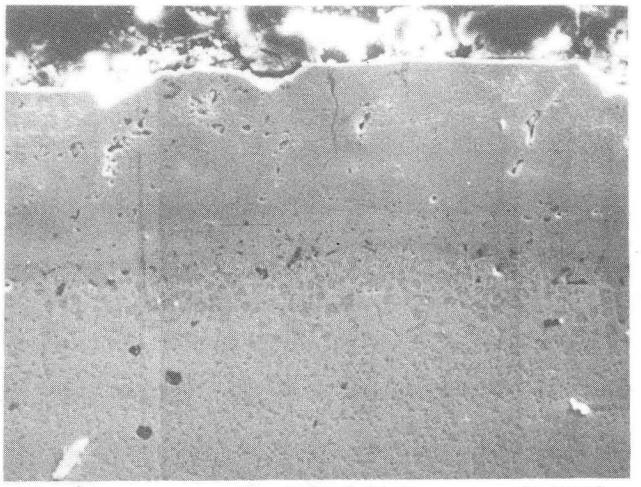

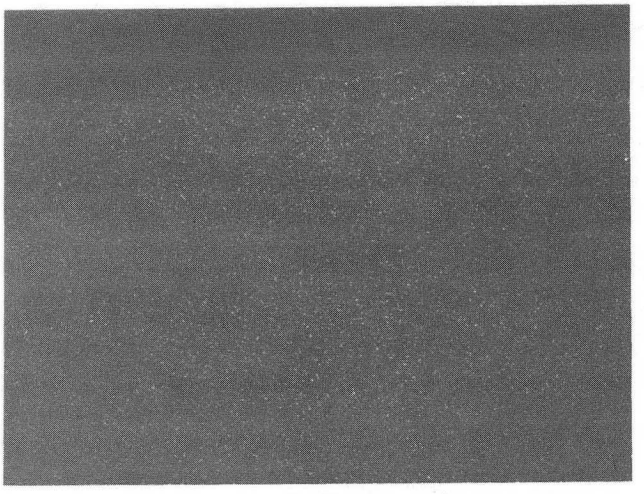

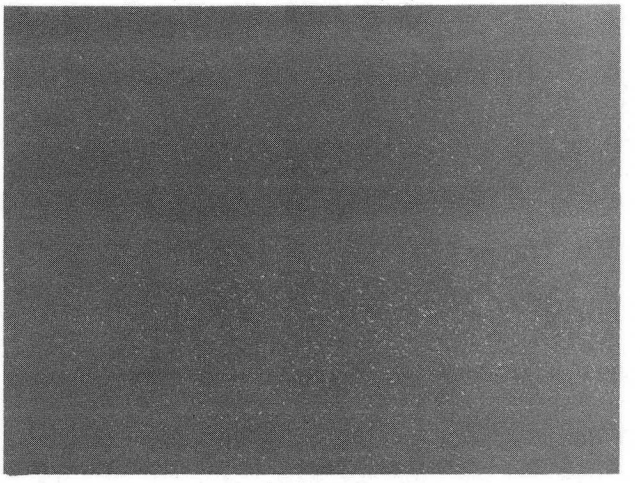

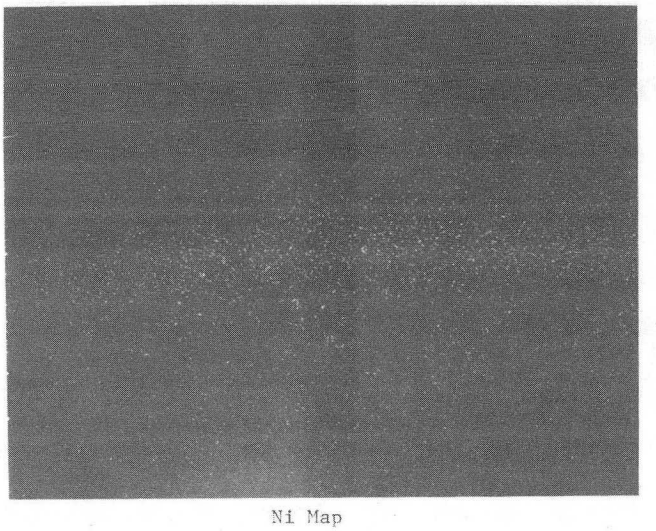

XBB 8210-8727

Fig. 60 SEM aluminized 347SS cross section from retort S-59

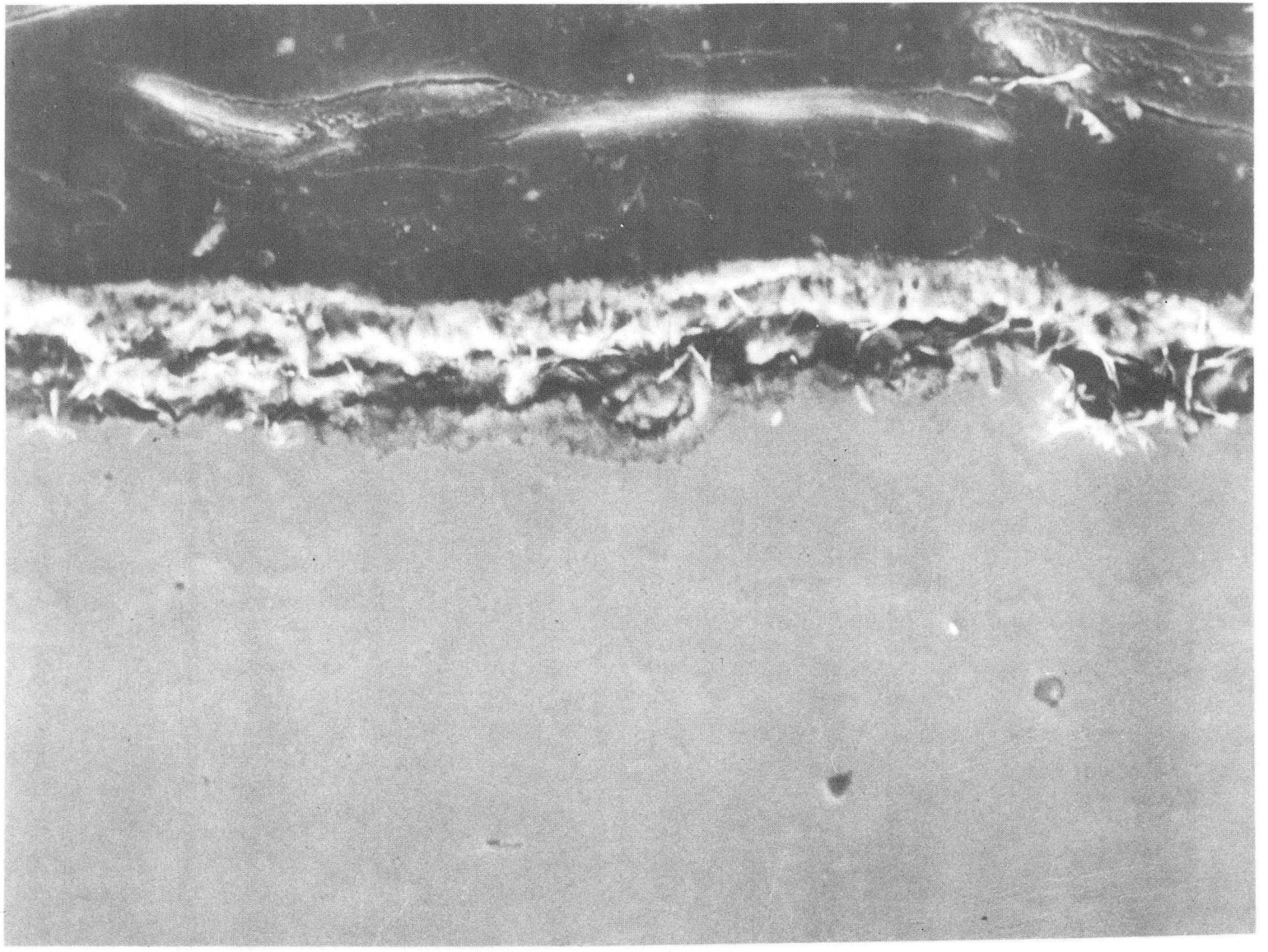

XBB 8210-8728

Fig. 61 1018 steel cross section from retort S-60

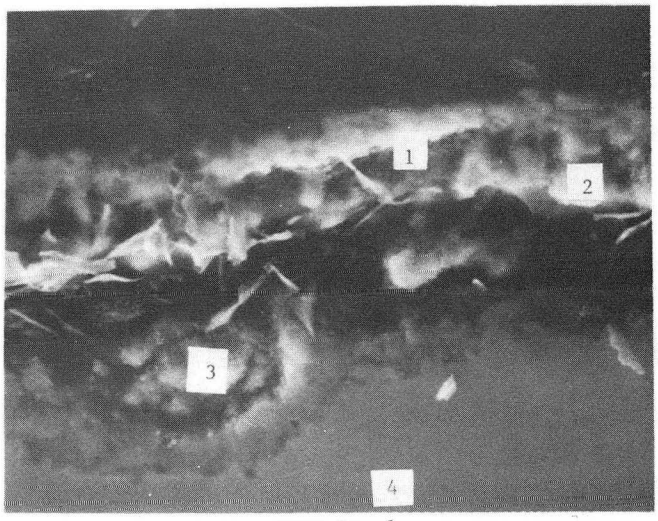

1018 Steel

40 μm

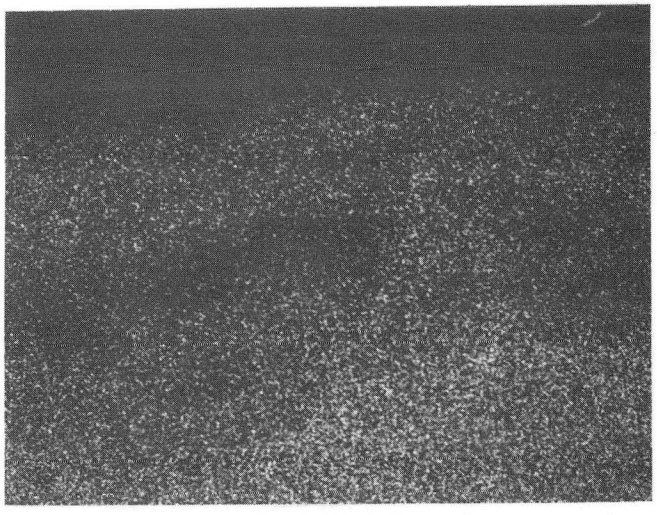

Fe Map

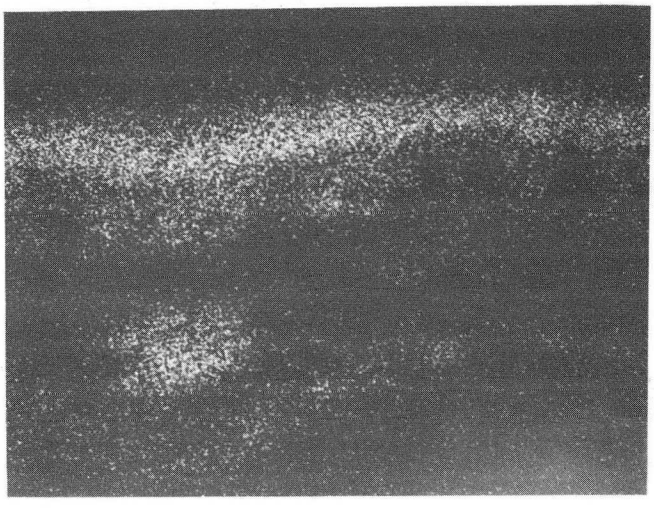

S Map

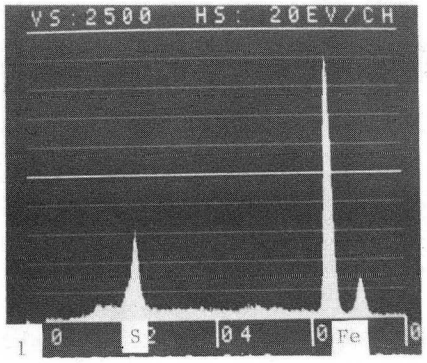

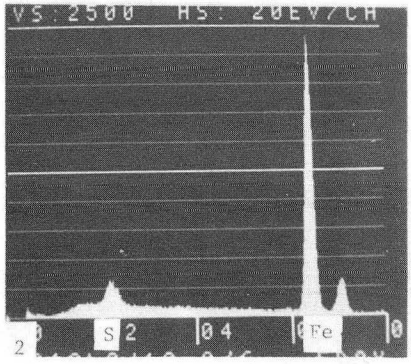

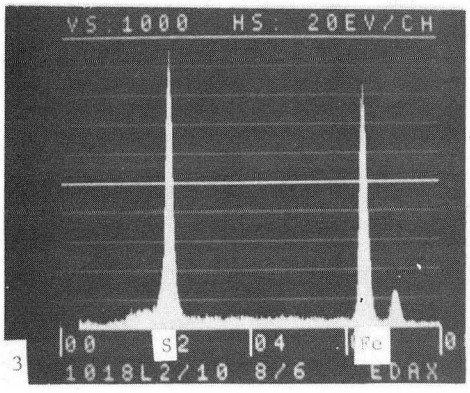

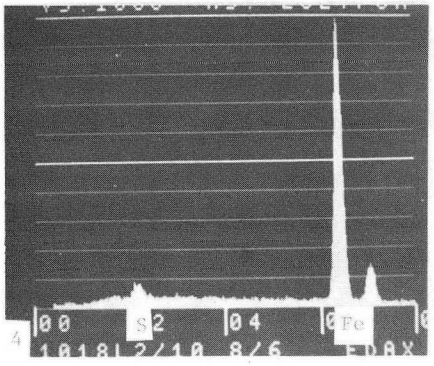

XBB 8210-8729

Fig. 62 High magnification cross section of 1018 steel from retort S-60

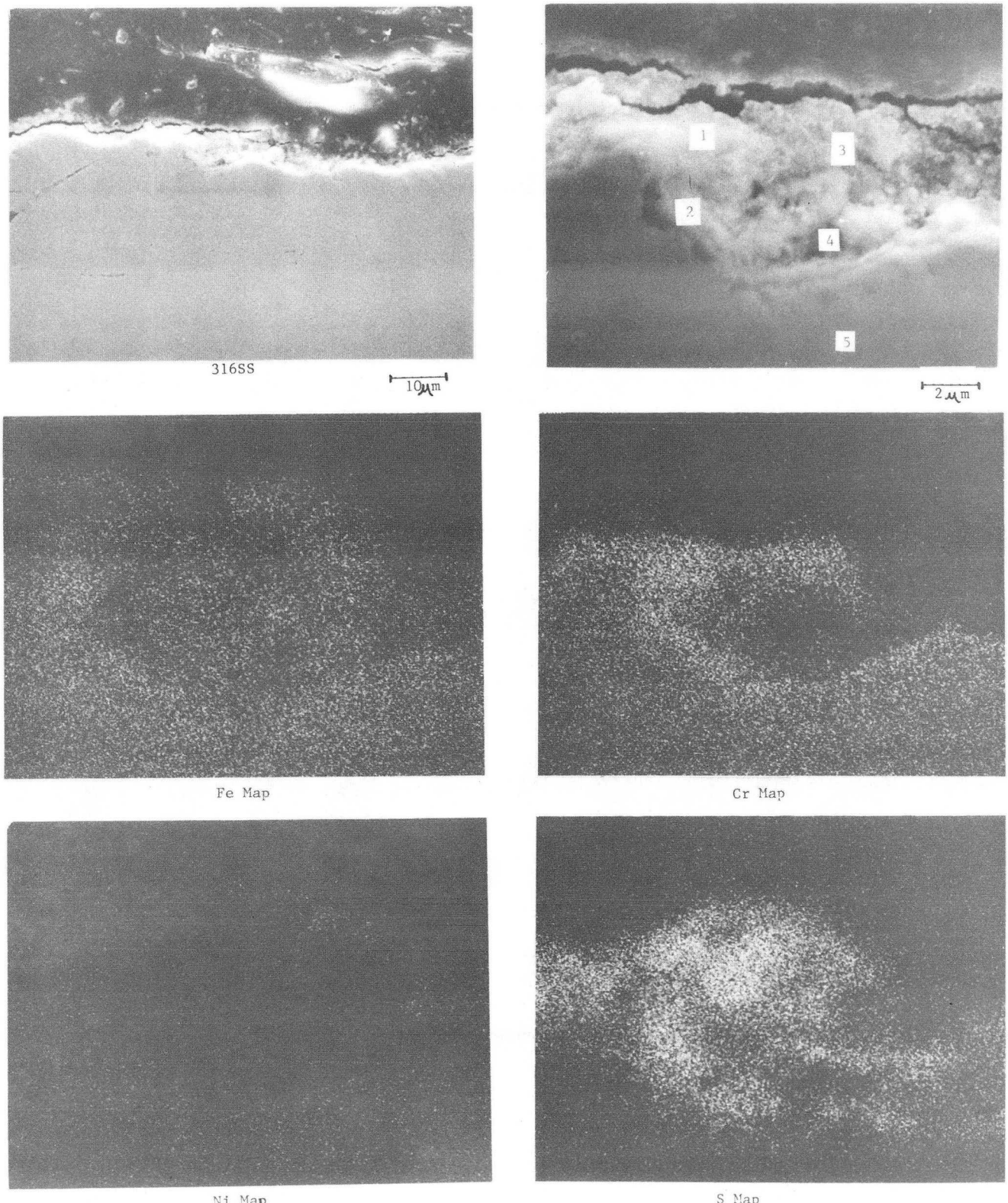

Fig. 63 316SS cross section from retort S-60

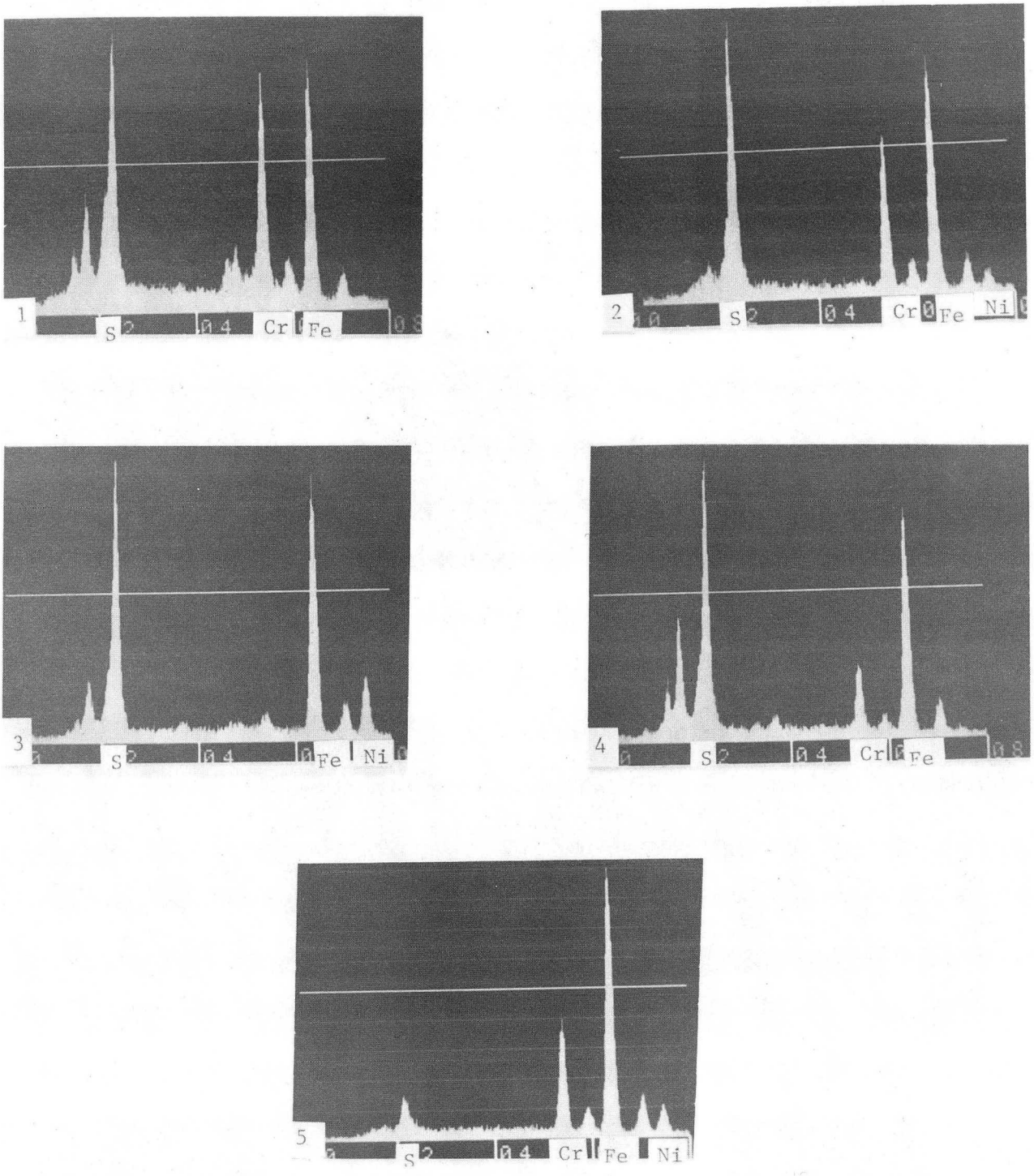

XBB 8210-8735

Fig. 64 EDAX peak analyses of 316SS cross section from retort S-60

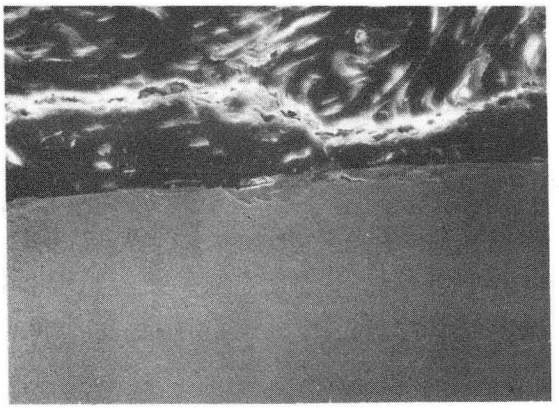

410SS

20 μm

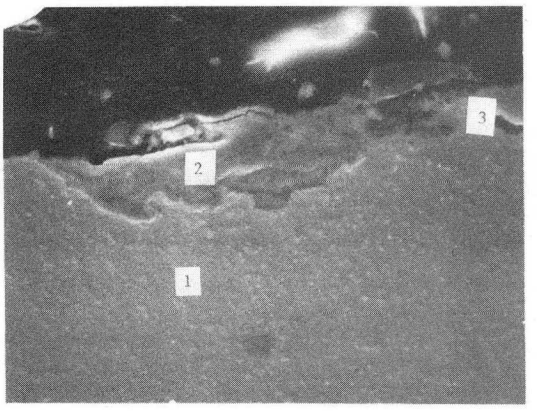

5 μm

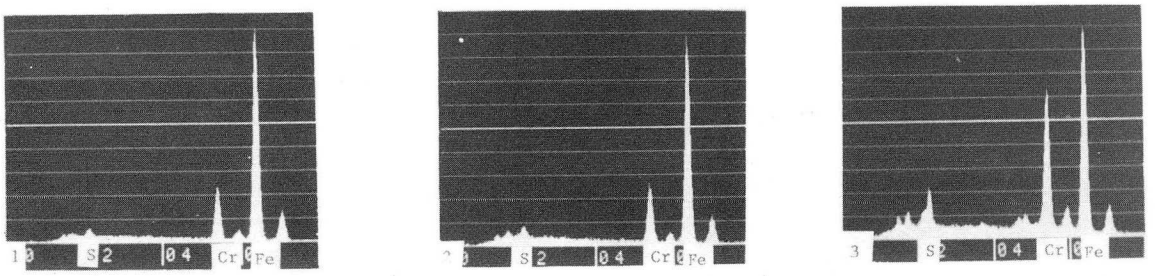

XBB 8210-8731

Fig. 65 410SS cross section from retort S-60

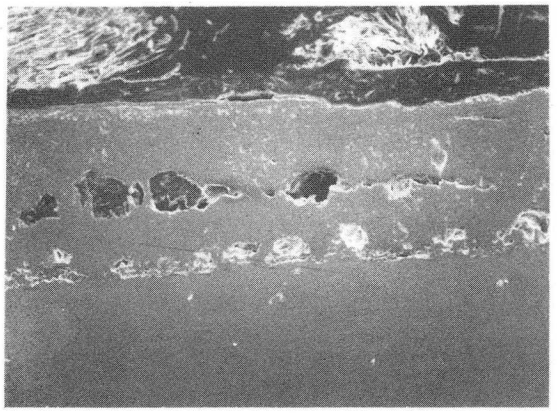

1018 Steel

100 μm

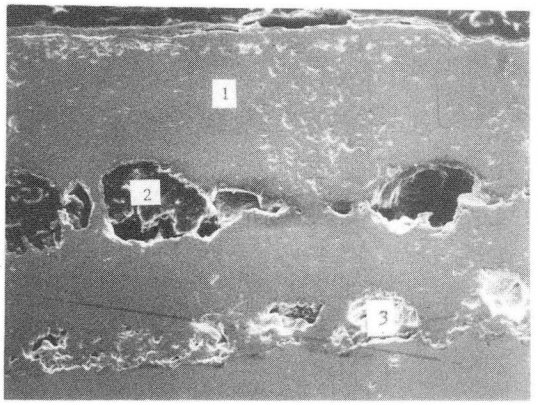

50 μm

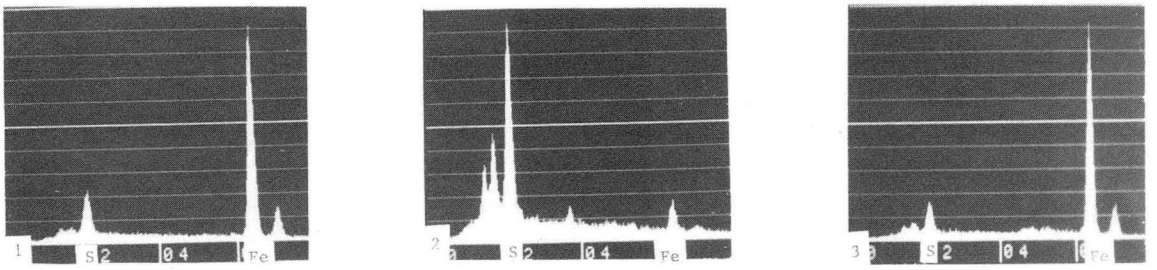

XBB 8210-8732

Fig. 66 Bare 1018 steel cross sections from retort L-2

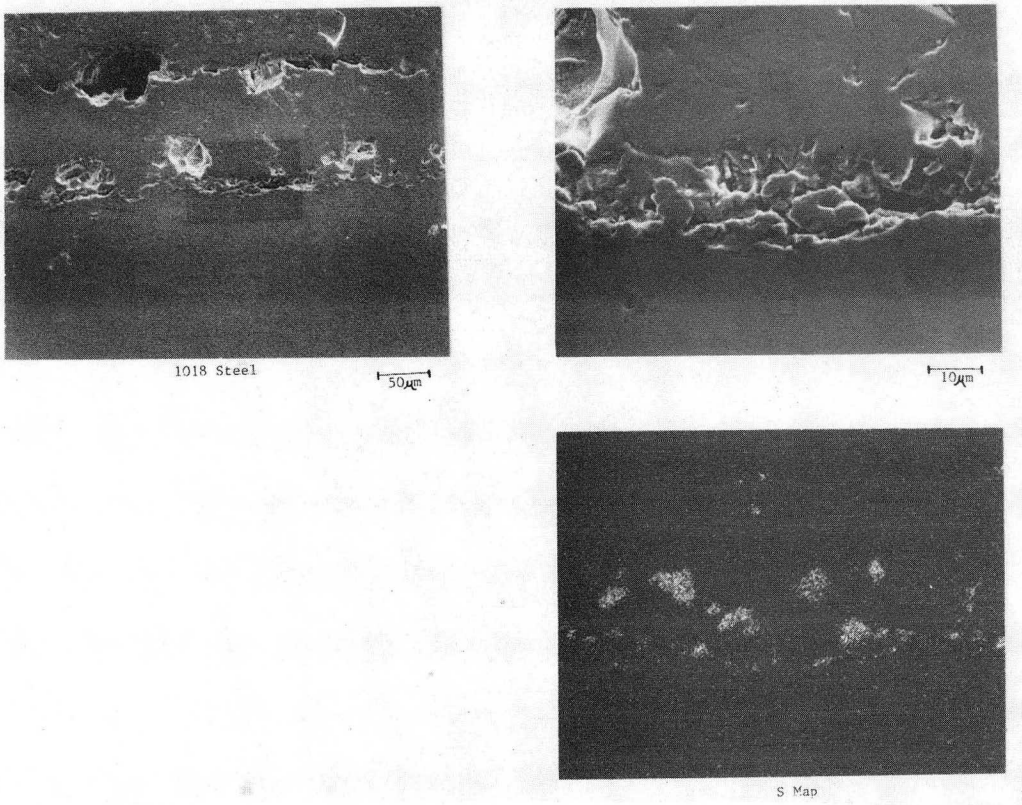

Fig. 67 Close up of inner band of mixed oxide-sulfide scale on 1018 steel from retort L-2

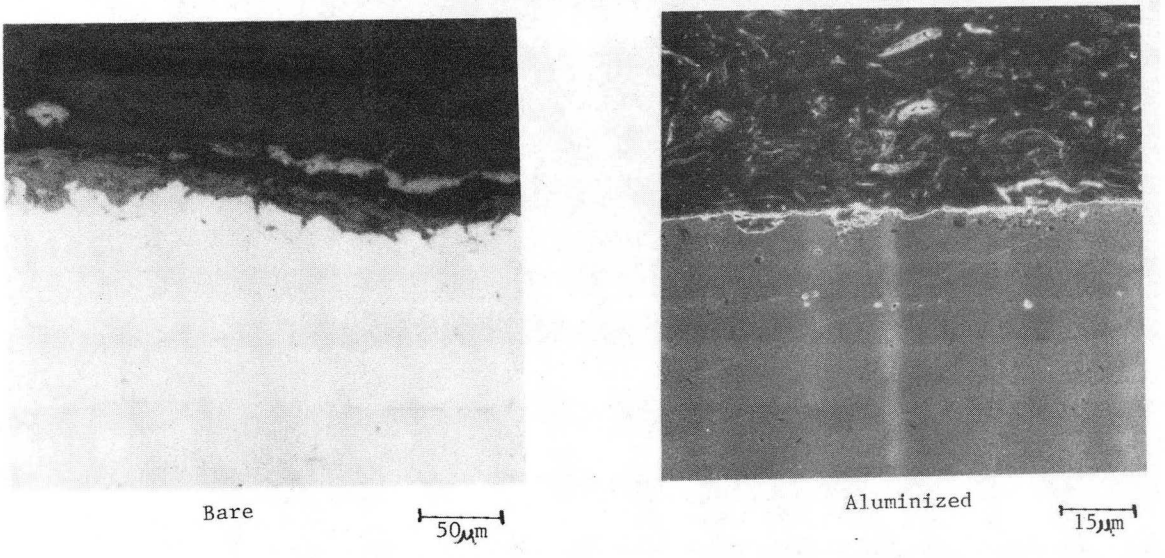

Fig. 68 Bare and aluminized 316SS cross sections from retort L-2

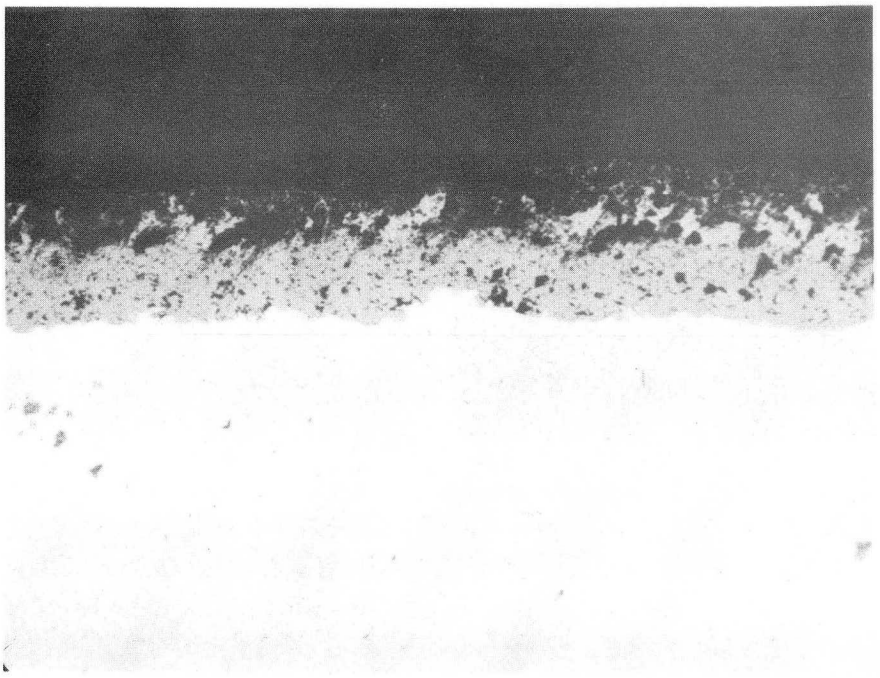

410SS

100μm

XBB 8210-8736

Fig. 69 410SS cross section from retort L-2

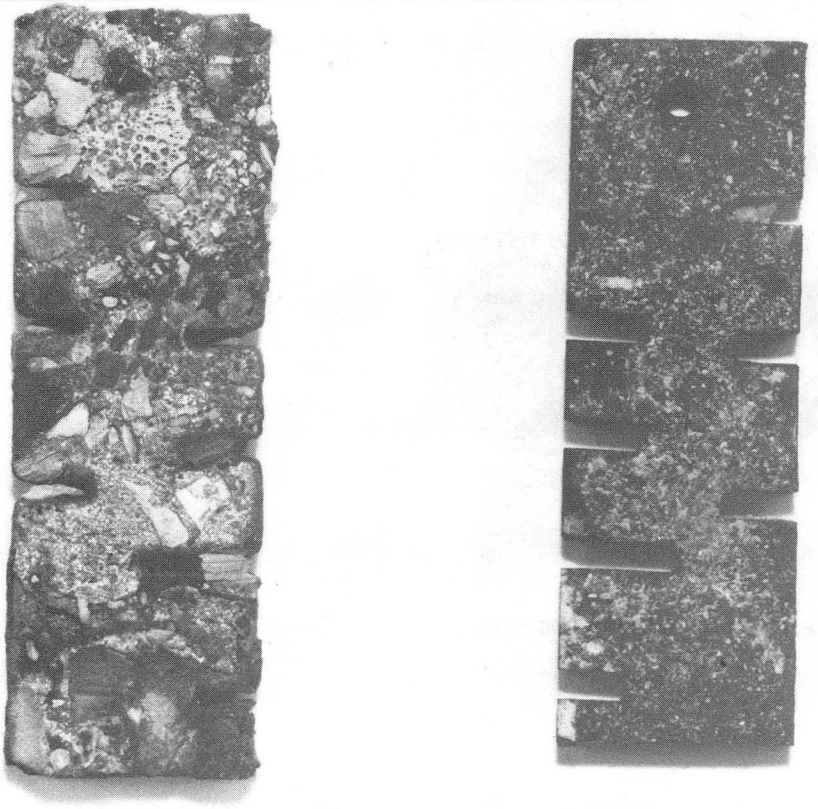

Rich Shale

2X

Lean Shale

1018 Steel

CBB 820-8742

Fig. 70 Overall view of 1018 steel specimens exposed in rich and lean shale in retort L-3

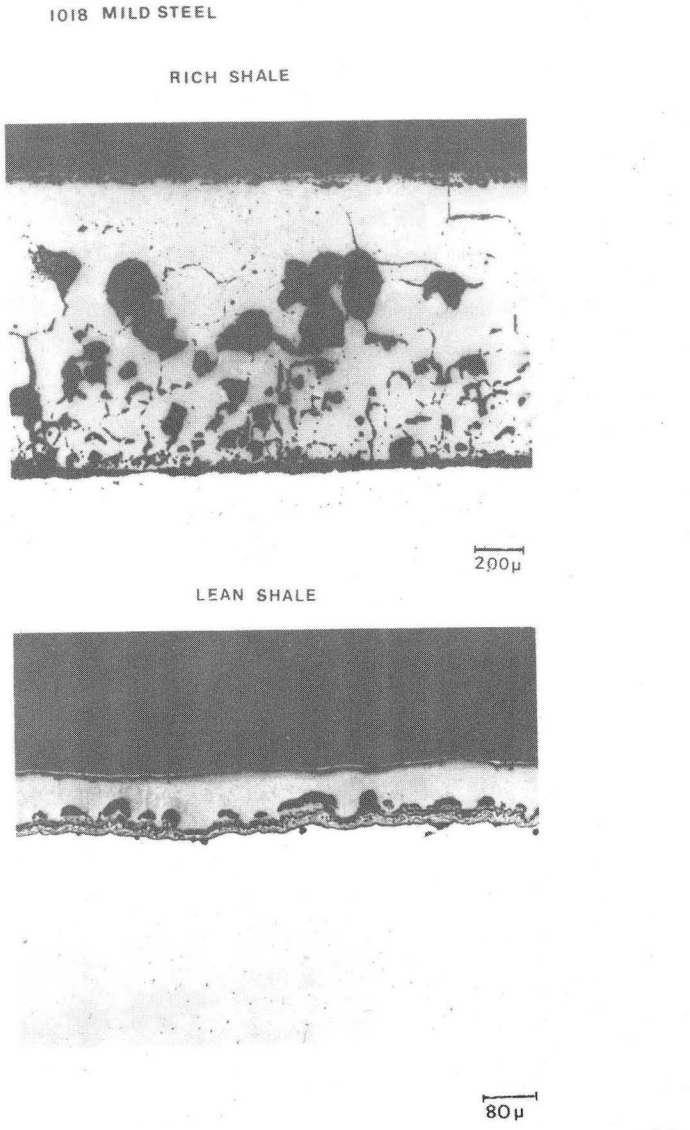

Fig. 71 1018 steel cross sections from rich and lean shale sections of retort L-3

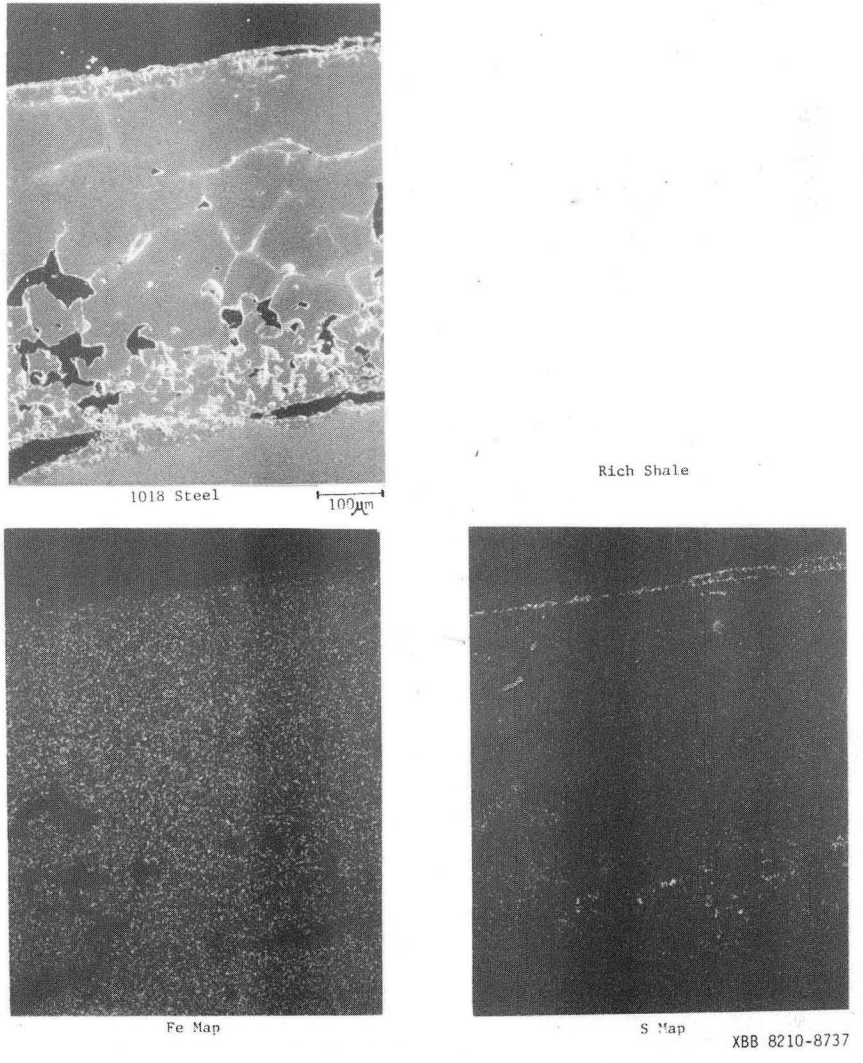

Fig. 72 SEM micrograph of 1018 steel with sulfur and iron x-ray maps from retort L-3, rich shale

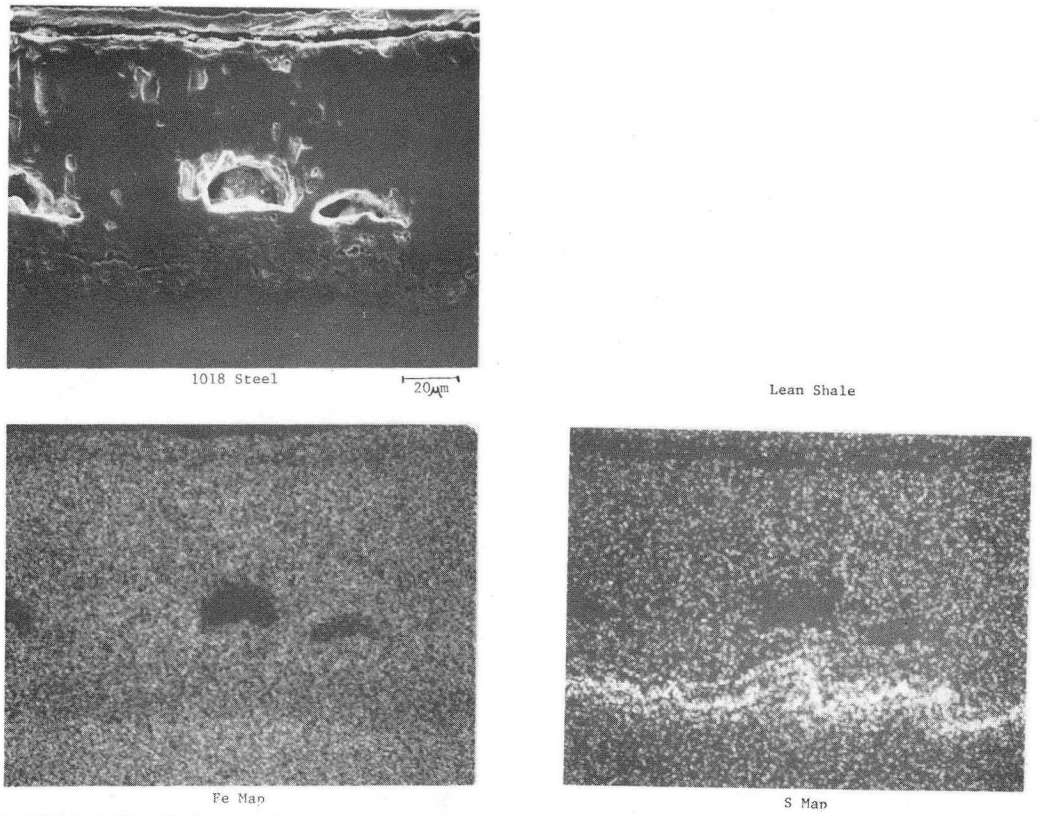

Fig. 73 SEM micrograph of 1018 steel with sulfur and iron x-ray maps from retort L-3, lean shale

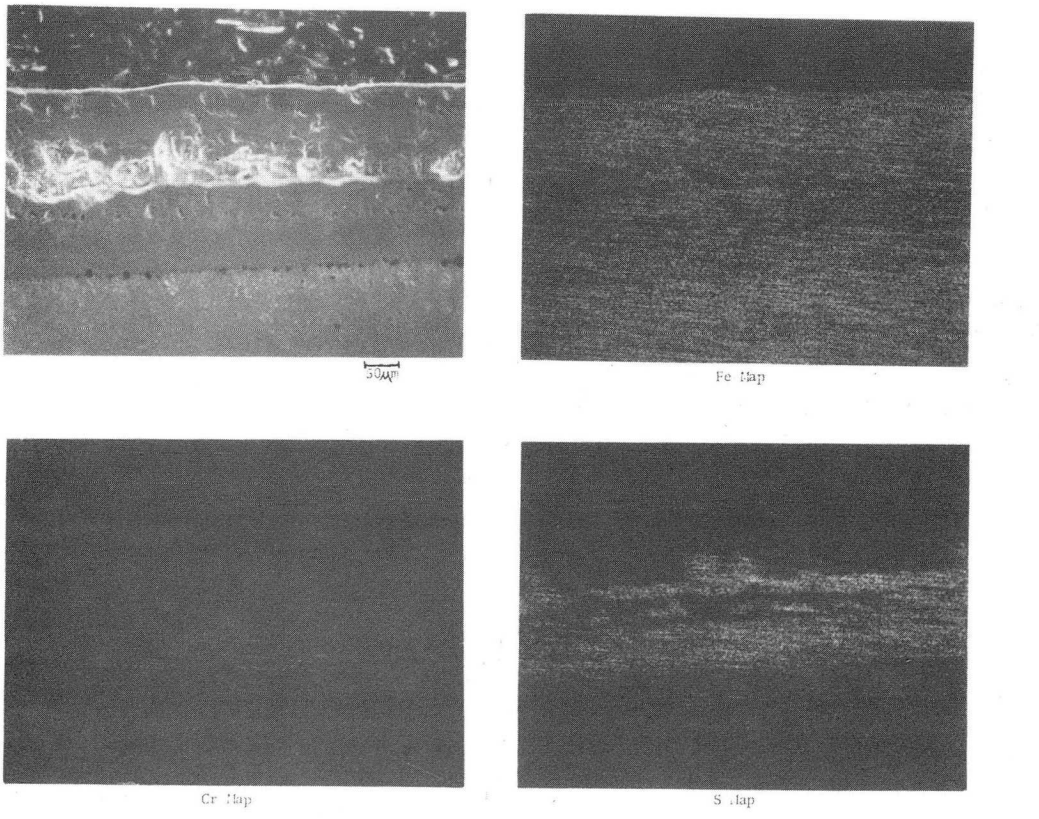

Fig. 74 SEM micrograph of 2¼Cr1Mo steel with x-ray maps from retort L-3, rich shale

410 SS

RICH SHALE

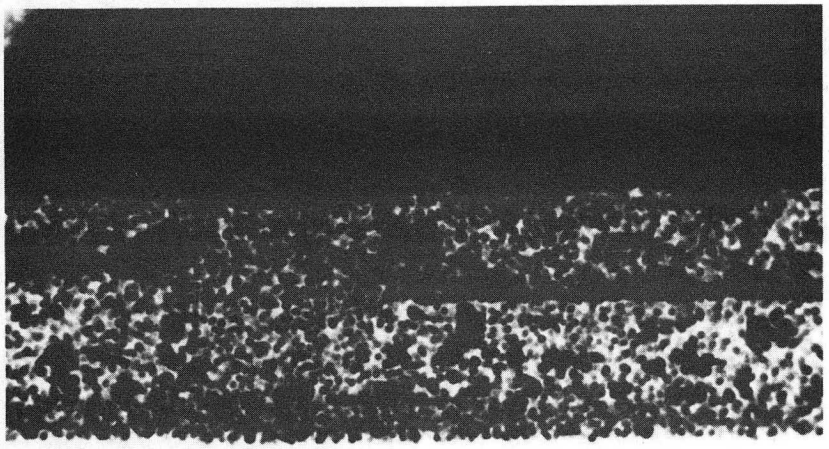

150μ

LEAN SHALE

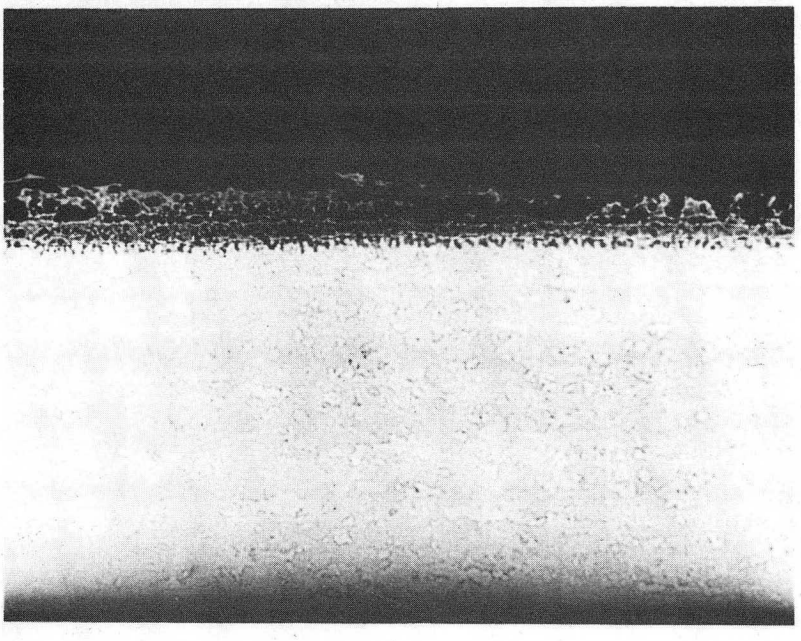

150μ

XBB 801-155

Fig. 75 410SS cross sections from rich and lean shale sections of retort L-3

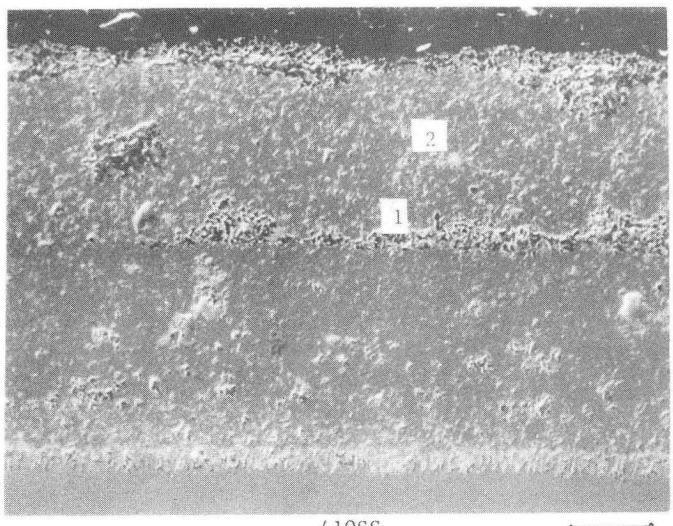

410SS

50μm

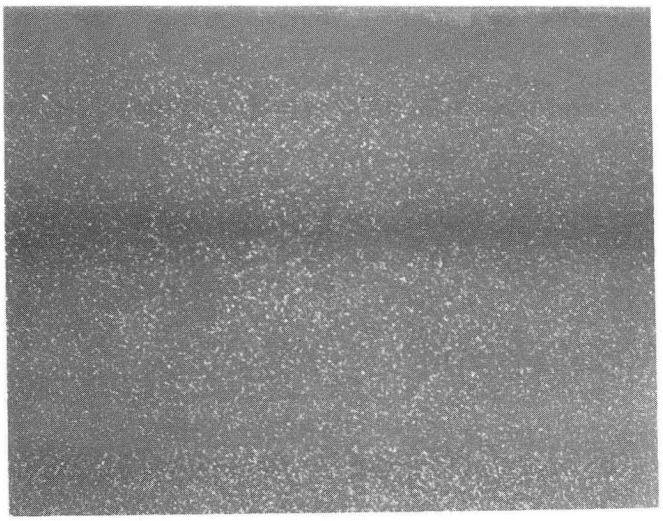

Fe Map

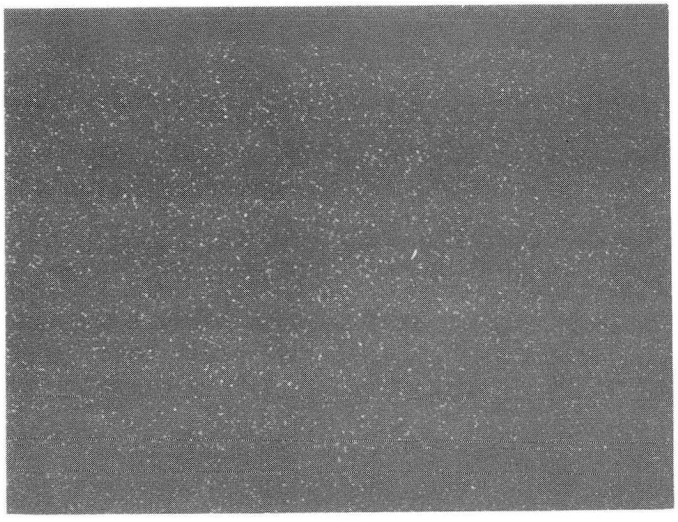

Cr Map

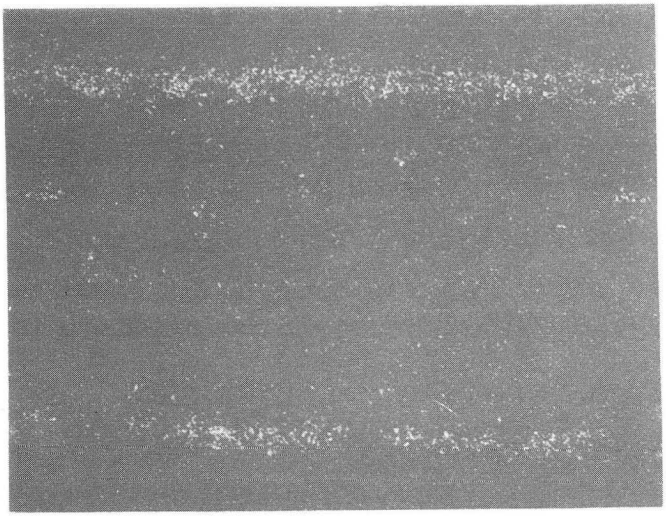

S Map

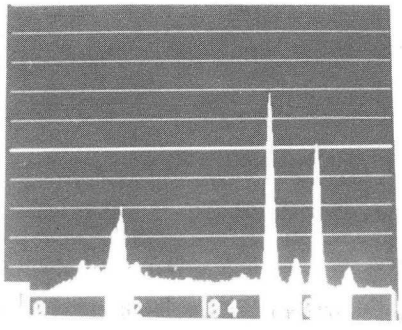

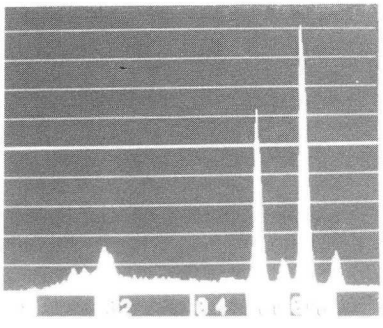

Rich

XBB 8210-8740

Fig. 76 Micrograph of 410SS with x-ray maps and EDAX peak analyses from rich shale section of retort L-3

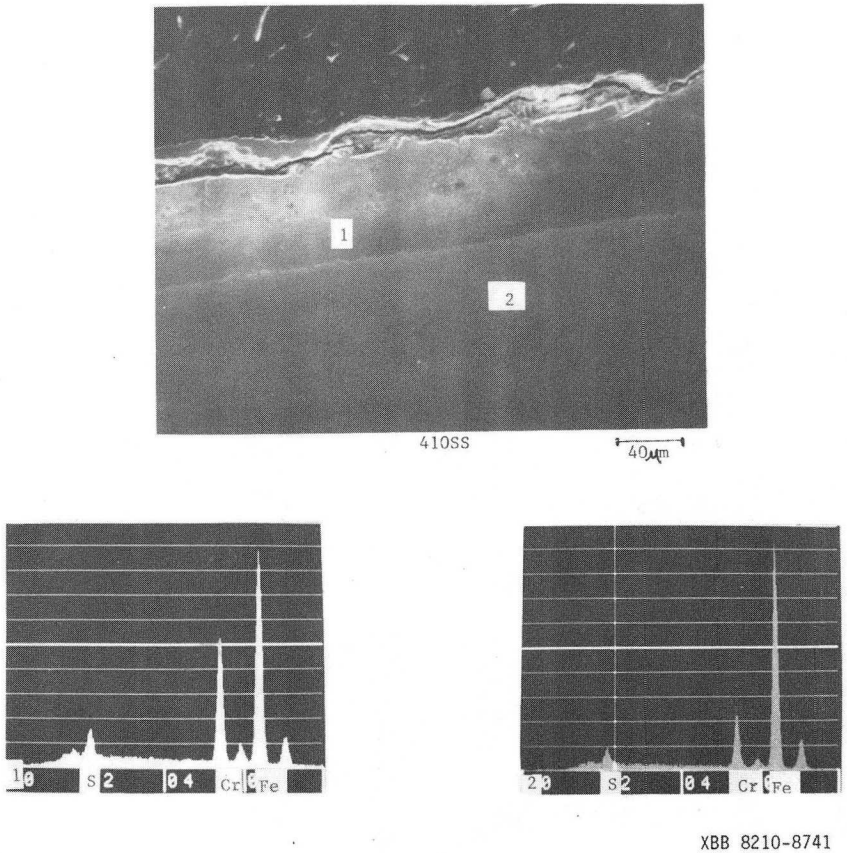

Fig. 77 Micrograph of 410SS with EDAX peak analyses from lean shale section of retort L-3

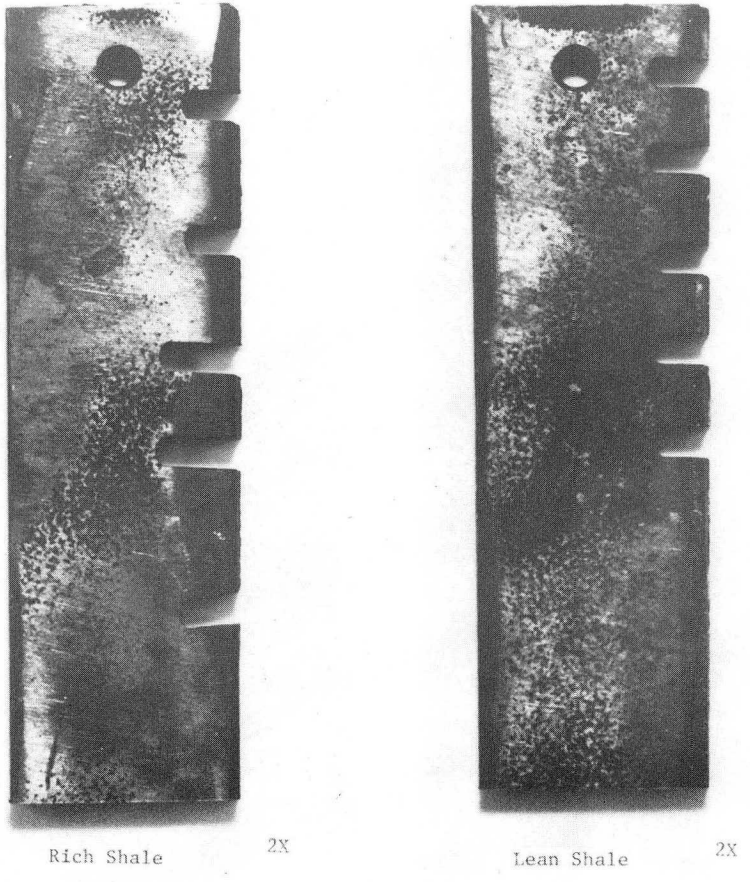

Fig. 78 Photos of the 310SS specimens exposed in the rich and lean sections of retort L-3

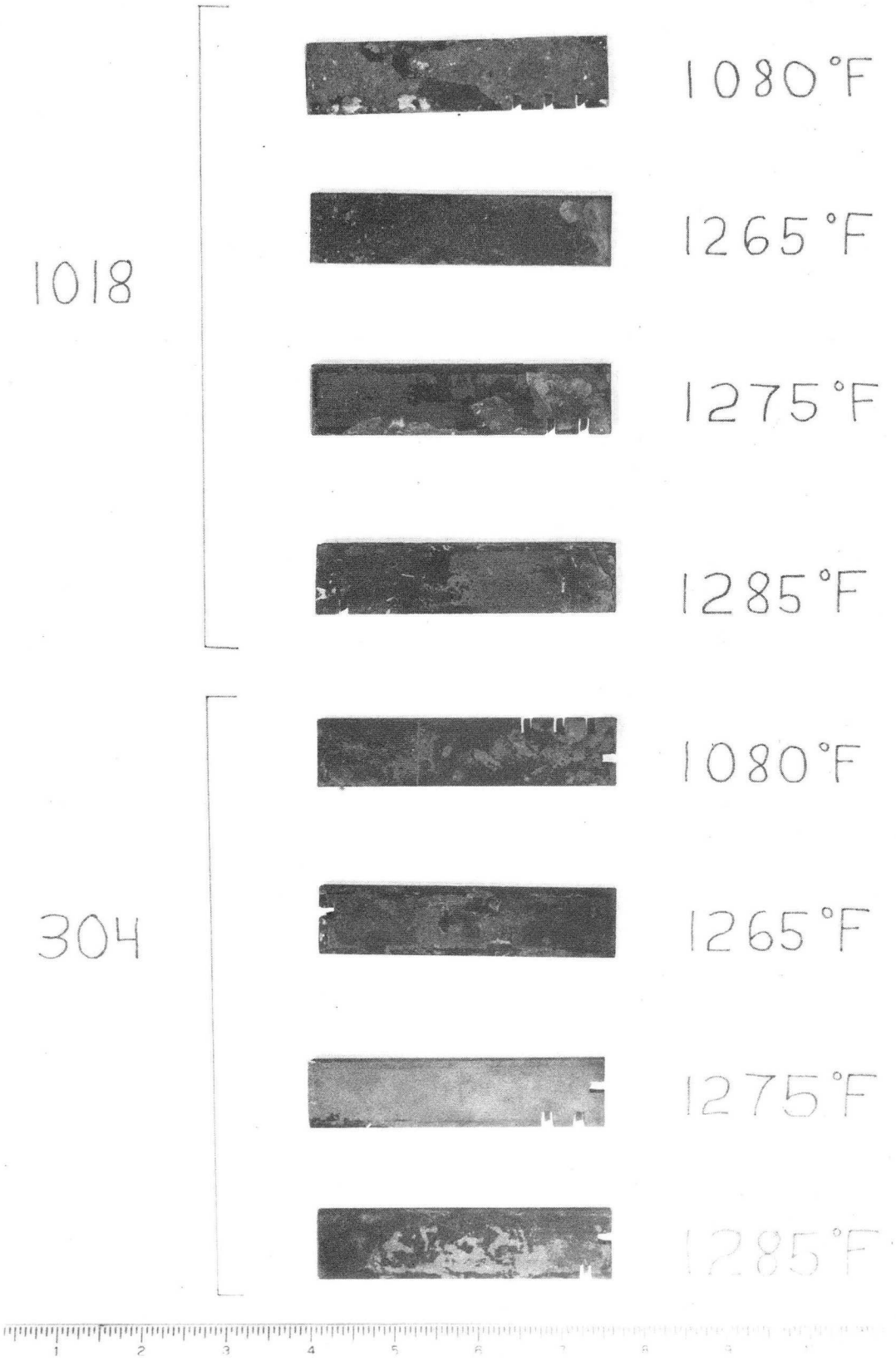

Fig. 79 Appearance of 1018 and 304SS exposed in controlled state retort, CS78

CBB 786-6948

304 Stainless Steel -
Controlled State Retort

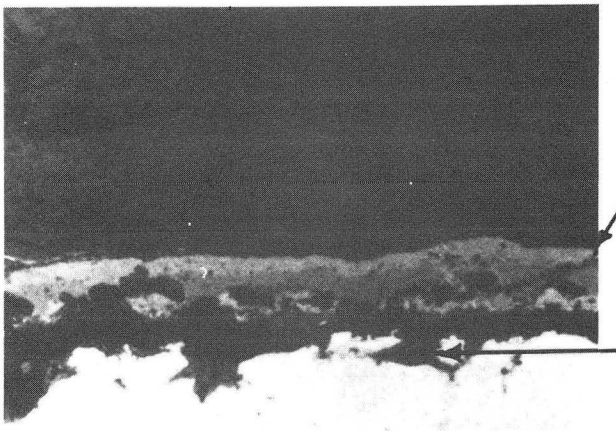

320x

Outer Scale

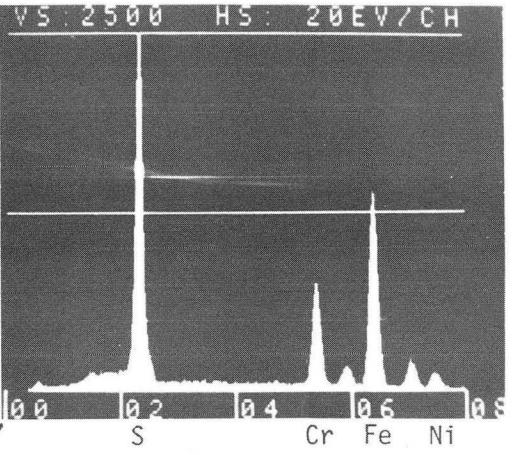

Inner Scale

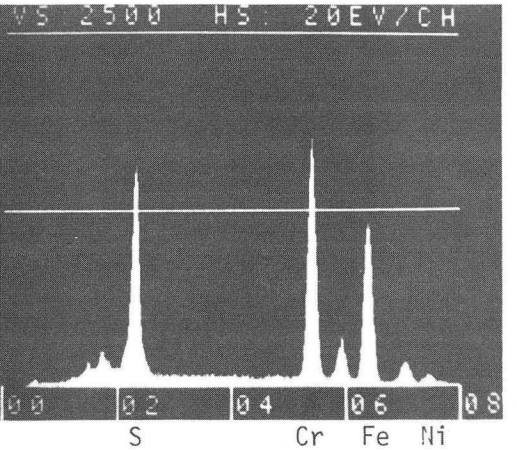

Base Metal

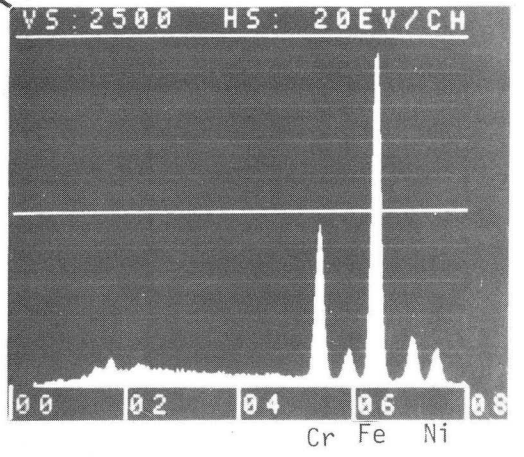

Fig. 80 Corroded 304SS from retort CS70 XBB 789-12295A

2 1/4 Cr-1 Mo Steel -
Controlled State Retort

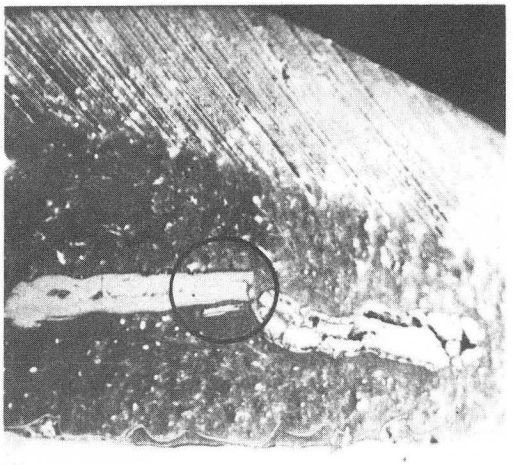

20x

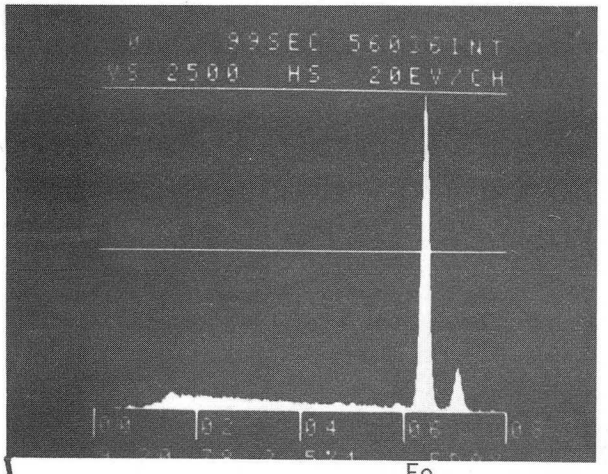

Outer Scale

Secondary Electron Image - 320x

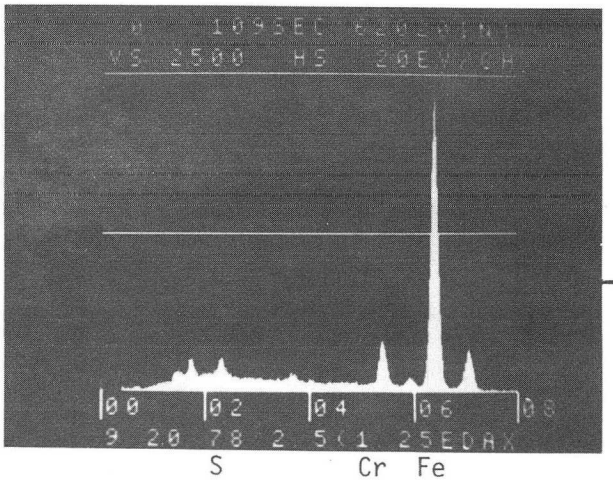

Inner Scale

.0040

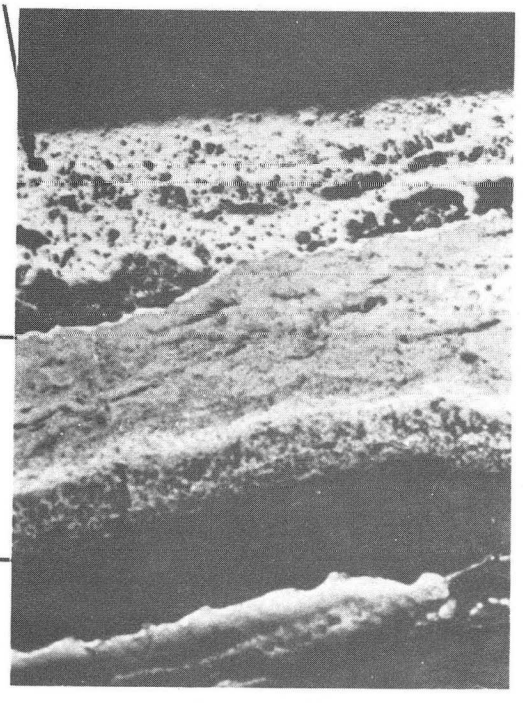

XBB 789-12296A

Fig. 81 Corroded 2¼ CrMo steel from retort CS79

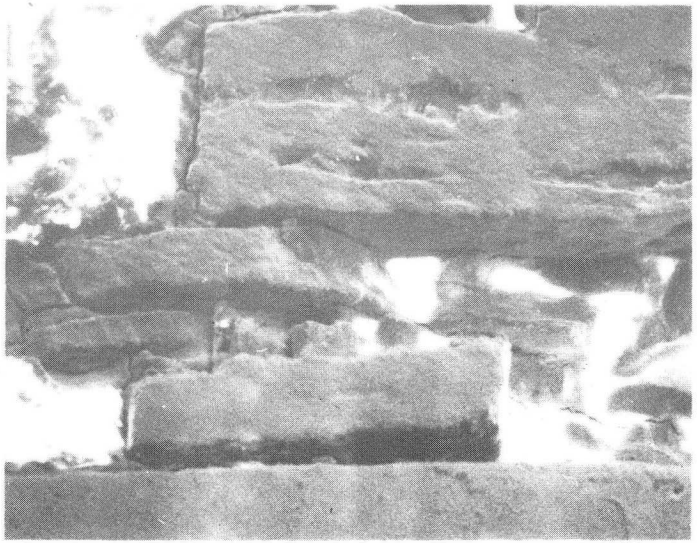

200x

1 1/4 Cr-1/2 Mo Steel -
Controlled State Retort

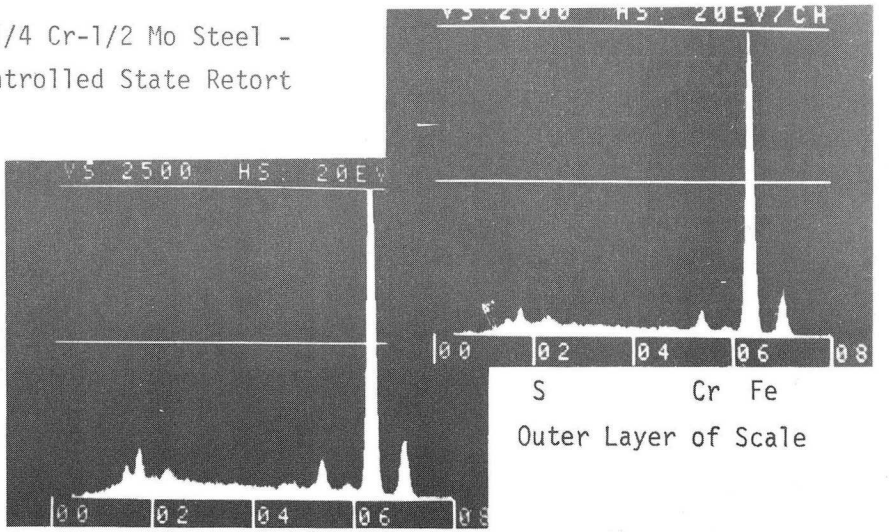

Fe Map 200x

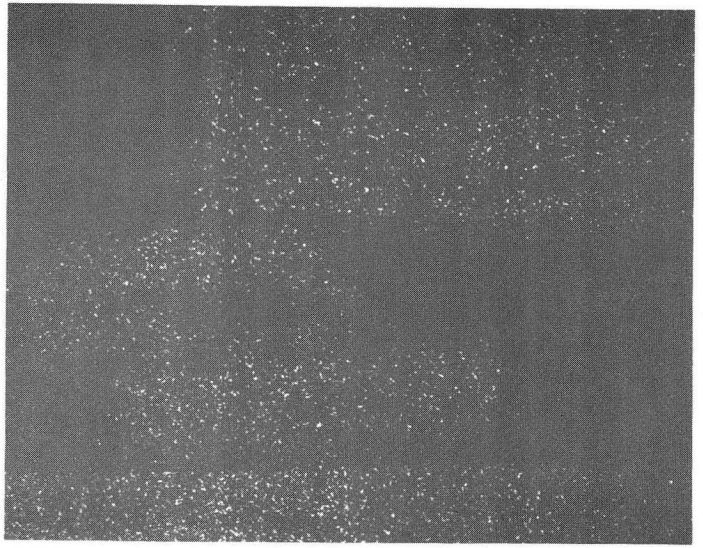

Cr Map 200 x

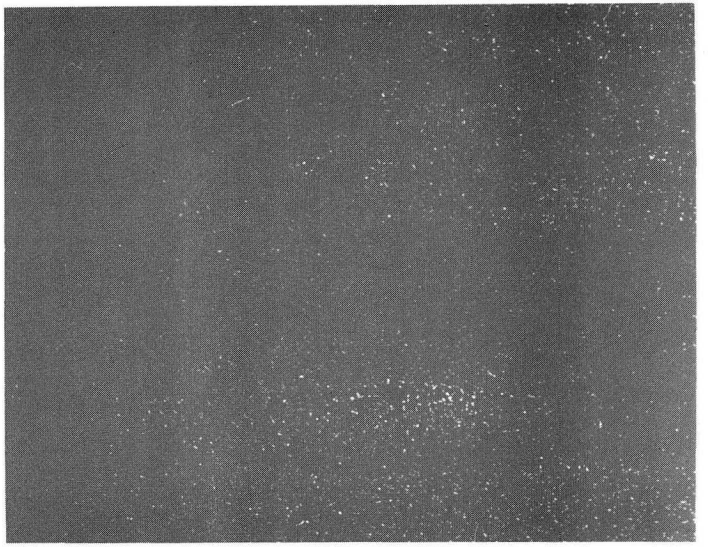

XBB 789-12297A

Fig. 82 Corroded 1¼Cr½Mo steel from retort CS79

Incoloy 800 - Controlled
State Retort

2000X

Ni Map 2000X

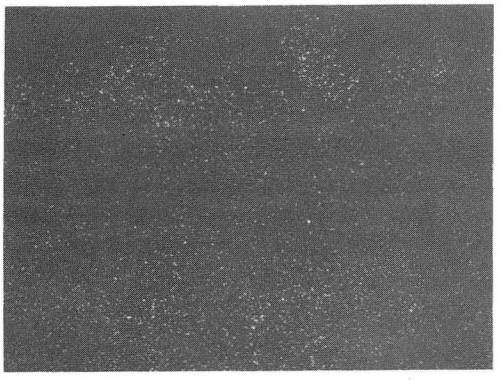

Cr Map 2000X

S Map 2000X

Fe Map 2000X

XBB 789-12301A

Fig. 83 Corroded Incoloy 800 from retort CS79

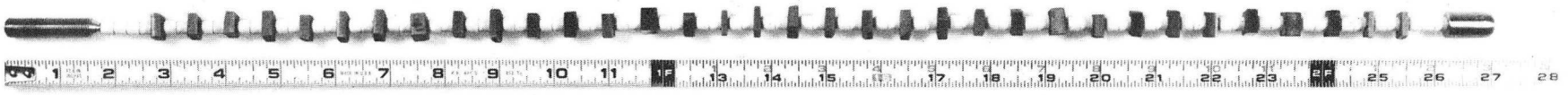

XBB 793-3129

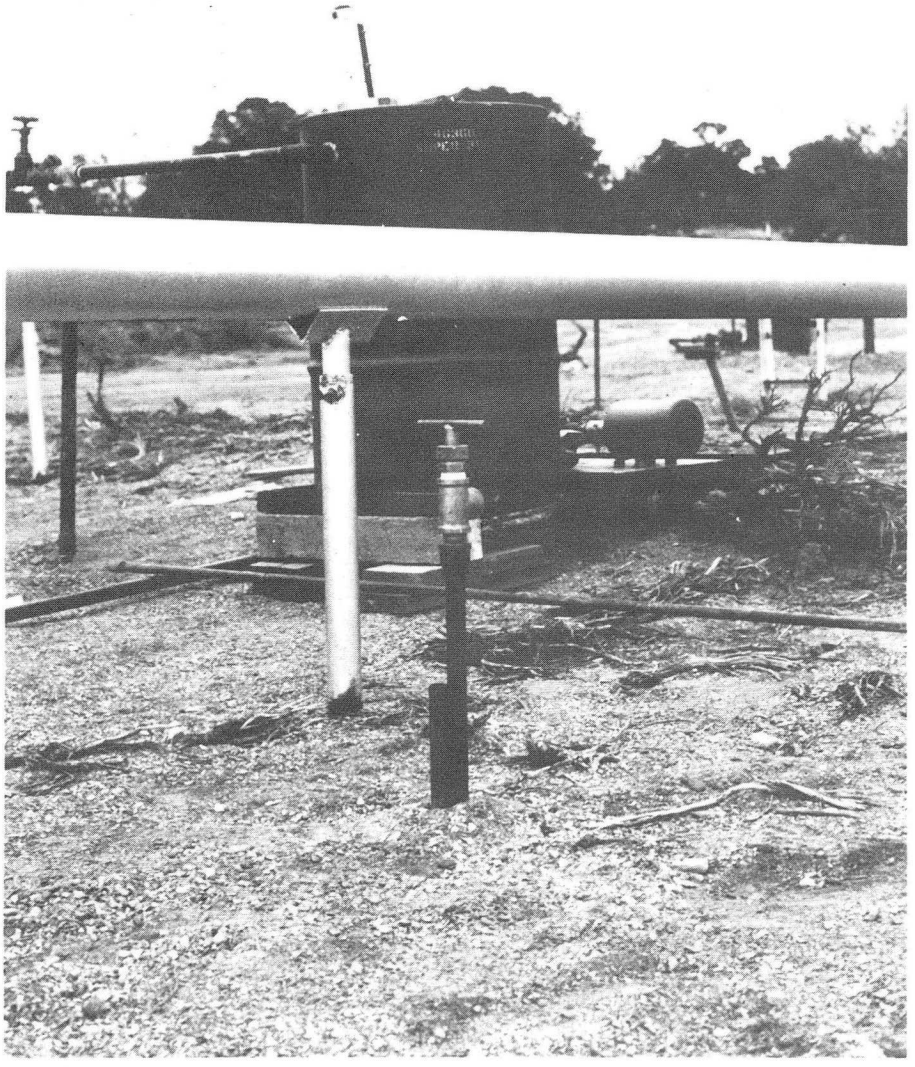

CBB 794-4495

Fig. 85 Above ground terminus of specimen exposure rod

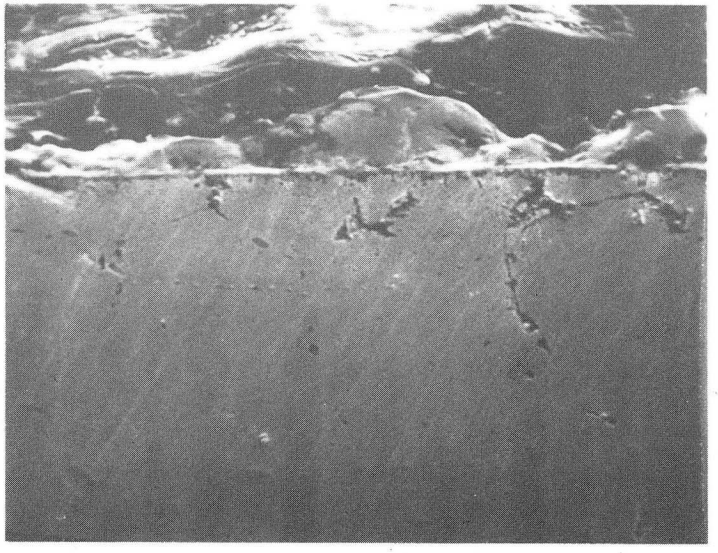

$\overline{10_{\mu m}}$

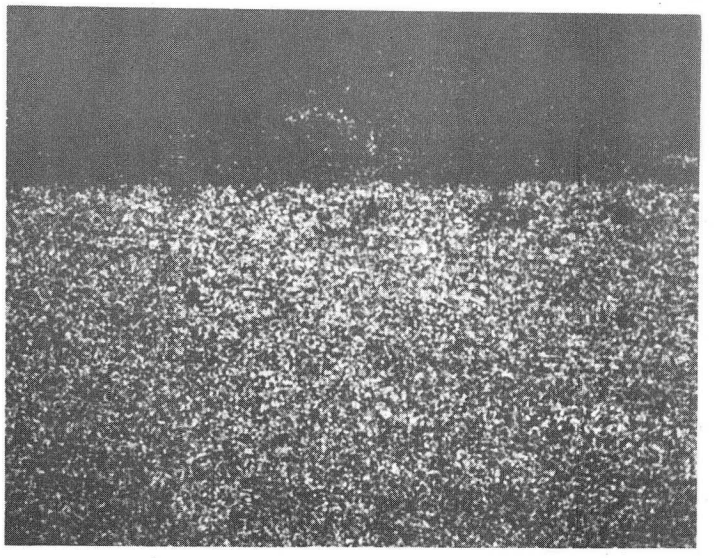

Fe Map

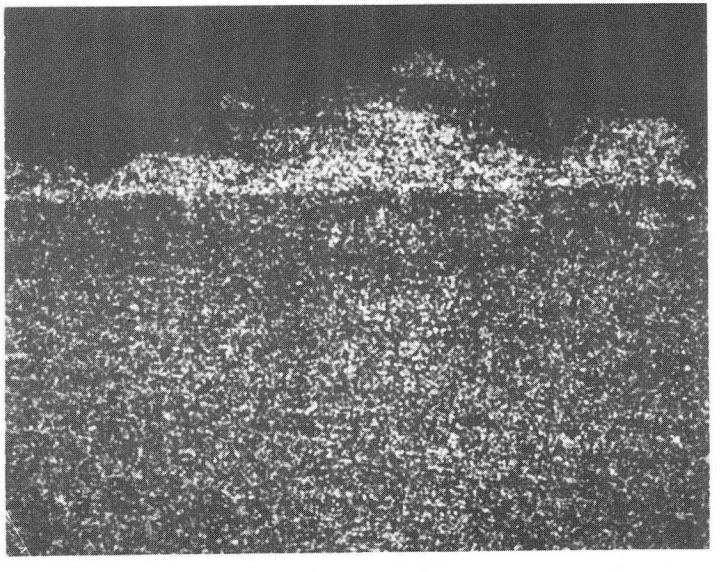

Cr Map

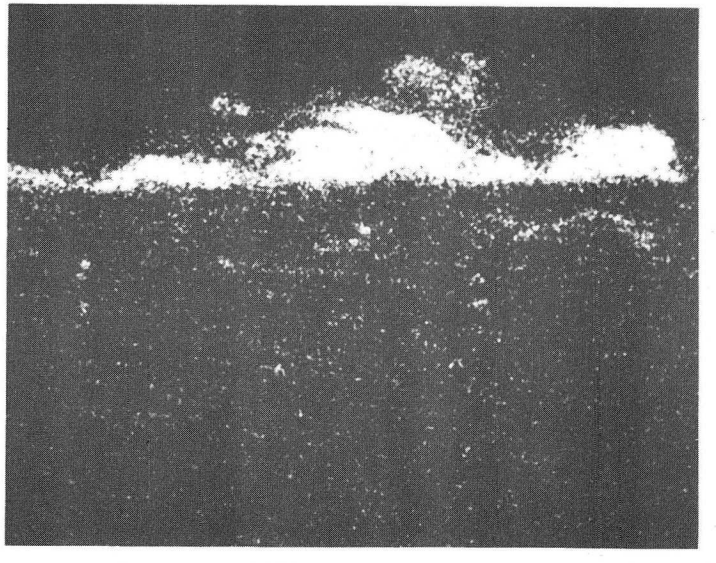

S Map

XBB 810-11952

Fig. 86 Corrosion scale formed on 304SS after 48 hour exposure at 1000°C in lab crucible

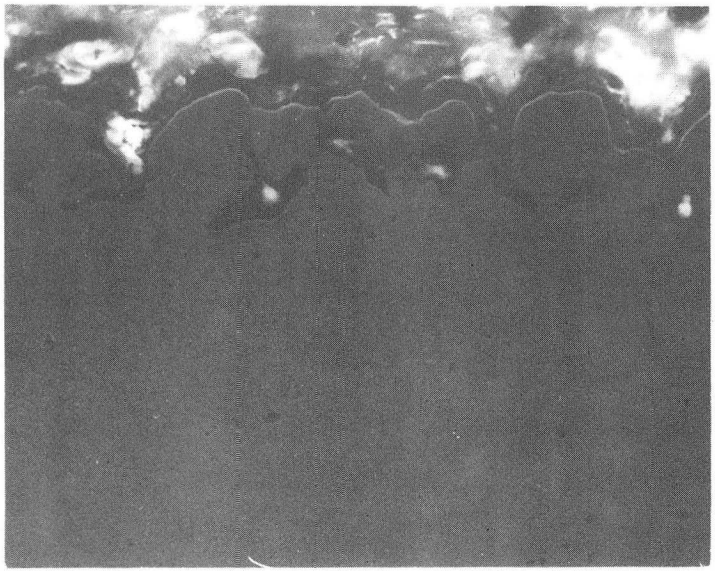

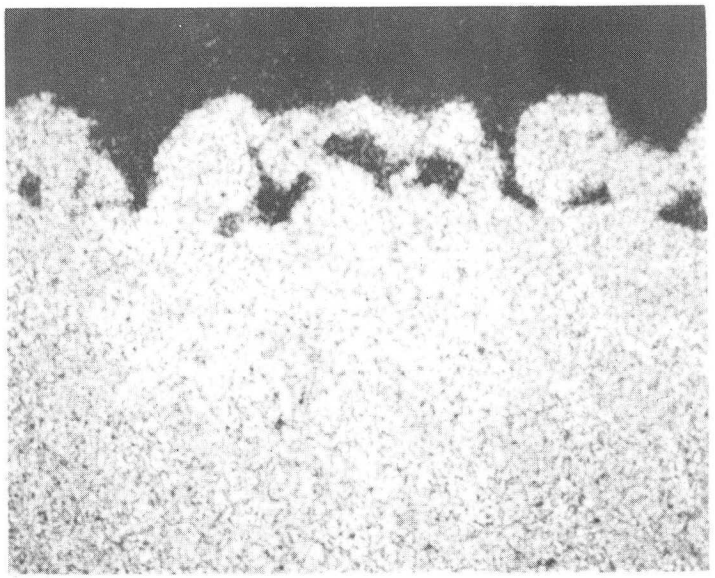

Fe Map

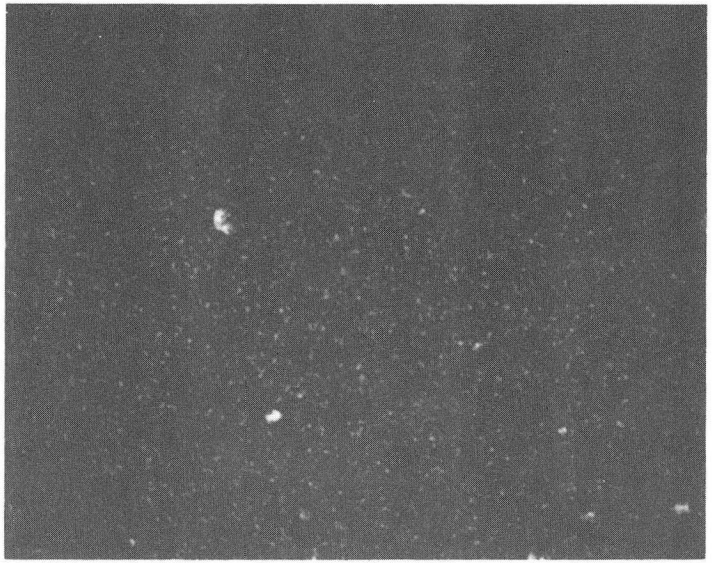

1018 Steel

S Map

Fig. 87 Cross section of 1018 steel from crucible test

XBB 821-525

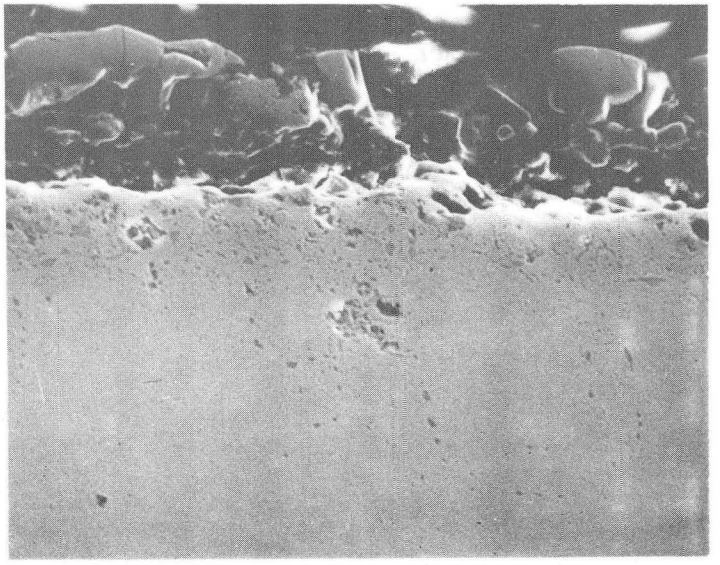

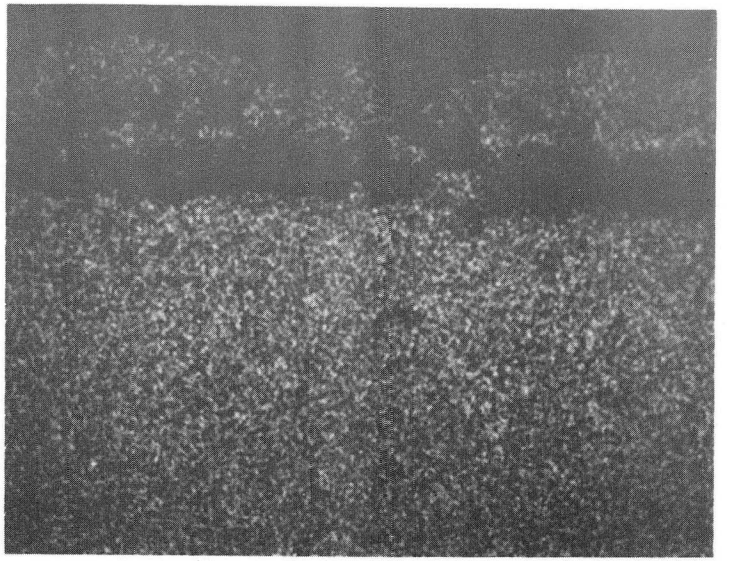

Fe Map

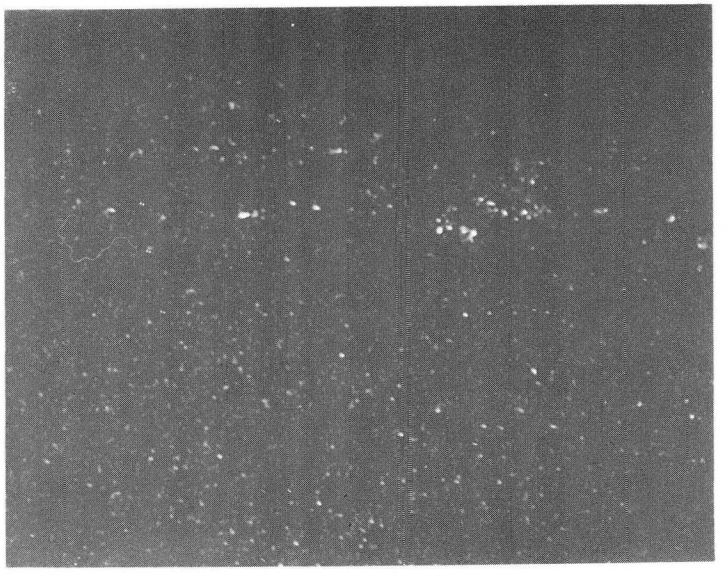

Cr Map

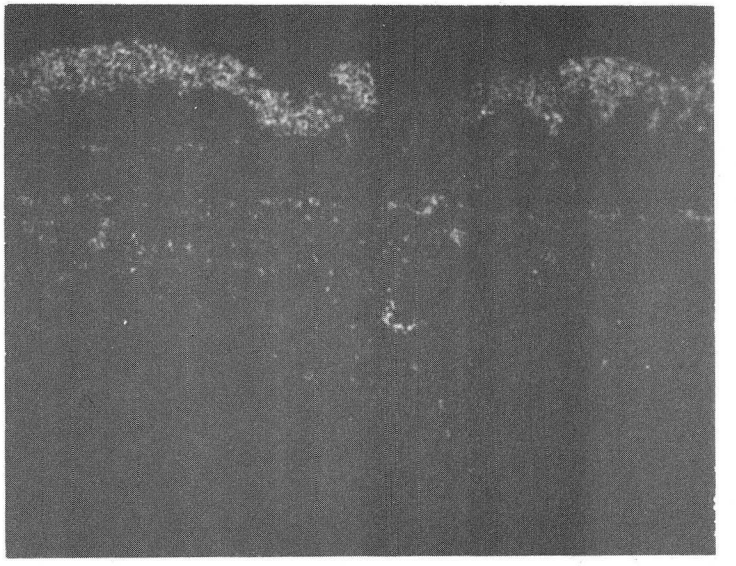

S Map

XBB 821-526

Fig. 88 Cross section of 2¼Cr1Mo steel from crucible test

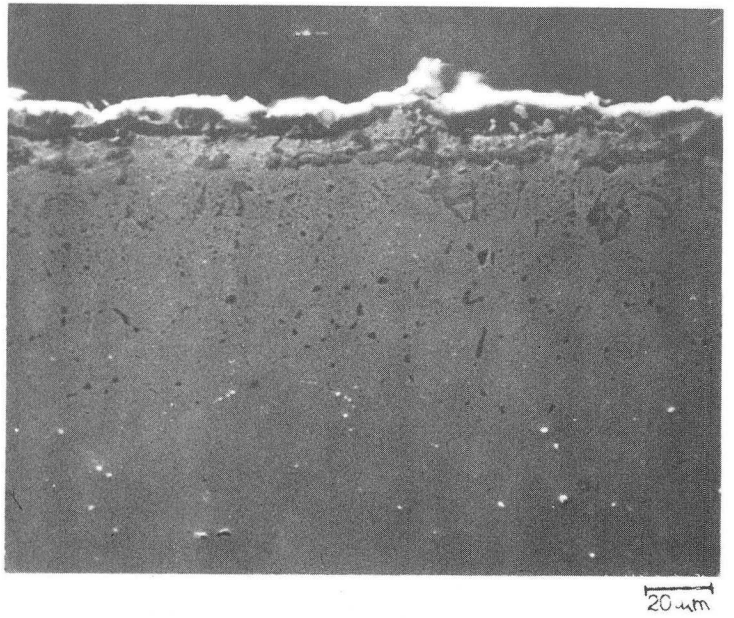

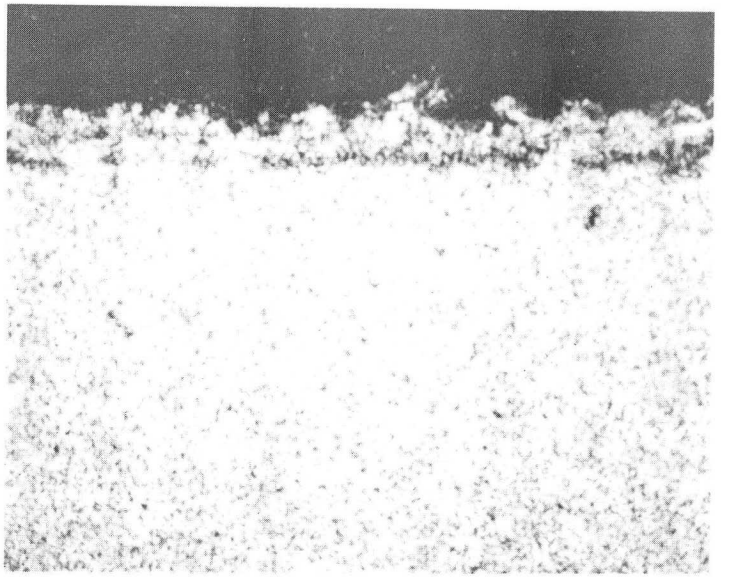

Fe Map

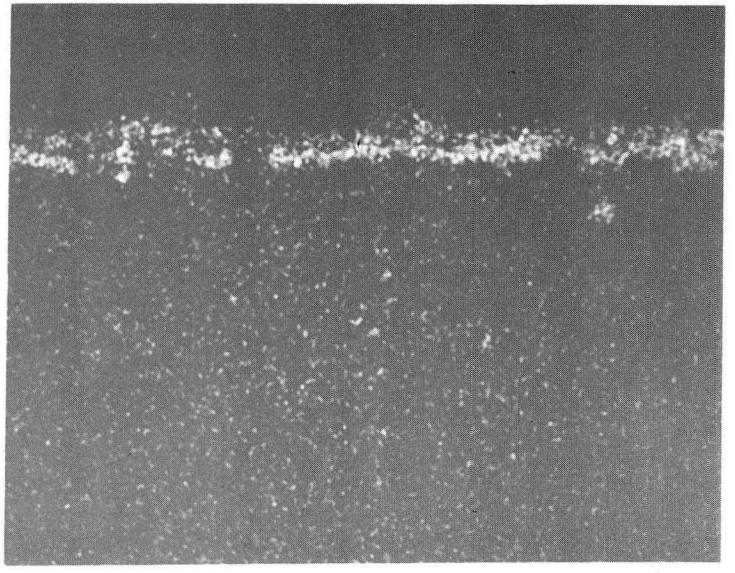

Cr Map

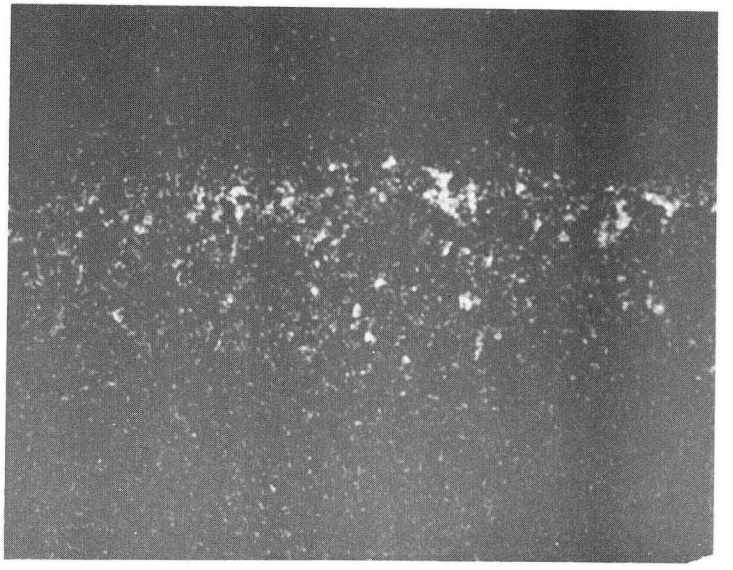

S Map

Fig. 89 Cross section of 5Cr½Mo steel from crucible test

XBB 821-527

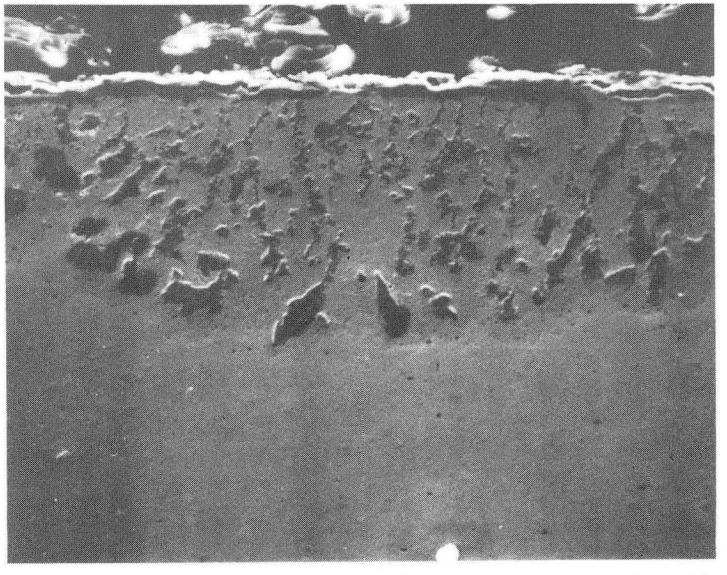

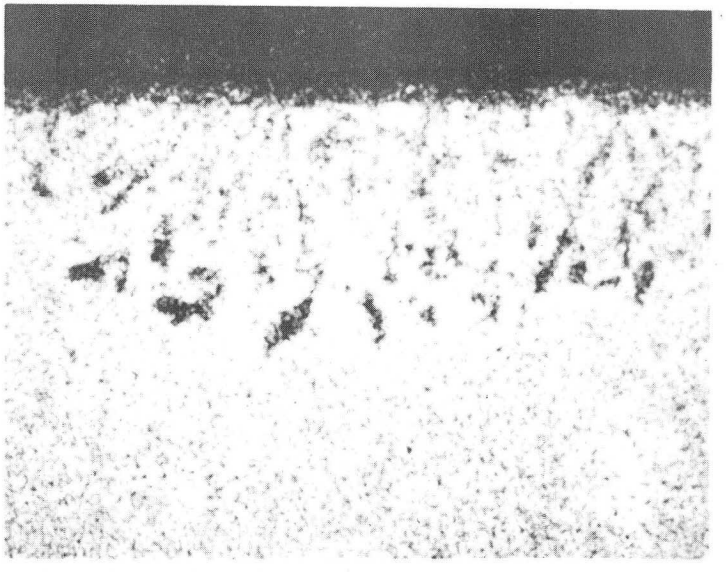

Fe Map

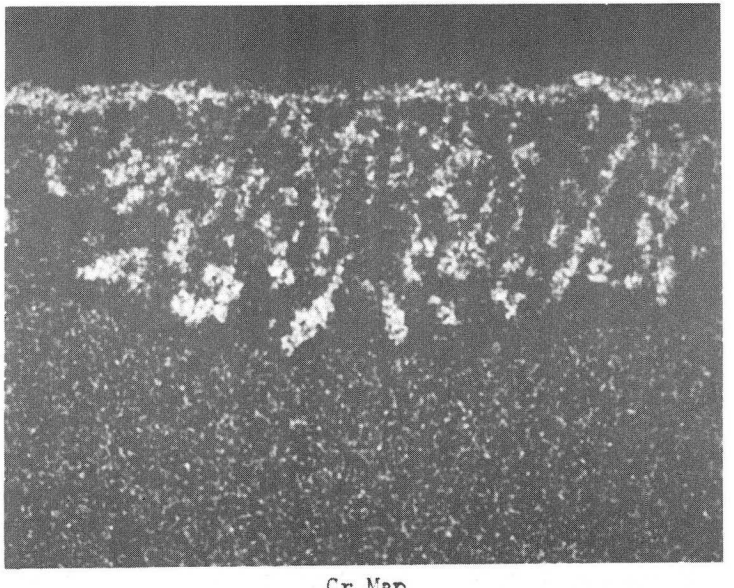

Cr Map

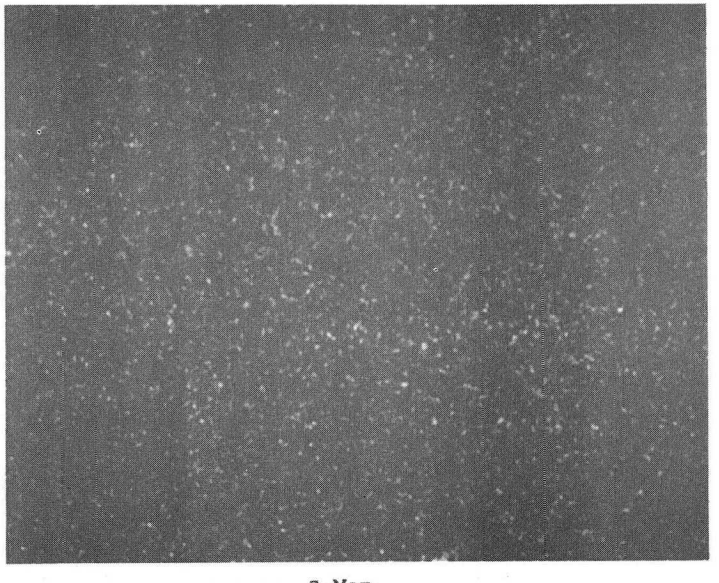

S Map

Fig. 90 Cross section of 9Cr1Mo steel from crucible test

XBB 821-528

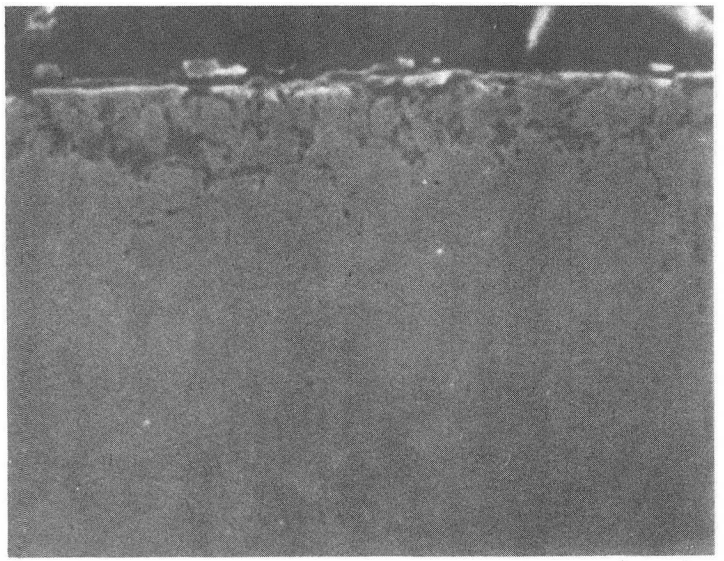

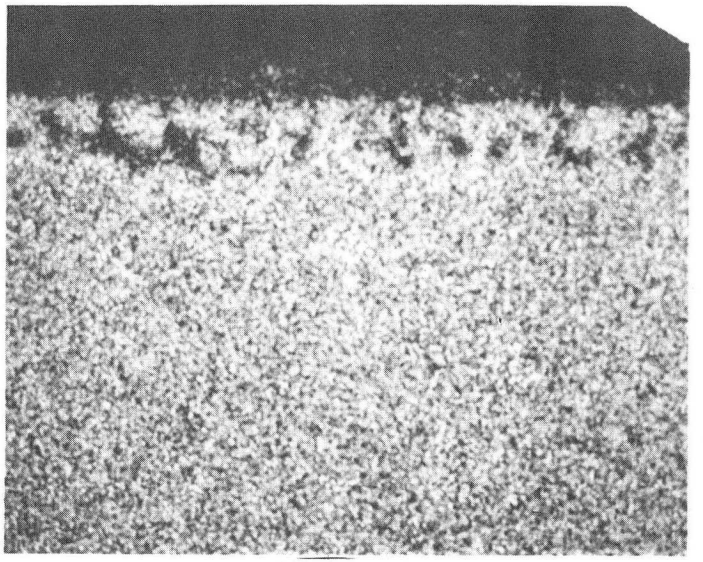

Fe Map

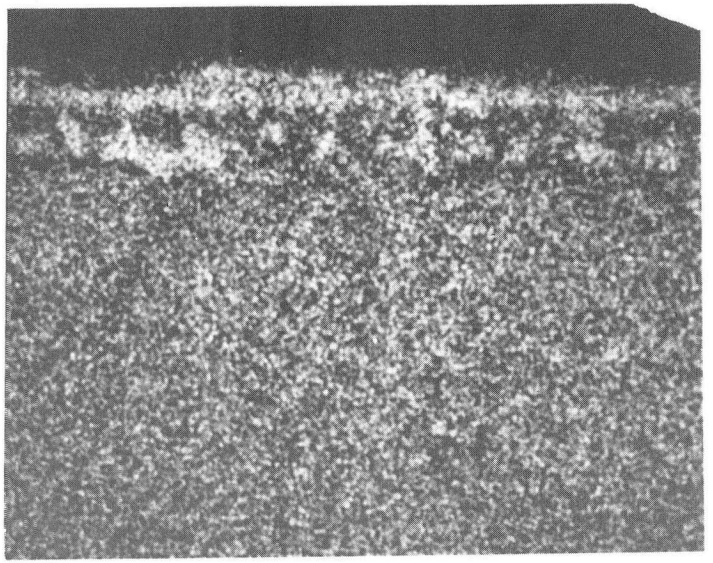

Cr Map

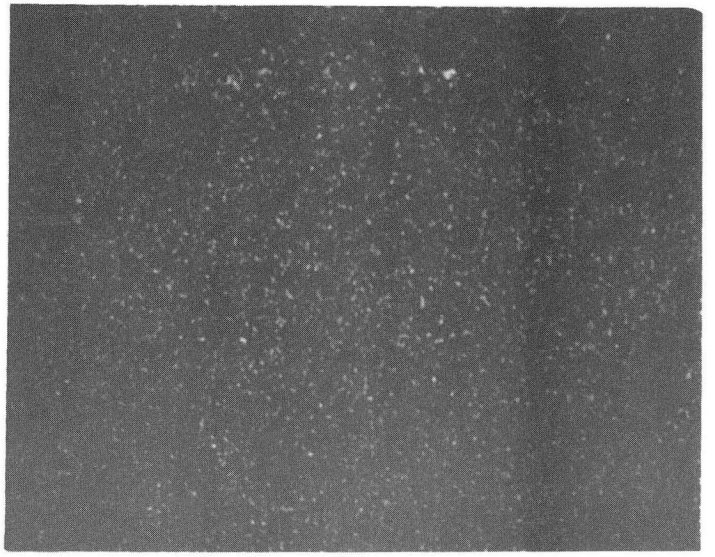

S Map

XBB 821-662

Fig. 91 Cross section of 310SS steel from crucible test

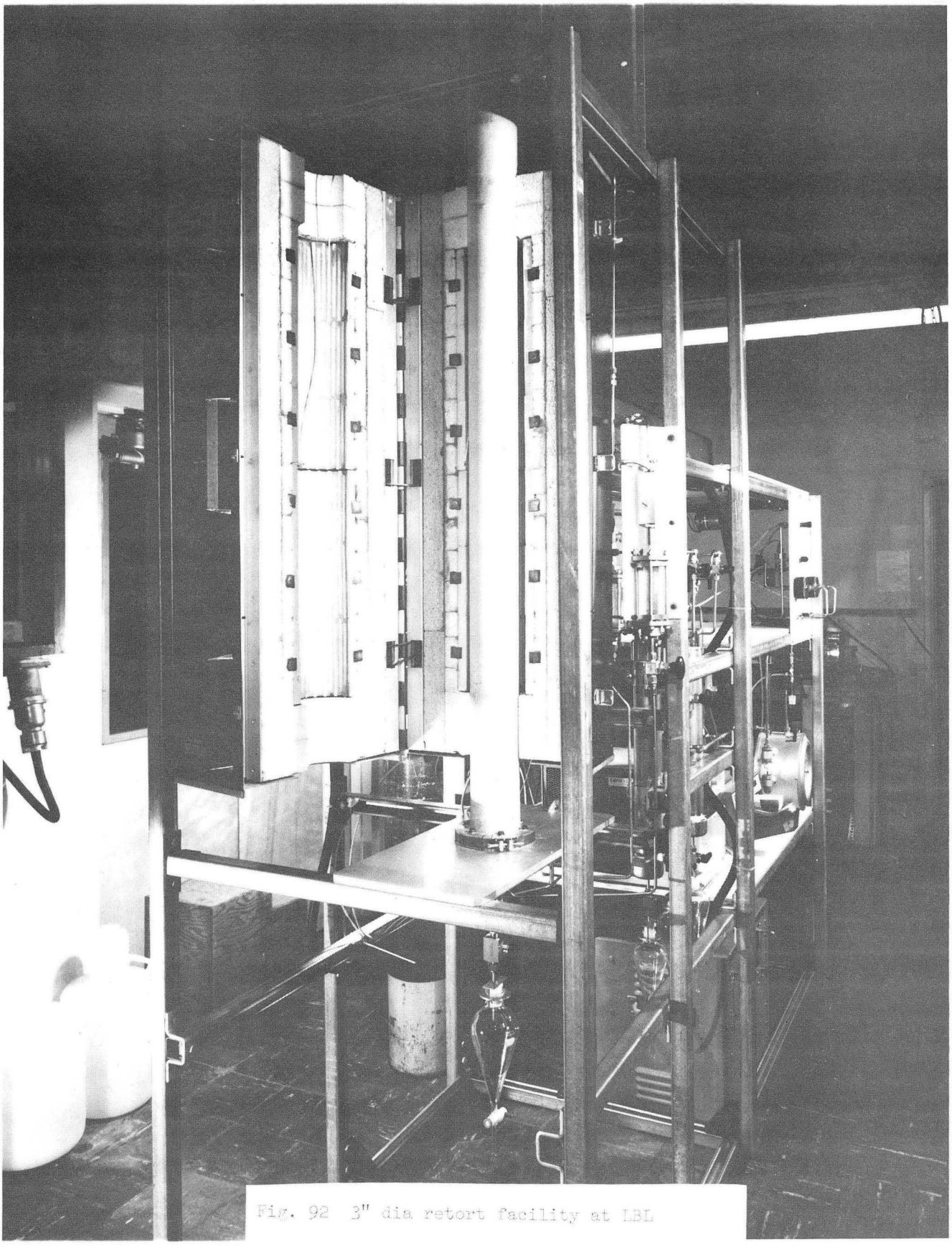

Fig. 92 3" dia retort facility at LBL

XBB 798-10750

This report was done with support from the Department of Energy. Any conclusions or opinions expressed in this report represent solely those of the author(s) and not necessarily those of The Regents of the University of California, the Lawrence Berkeley Laboratory or the Department of Energy.

Reference to a company or product name does not imply approval or recommendation of the product by the University of California or the U.S. Department of Energy to the exclusion of others that may be suitable.

TECHNICAL INFORMATION DEPARTMENT
LAWRENCE BERKELEY LABORATORY
UNIVERSITY OF CALIFORNIA
BERKELEY, CALIFORNIA 94720